Ion Transport Properties of Some Mixed Halide Based Oxide Dispersed Composite Electrolyte Systems

A

Thesis

Submitted for the Award of

the Degree of

DOCTOR OF PHILOSOPHY

By

Archana

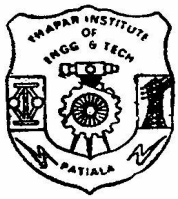

SCHOOL OF PHYSICS AND MATERIALS SCIENCE

THAPAR INSTITUTE OF ENGINEERING AND TECHNOLOGY

(DEEMED UNIVERSITY)

PATIALA – 147 004

INDIA

CERTIFICATE

This is to certify that this thesis entitled **"Ion Transport Properties of Some Mixed Halide Based Oxide Dispersed Composite Electrolyte Systems"** which is being submitted by **Archana** in fulfillment of the requirements for the award of the Degree of Doctor of Philosophy in the School of Physics and Materials Science, Thapar Institute of Engineering and Technology (Deemed University) Patiala, Punjab, India is a record of candidate's own work carried out by her under our supervision. The matter presented in this thesis has not been submitted in part or full for the award of any degree in any other university or Institute.

Supervisors

(Dr. Anjan Sil)
Associate Professor
Department of Metallurgical & Materials Engg.
Indian Institute of Technology Roorkee
Roorkee – 247 667
INDIA

(Dr. N. K. Verma)
Professor & Head
School of Physics & Materials Science
Thapar Institute of Engg. & Tech.
Patiala – 147 004
INDIA

DECLARATION

I hereby affirm that the work presented in this thesis is exclusively my own and there are no collaborators. It does not contain any work for which any other university has awarded a degree.

Archana

(Archana)

Date: Sept 20, 2004

Countersigned

Anjan Sil

(Dr. Anjan Sil)
Associate Professor
Department of Metallurgical & Materials Engg.
Indian Institute of Technology Roorkee
Roorkee – 247 667
INDIA

(Dr. N. K. Verma)
Professor & Head
School of Physics & Materials Science
Thapar Institute of Engg. & Tech.
Patiala – 147 004
INDIA

ACKNOWLEDGEMENT

The present work will remain incomplete unless I express my feelings of gratitude towards a number of persons who delightfully cooperated with me in the process of this research work.

No amount of words can adequately express the debt I owe to my revered teacher and supervisor Dr. Anjan Sil (Associate Professor, Department of Metallurgical and Materials Engineering, IIT Roorkee, Roorkee) for his constant encouragement, able guidance and thoughtful discussions during the course of the present investigation. I shall always treasure his guidance, wise criticism and wholehearted co-operation.

It is my privilege to acknowledge with a sense of gratitude and devotion the keen interest rendered by my supervisor Dr. N. K. Verma, Professor and Head, School of Physics and Materials Science, TIET, Patiala.

The thanks are also due to Dr. K. K. Raina, Dr. O. P. Pandey, Dr. Kulvir Singh and Dr. Manoj Kr. Sharma and Mr. Piyush Verma for their sustained encouragement.

I am grateful to Dr. (Mrs.) Ravinder Sidhu, Mr. Rath, Mr. Sarabjit Singh and especially Mr. Jant Singh, TIET, for their kind support.

Words will be inadequate in expressing my sincere thanks to my friends and labmates Dr. (Mrs.) Jasjit Kaur Sarang, Mr. Puneet Sharma, Dr. (Mrs.) G. Sumana, Mr. Praveen, Mr. Pankaj and Mrs. Raminder Kaur Pabla and especially Mrs. Shaveta Singla, who helped me in various ways, most of all for their cheerful companionship during the course of work.

How can I forget my Parents' support and my husband for his constant encouragement and always audaciously pushing me to get on with my work.

PREFACE

Composite solid electrolytes are a one class of electrolytes. The primary concern of these electrolytes is ionic conductivity (σ) based on various transport characteristics. Though the alkali halides are intrinsic ionic conductors, they rarely meet the technological demands due to the limitation in their conductivities (typically for α–AgI~1.0 $\Omega^{-1}cm^{-1}$ at 150^{o}C, α–CuBr~5.0 $\Omega^{-1}cm^{-1}$ at 480^{o}C, α-CuI~9.0× 10^{-2} $\Omega^{-1}cm^{-1}$ at 450^{o}C etc.). Therefore there was a genuine need to synthesize / tailor-make solid electrolytes which can have high conductivities. This could be realized by making the composite electrolytes with insulating oxide dispersions. Although the idea of composite electrolytes and thereby enhancing the ionic conductivity was proposed as early as 1973 when Liang [76] reported a 50 time increase for the $LiI+Al_2O_3$ system. Since then a large number of systems were developed and investigated for a search of higher and higher conductivities. A reasonably large number of studies on oxide dispersed metallic halides and alkali halides were conducted and reported by various researchers across the world. All these works were essentially targeted to develop electrolytes for the power sources for various applications such as cell phones, pagers, computers, light shutters, smart windows etc. The ever-increasing demand of power sources for modern electronic devices strongly motivate researchers to develop and investigate newer and newer electrolytes, which are the key components of power source / solid state battery. In view of the above requirements, the solid electrolyte preparation and their physical and electrical characterizations were carried out in the present thesis. In order to demonstrate the superiority of mixed matrix base for the oxide dispersion as compared to the case of single halide matrix and the resulting oxide dispersion characteristics-both in single and mixed matrices, a number of electrolytes in the following systems were prepared: (i) $(KCl)_{1-x}+(ZrO_2)_x$; (ii) $[(KCl)_{1-x} + (NaCl)_x]_{1-y}+(ZrO_2)_y$; (iii) $[(KCl)_{1-x} +(CuCl)_x]_{1-y} + (SnO_2)_y$; (iv) $[(BaCl_2)_{1-x}+(KCl)_x]_{1-y} + (ZrO_2)_y$ and (v) $[(KCl)_{1-x}+(KI)_x]_{1-y}+(ZrO_2)_y$. These mixed systems were chosen to address the issues of the characteristics of oxides dispersed in mixed matrices in relation to that of single matrix composite electrolytes. In the systems (ii) and (iii), the essential charge carriers are cations, whereas, in systems (iv) and (v), the conduction is executed essentially by anions. The reason for choosing the KCl-based matrix is due to the fact that it does not undergo phase transformation before melting, thereby accommodating the effect of wide variation of temperature on transport characteristics to develop an empirical relationship of conductivity (σ) and ionic mobility (μ) with temperature. In a majority of the present studies, the dispersoid taken is ZrO_2 particles (size ~1μm). This is due to the

fact that in general, alumina is used as dispersoid for which systems were well studied and reported by other researchers. However, to the best of author's knowledge, no systematic studies on ZrO_2-dispersed composite electrolytes are reported in the literature.

The entire work has been presented in the following five chapters:

Chapter I

Chapter I presents an introduction to electrical conductivity of ionic solids. A review of research findings reported in the area of solid electrolytes and their applications in different fields are also presented. The fundamental characteristics, ions transport mechanisms, temperature dependent conductivity behaviour and defect chemistry of the solid electrolytes have been discussed too. The electrical conductivity behaviour of the two-phase composite electrolytes and, the methods by which the conductivity enhancement can take place are also explained. Several phenomenological theories and the associated models viz. space charge model, adsorption-desorption model etc., that were proposed by various researchers to explain the conductivity enhancement in the oxide dispersed composite electrolyte systems, are also discussed. The scope of the present work, reported in the thesis, is given towards the end of this chapter.

Chapter II

Chapter II deals with the materials requirement, sample compositions, methods of sample preparation, the physical characterization and electrical measurements of the samples. The samples were prepared from powder processing route, following compaction and solid state sintering. The following physical characterization methods have been used: X-ray diffraction (XRD) and Thermal Analyses (DTA/TG) to detect the formation of any new phases / chemical changes that may occur in the material during heat treatment, and Scanning Electron Microscopy (SEM) to reveal the microstructure development especially showing the halide-dispersoid interface formations. The methods of conductivity measurement by impedance spectroscopy technique, ionic mobility estimation by transient ionic current technique and the determination of ionic transference number by Hebb Wagner polarization method are also explained.

Chapter III

Chapter III presents the preparation, characterization and transport characteristics namely σ and μ of KCl-based solid electrolytes dispersed with ZrO_2 particles. This was studied with a view to understand the effect of oxide dispersion in single halide base matrix. The samples were prepared by ceramic powder processing technique. The XRD analysis and the microstructural studies of the sintered composite electrolyte samples were carried out. The ionic conductivity arises due to the combined effect of mobility (μ), concentration (n) and charge $(q=Ze)$ of ions, and this is given by the relation $\sigma = n\,q\,\mu$. As the σ and μ values are temperature dependent, the measurements of these parameters were made as a function of temperature. These temperature dependent studies helped to determine the predominant factor, i.e. μ or n for conductivity increase with temperature.

Chapter IV

Chapter IV demonstrates the preparation of mixed halide matrix and oxide dispersion into the matrix. The systems $[(KCl)_{1-x}+(NaCl)_x]_{1-y}+(ZrO_2)_y$ and $[(KCl)_{1-x}+(CuCl)_x]_{1-y}+(SnO_2)_y$ were studied to fulfill the objective. The details of preparation of mixed matrix for different compositions by melt quench technique and subsequent oxide dispersion by wet mixing technique in the highest conducting mixed matrix compositions are presented. The samples were characterized by SEM, XRD and DTA / TG to explain the conductivity behaviour of the materials. In order to show the effect of dispersoid particle size, the conductivity studies were also carried out on the samples in the system $[(KCl)_{1-x}+(NaCl)_x]_{1-y}+(ZrO_2)_y$ prepared by finer particles sizes (size~20-50 nm) of ZrO_2 also.

Chapter V

Chapter V deals with anionic conductors in mixed halide base. The following systems $[(BaCl_2)_{1-x}+(KCl)_x]_{1-y}+(ZrO_2)_y$ and $[(KCl)_{1-x}+(KI)_x]_{1-y}+(ZrO_2)_y$ were studied. The mixed matrices for different compositions were prepared by melt quench technique and the oxide dispersions were made. The temperature dependent transport characteristics, σ and μ were studied for $[(BaCl_2)_{1-x}+(KCl)_x]_{1-y}+(ZrO_2)_y$ system. The highest conducting electrolyte samples in this system were characterized by SEM and XRD. The conductivity characteristics in the system $[(KCl)_{1-x}+(KI)_x]_{1-y}+(ZrO_2)_y$ were studied and the optimally high conducting composition in this system was established.

At the end, the entire study is concluded and a few points on the scope of future work are suggested. The net conclusion is that with oxide dispersion the conductivity enhancement has been found with respect to the base single matrix. Further enhancement in conductivity was found by base matrix modification, i.e. by making mixed halide as base matrix. The list of papers published, presented and communicated is also appended.

TABLE OF CONTENTS

Chapter I

Introduction to composite solid electrolytes

Overview

This chapter presents a review of the research work reported in the area of solid electrolytes. A detailed description of the solid electrolytes and their different applications is presented. The ionic conductivity is the key feature of the solid electrolytes from their application point of view. The possible mechanisms constituting various proposed models for understanding conductivity enhancement in solid electrolytes are explained. The parameters that govern the properties of the solid electrolyte systems are also mentioned. The scope of the present dissertation is explained towards the end of this chapter.

1.1 Alkali halides

The alkali halides such as LiCl, NaCl, RbCl etc. are the most interesting ionic solids as these are fully ionizable. The alkali halide crystals have always been at the center stage of solid state physics and these have been treated as “model crystals” for verifying many solid state theories. In present decades, these have proved to be useful in several applications ranging from X-ray monochromators to tunable lasers. Because of the dual importance – purely scientific and technological – a vast amount of information has been generated on various aspects of the alkali halides. The study of alkali halides has played an important part in the development of theory of point defects in crystalline solids. In particular, the measurements of ionic conductivity and coefficient of self diffusion can give valuable information regarding the number and type of defects in the crystal lattice; the energy for the formation of different defects, their mobility and interactions between them. The ionic transport both in pure alkali halide crystals and doped alkali halides at elevated temperatures is used to estimate defect concentrations, enthalpies of defect formation, activation energies for ion migration and other physical parameters. It is generally considered that Schottky defects are present in most of the alkali halides with concentrations far higher than that of other type of defects i.e. Frenkel defects. The defect structure and defect concentration can be predicted clearly in the case of Schottky vacancies.

1.2 Electrical conductivity

Electrical conductivity (σ) is an indicator of the ease with which a material is capable of conducting an electric charge. The electrical conductivity is the inverse of resistivity i.e. $\sigma = \frac{1}{\rho}$. Ohm’s law relates the current I (i.e. the rate of charge flow) passing in a material to the applied voltage as $V = IR$, where R is the resistance offered by the material against the current. The resistivity ρ is independent of the specimen geometry and is given by the expression $\rho = \frac{RA}{l}$, where l is the distance between the two points along the current path across which the voltage is measured and A the cross-sectional area perpendicular to the current. Alternatively, σ may be defined as the proportionality

constant in the linear relation of current density (j) with the applied electric field (E) such that $j = \sigma E$. The magnitude of the electrical conductivity as given by the relationship $\sigma = n e Z \mu$ is determined by (i) n, the density of charge carrier; (ii) $q = (eZ)$, the charge on a carrier; and (iii) μ, the average drift velocity of the charge carriers per unit electric field defined as mobility. Commonly used unit of conductivity is S cm^{-1} where 1 siemen, $S = 1\Omega^{-1}$.

The charge carriers can be ions (cations and / or anions) and / or electrons (or holes). As the cations and anions possess electric charge, they are able to migrate when an electric field is applied, resulting in an electric current in addition to that due to any electron motion in the solid. The total conductivity for an ionic material σ_{total} is thus equal to the sum of both electronic and ionic contributions expressed as $\sigma_{total} = \sigma_{ionic} + \sigma_{electronic}$. Solids are classified as first type conductors if the charge carriers are mainly electrons and second type conductors when the carriers are mainly ions. Materials that have conductivity due to both electrons and ions are regarded as mixed conductors. This classification of conductors is, however, based on their room temperature conductivity. The material, for example, yttrium stabilized zirconia (YSZ) (0.92 ZrO_2 + 0.08 Y_2O_3) [1], which is insulator at room temperature, may have significantly high conductivity at higher temperatures. The conductivity in YSZ is predominantly due to oxygen ions, and negligibly by electrons. Table 1.1 gives classification of solid materials according to their typical conductivity range at room temperature.

Table 1.1 Typical values of electrical conductivity

	Material	**Conductivity (Ω^{-1} cm^{-1})**
Ionic conduction	Ionic crystals	$< 10^{-18} – 10^{-4}$
	Solid electrolytes	$10^{-3} – 10^{1}$
	Strong (liquid Electrolytes)	$10^{-3} – 10^{1}$
Electronic conduction	Metals	$10^{1} – 10^{5}$
	Semiconductors	$10^{-5} – 10^{2}$
	Insulators	$< 10^{-12}$

1.3 Applications

The discovery of transistors in the 1950s revolutionized the field of semiconductor electronics and a new branch of science named as solid state electronics was emerged. This branch of science mainly deals with the physics, engineering and technological aspects of electronic materials and has made tremendous strides, especially in the area of integrated electronics. Until the late 1960s, a very few devices based on ion conducting materials, were available. Out of the known devices, the majority of them were based on liquid aqueous electrolytes. These devices were reported [2-5] to suffer from a number of major shortcomings such as:

(i) they have limited temperature range of operation; the devices would fail to function below freezing and above boiling temperatures of liquid electrolytes,
(ii) they are less rugged,
(iii) they have limited shelf life due to the corrosion of electrode materials by the electrolytic solution resulting in leakage,
(iv) difficulty in constructing in miniature thin film.

In order to eliminate the above shortcomings, there was a need to replace the liquid electrolytes with some suitable ion conducting solids. As an early attempt, the ion conducting solids such as alkali halides, silver halides etc. were used. However, due to the fact that these solids were poor conductors, they remained unsatisfactory choices as

replacement of liquid electrolytes. However, the search for solids having high ionic conductivity continued rigorously. Eventually, the situation took a dramatic turn in the year 1967 when two new kinds of solid systems namely MAg_4I_5 (where M = Rb, K, NH_4) [6-8] and Na β – alumina [9], exhibiting exceptionally high Ag^+ and Na^+ ion conductivity ($\sigma \sim 10^{-1}\ \Omega^{-1}cm^{-1}$) in the respective electrolytes at room temperature and also moderately high temperature were discovered. A large number of fast ion conducting solids with various mobile ion species, namely H^+, Li^+, Na^+, K^+, Ag^+, Cu^+, F^-, O^{-2} etc. have, so far, been reported. In fact, the year 1967 has been marked as the beginning of a new era in the field of materials science, which currently bears the name solid state ionics, a terminology used parallel to solid state electronics.

Energy generation, which, to date, has largely been based on fossil fuels, is a major source of anthropogenic green house gas emissions and other pollutants. However, future energy generation must be sustainable in terms of (i) cost factor, (ii) fuel resource availability and (iii) environmental acceptability. Much effort is being made on sustainable energy supply through different measures such as the development of more efficient energy generation technologies, increased end use efficiency and greater use of new renewable energy sources such as solar, wind and biomass. At the same time there is an increasing emphasis on small-scale distribution electricity generation. Fuel cells have the potential to play a dominant role in the future distributed energy generation network, with their high fuel conversion efficiencies, and as a clean source of power (significantly lower pollution and green house gas emissions compared to those of conventional, centralized power generation). Furthermore, the use of fuel cells in transport vehicles as an auxiliary power unit or a replacement for internal combustion engines will bring substantial benefits in terms of clean urban area and by extending the life of existing fossil fuel resources. While solid oxide (SOFC) and polymer electrolyte membrane (PEMFC) fuel cells and oxygen sensors are perhaps the best known and prominent applications of Solid State Ionics (SSI) in the field of energy generation, other potential areas are starting to emerge. These include hydrogen production from solar energy and novel methods of oxygen separation from air. Efficient and cost effective energy storage systems are crucial for new load levelling and electricity supply applications. The wider

use of solar and other renewable energy sources are in both stationary and mobile power applications. Storage technologies such as advanced batteries and high power delivery supercapacitors will play key roles, while hydrogen generated from renewable energy is seen as the fuel for the future [10]. SSI technologies which are set to play increasingly important roles in sustainable energy systems include :

- fuel cells (PEMFC and SOFC);
- advanced batteries (based on Li^+, Na^+ and H^+ etc ion conductors);
- supercapacitors (polymer membrane capacitors);
- ionic transport membranes (gas separation and chemical reactors);
- advanced sensors for process control and safety;
- electrochromic smart windows for optical modulation and energy efficient buildings.

Several of these technologies are presently being commercialized [11,12], while the others are at various stages of the development. All are set to play increasingly important roles across the entire spectrum of sustainable energy generation and supply. Electrochemical devices have been proven to be products for a full range of corrosion control applications. Electrochemical devices based on ceramic electrodes and electrolytes are becoming increasingly important for energy generation, oxygen separation, coal gasification, and selective oxidation of hydrocarbons. Major portion of the cost of manufacturing these devices is due to the raw materials.

1.3.1 Electrochromic display devices

The increase in the interaction between man and machine has made display devices indispensable for visual communication. The information, which is to be communicated from a machine, can be often in the form of colour images. Electrochromic display device (ECD) is one of the most powerful candidates for this purpose and has various merits such as multicolour, high contrast, optical memory, and no visual dependence on viewing angle [13]. Electrochromism can be defined as the colour change in a material by an applied electric field or electric current as optical properties of these materials change when a voltage is applied across it. The optical properties should be reversible i.e. the original state should be recoverable if the polarity of the voltage is reversed. Some of the

mechanisms which are responsible for the colour change in solids or liquids are given below [14] :

(i) Electrolyte colouration or colour center

When electrons are injected into solids, colour centers are produced as a result of electron trapping.

(ii) Charge transfer

In this mechanism, the electric field causes a charge to be transferred from one type of impurity center to another. An absorption band associated with one type of impurity center grows at the expense of that of the other type.

(iii) Franz – Keldysh effect

In this case, the electric field induces a shift in the absorption band and hence colour due to a tunneling effect results.

(iv) Electrochemical redox reaction

Some ions or molecules can be reduced or oxidized electrochemically with the change in colour.

Based on above mechanisms, electrochromic devices can be categorized according to the type of electrolyte or ion conductor. Liquid electrolytes are convenient for research and exploratory work. However, solid inorganic or organic materials are preferred for practical devices.

In an inorganic electrochromic display device, $RbAg_4I_5$, β–alumina and $HUO_2PO_4.4H_2O$ have been tested as solid electrolytes. An example of a complete cell configuration consisting of such electrolytes is given below:

Ag (1) / $RbAg_4I_5$ / WO_3, SnO_2, Ag (2)

The cell is initially transparent with a faint milkiness due to $RbAg_4I_5$. When a low dc voltage is applied across the cell with WO_3 as the cathode, a blue colouration develops

over the region of the electrolyte. Even after the removal of the electric field, the film remains coloured. On reversing the potential, the colour (blue) disappears. These properties make electrochromic materials of considerable interest for optical devices of different types, such as elements for information display, light shutters, smart windows, variable reflectance mirrors and variable emittance thermal radiators.

1.3.2 Solid electrolyte thermometer

Solid electrolytes are also used as high temperature electrochemical thermometer. Such a thermometer has an advantage that it can be used at high temperatures (>1000^{o}C) because the materials used are ceramics. Generally gas thermometry is limited to a maximum of ~ 1000^{o}C due to lack of suitable materials. Such a thermometer has the cell geometry

$$Pt / O_2 (P_1) / \text{Solid electrolyte} / O_2 (P_2) / Pt$$

The temperature can be calculated from the oxygen pressure levels P_1 and P_2.

1.3.3 Electrochemical pumps

Solid electrolytes can also be used for gas separation because of their selectivity to only one type of charge carrying species. In the case of Zirconia based electrolytes, only O^{2-} ions migrate. Therefore on application of an electric field across the cell, pure O_2 gas can be generated at the anode. Such devices can be used electrochemically to pump oxygen in or out of both a stationary and a dynamic system. They also find applications in food packaging industry as well as in the medical field if the cells can be made to economically produce large quantities of oxygen for low energy consumption [15].

1.3.4 Thermoelectric generators

A thermoelectric generator is a unique heat engine in which charge carriers serve as the working fluid [16]. These generators convert a part of the heat flowing from a hot body to a cold body into electricity. The portion of the thermal power that converts into electrical power is referred as efficiency. The operation is based on the principle that an EMF is generated when a solid electrolyte with its two opposite faces either at (i) different

temperatures, or with (ii) different pressures resulting in different electrochemical activity of the mobile species.

In 1974, the design of a thermoelectric generator with β - alumina electrolyte was suggested in which different sodium activities at the two faces were maintained as a result of a temperature difference. Thermoelectric power generators have, so far, been primarily employed in space and military applications. Generators are reliable because they produce electricity without moving parts which may fail or wear out. This high degree of reliability is especially important in space applications, where the investment is quite high and repair or replacement of equipment is not feasible [17].

1.3.5 Solid state battery

A battery is a device that converts chemical energy contained in its material constituents into electrical energy. The earlier electric power sources used liquid electrolytes. However, solid state batteries have some distinct advantages over those with a liquid electrolyte. The primary advantage is the avoidance of electrolyte leakage into the electrodes, which can cause the damage to the performance of electrodes. So solid state batteries have longer life and are inherently safer than liquid electrolyte cells. A number of solid state high energy density storage batteries based on ceramic superionic conductors are being developed for utility load levelling and vehicle traction application [18-21]. The first sodium / sulfur battery using Na^+ β - alumina solid electrolyte [22] is under testing in several countries for use in, for example, electric cars and power station load levelling. The normal temperature of its operation is between 300–350^oC.

Other types of cells which are in applications are miniature primary cells which operate at room temperature and have long life rather than a high power output. They are used in electronic watches, heart pacemakers and in military applications.

1.3.6 Fuel cells

A fuel cell operating as a sort of continuously replenished battery provides an alternative whereby electrical energy can be made available with small losses. It operates like a battery but does not need to be recharged. It continuously produces power to convert

gaseous fuels (hydrogen, natural gas, gasified coal) directly into electricity via an electrochemical process. These devices are capable of generating continuous voltage and current. They offer a clean and pollution free technology for electricity generation. The basic elements of a typical fuel cell as depicted in figure 1.1 consist of an electrolyte in contact with a porous anode and a porous cathode. The fuel and oxidant gases flow along the surface of the anode and the cathode respectively and they react electrochemically in the three-phase boundary region established at the gas-electrolyte-electrode interface.

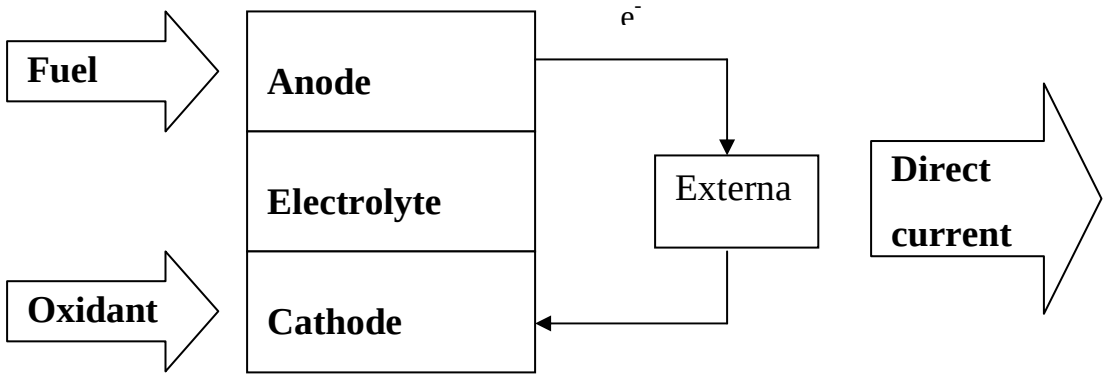

Fig. 1.1 Schematic representation of a planar fuel cell.

A fuel cell produces electrical energy for as long as fuel and oxidant are fed to the porous electrodes. Hydrogen, ethanol, methanol etc. are used as fuels, while oxygen or air can be used as oxidant.

In 1899, Nernst [1] discovered the solid oxide electrolyte stabilized Zirconia for the fuel cell. In the middle of the 20^{th} century, a rapid development in this area has taken place. At present several types of fuel cells are available in the consumer market and the following five types of fuel cells are commonly employed [23,24]:

- the solid polymer proton conductor fuel cell (SPFC);
- the alkaline fuel cell (AFC);
- the phosphoric acid fuel cell (PAFC);
- the molten carbonate fuel cell (MCFC);
- the solid oxide fuel cell (SOFC).

Low temperature fuel cells (AFC, SPFC and PAFC) have a potential for propulsion of cars, where a short heating time is needed and the efficiency has to be compared with that of a combustion engine (~ 20%) given by the limitations of the Carnot cycle.

High temperature fuel cells (MCFC and SOFC) are suitable for continuous power / heat production, where the cell temperature can be maintained. In general the high temperature fuel cells exhibit higher efficiency and are less sensitive to fuel composition than the case with low temperature fuel cells. At higher temperatures, natural gas can be applied directly as a fuel.

1.3.7 Ceramic sensors

There is a continuous need for the development of rugged and reliable sensors capable of making measurements in crucial environments in industries viz. steel manufacturing, heat treatment, metal casting, automotive, aerospace, utility and power industries, etc. [25-27]. The application of sensor and measurement technology has resulted in many benefits including improved energy efficiency, better quality, and lower scrap or off specification products and reduced emissions. The automotive industry is an excellent example where increased use of sensor and measurement technology has led to an improvement in engine performance, higher energy efficiency and reduced pollutant emissions. Solid electrolytes of the mobile M^{Z+} ions may be used to control the element concentration in various environments by electrode reaction of the first kind (M/M^{Z+}) [28]. The high alkali ion reactivity allows the use of alkali ion conducting solid conductors for monitoring of various gases. While low temperature sensors have been commercially successful, their high temperature counterparts have been less so.

1.4 Solid electrolytes

New types of electrochemical devices, including lithium batteries, electrochemical capacitors, electrochromic windows, fuel cells and photo electrochemical solar cells demand a variety of special properties of the ubiquitous electrolyte contained therein. Materials such as solid polymer electrolytes, molten salts, ceramic fast ion conductors and fast ion conducting plastic crystals are currently in focus world-wide for the

applications mentioned above. The solids exhibiting high ionic conductivity are termed as superionic conductors or solid electrolytes or fast ion conductors or hyperionic solids.

The term superionic conductors is used to describe a class of materials which may be crystalline, glassy or polymeric through which the transport of ions is fast due to the application of an electric field, and has insignificant electronic conductivity. These materials are intermediate in structure and property between, on the one hand, normal crystalline solids with regular three dimensional structures and immobile atoms or ions and on the other hand, liquid electrolytes which do not have regular structures, but do have mobile ions as shown in figure 1.2.

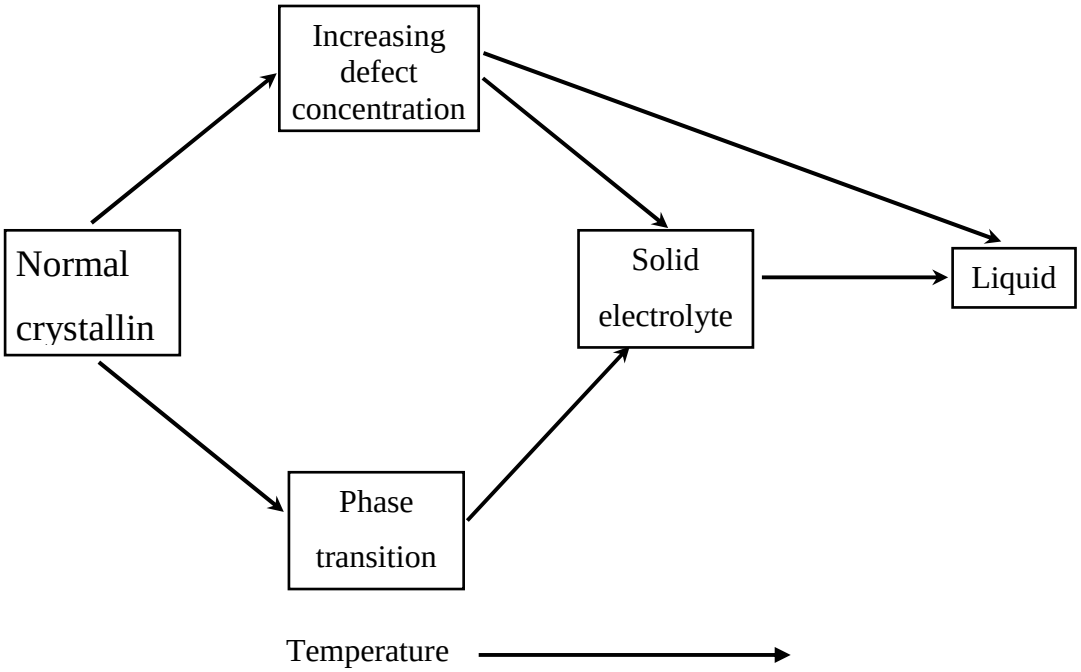

Fig. 1.2 Solid electrolytes as intermediate between normal crystalline solids and liquids.

The high ion conductivity in solids, such as α–AgI [29], MAg_4I_5 (where M = Rb, K, NH_4) [6,8] and Na β–alumina [30,31], approach similar values (10^0-10^{-3} $\Omega^{-1}cm^{-1}$) as that of liquid salt solutions or melted salts (electrolytes). Such materials are called solid electrolytes. Their conductivity is caused by a delocalization of Ag^+ and Na^+ cations over a wide range of interstices in an immobile sub lattice. The high ion conductivity for solid materials is rather unusual at moderate temperatures (i.e. 20° - 300°C). Most of the solids

show certain ion localization. However, in some compounds at certain temperatures, a phase transition is possible, where the localized cation sublattice gets disordered over a numerous interstices. Such a phase transition is observed in AgI ($\beta \rightarrow \alpha$ phase transition at 147°C) and Ag_4RbI_5 (at 122 K). The conductivity spontaneously increases by several orders of magnitude upon the melting of cation sublattice. Therefore, the term "solid electrolyte" can rather be used to identify a particular state of solid material, when a sort of ion is quasi-freely (with low activation energy < 0.5 eV) moving around over numerous available sites in the rigid sublattice. However, many other materials with the lower ionic conductivity are also regarded as solid electrolytes.

Other type of solid electrolytes form due to a gradual increase in defect concentration with increasing temperature. For example ZrO_2 in which the concentration of anion vacancies above ~ 600^oC is sufficiently large and therefore is a good high temperature oxide ion conductor. The distinction between normal ionic solids and solid electrolytes is often not well defined, especially for material such as ZrO_2, which undergoes a gradual change in behaviour with increasing temperature.

Ratner and Nitzan [32] gave a general definition of the solid electrolyte as a solid that exhibits a characteristic ionic conductivity, more typical of liquids, lying in the range from 10^{-6} to 10^{-1} $\Omega^{-1}cm^{-1}$ near ambient temperature. "High temperature solid electrolyte" refers to the material such as YSZ. This is a poor conductor at room temperature (σ < 10^{-10} $\Omega^{-1}cm^{-1}$) but has high ionic conductivity of 0.15 $\Omega^{-1}cm^{-1}$ at 1000°C [33].

1.4.1 Fundamental characteristics

Since the mid 1960s, a very active field of research namely solid electrolyte has been under the investigation. Many of these searches were carried out on a 'try and see' basis because the crystal structures of the materials were not known at that time. However, it was possible to study other materials whose crystal structures contain open channels, layers etc., with an idea that these channels may provide pathways for easy ionic transport. Although many theories have been proposed to account for solid electrolyte behaviour, it is still very difficult to make a priori reliable predictions about the value of σ in a particular material whose crystal structure is known. The following are the

guidelines, which show the likely structural characteristics that are a prerequisite for high ionic conductivity [34]:

(i) A large number of the ions of one species should be mobile i.e. a large value of n in the equation $\sigma = n e Z \mu$.

(ii) There should be a large number of empty sites available for the mobile ions to jump into.

(iii) The empty and occupied sites should have similar potential energies with a low activation energy barrier for jumping between neighbouring sites.

(iv) The structure should have a framework, preferably three dimensional, permeated by open channels through which mobile ions may migrate.

1.4.2 Ion transport mechanism

Even though crystals are defined as ordered arrangements of atoms or ions, they are not perfect. They always possess defects, the types of which can be divided into two broad categories; point defects and extended defects. The examples of extended defects are dislocation, grain boundary etc. In materials having high ionic conductivity, conduction occurs mainly through point defects e.g. vacancies, interstitial and substitutional impurities. A point defect can be developed by (i) intrinsic and / or (ii) extrinsic mechanisms. An intrinsic defect (due to thermal effect) is one that is inherent to the material; Schottky and Frenkel defects are in this class. While an extrinsic defect occurs due to the addition of an aliovalent impurity. This can be visualized by taking an example of Yttria stabilized Zirconia (YSZ) in which Zr^{4+} is replaced by additive Y^{3+}.

A Schottky defect consists of a cation and an anion vacancies. These vacancies move from the lattice site to the surface. A Frenkel defect is the result of movement of an ion to produce a simultaneous interstitial and a vacant lattice site. Figure 1.3 (a) and (b) schematically show Frenkel and Schottky defects respectively. As the size of the ion is important, the defects are limited to the sub lattice of the smaller ion, usually cation.

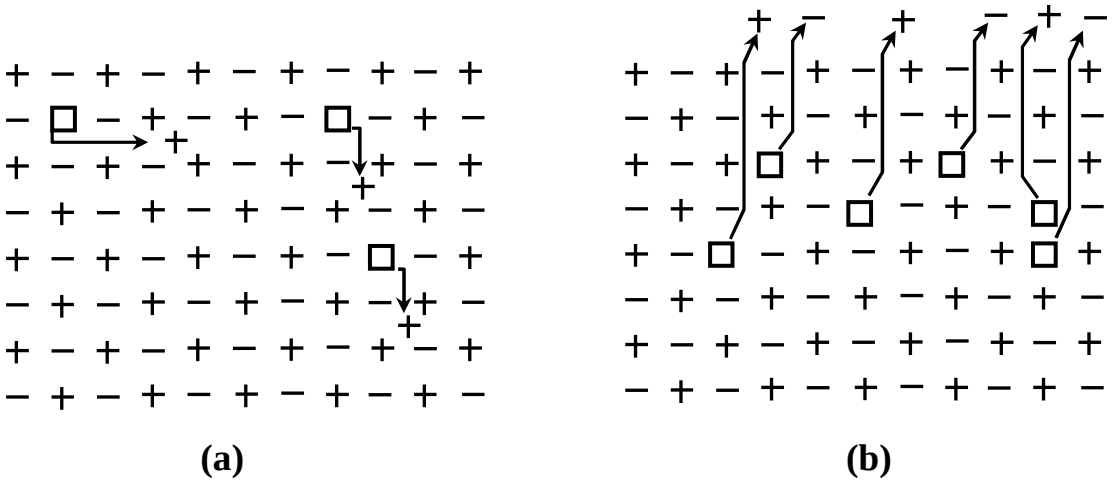

Fig. 1.3 Schematic representation of (a) Frenkel defects and (b) Schottky defects.

Very few ionic solids exhibit conductivity due to the intrinsic defects. One notable exception is the class of halides. Due to the thermal vibrations, when ions receive enough energy to be pushed into an interstitial site or to a nearby vacant lattice site, ion conduction takes place in the solid. For understanding the factors determining the ion conductivity in crystals, let us consider a binary AB ionic crystal which is basically a Schottky disordered solid. The Schottky disorder has $n_{Av} = n_{Bv} = n_S$, where n_{Av}, n_{Bv} are the number of A type and B type ion vacancies respectively and n_S is the number of Schottky pairs. In ionic crystals, conductivity may be described as transport of such defects given by the well-known general equation

$$\sigma = \sum_i n_i e Z_i \mu_i \tag{1.1}$$

where n_i, eZ_i and μ_i are concentration, charge and mobility respectively of the ith species of the carrier ions.

The defect concentration is estimated from thermodynamics. In the case of Schottky defects, a change of the thermodynamic potential is given by

$$\Delta G = n_S \, g_S - T \, \Delta \, S_{config} \tag{1.2}$$

where g_S is the change in thermodynamic potential of the system caused by a single occurrence of a Schottky defect and ΔS_{config} is the corresponding change in the configuration entropy. Further the entropy change ΔS_{config} is given by the equation

$$\Delta S_{config} = k_B \ln w \tag{1.3}$$

where k_B is Boltzmann constant and w is the number of possible ways of arranging the Schottky defects. At thermodynamic equilibrium, $(\partial \Delta G / \partial n_S)_{P,T} = 0$ and from this condition, the number of Schottky defects can be derived as

$$n_S = N \exp(-g_S / 2\, k_B T) \tag{1.4}$$

where N represents the number of lattice sites. Analogously, the number of Frenkel defects can be given by

$$n_f = (N N')^{1/2} \exp(-g_f / 2\, k_B T) \tag{1.5}$$

where N' is the number of interstitial sites.

Ion transport in ionic crystals takes place by the jump mechanism (vacancy, interstitial or interstitialcy). The formation of defects changes the vibrational modes of the ions surrounding the defects. Following the Einstein Model, the probability P (per unit time) for a given ion to jump from one site to another is governed by

$$P = \upsilon_o \exp(-\Delta g / k_B T) \tag{1.6}$$

where υ_o is the vibrational frequency of the ions about their mean position in a potential well of barrier height Δg, which is termed as Gibb's free energy for migration of ions. Gibb's free energy is expressed as

$$\Delta g = \Delta h - T \Delta S \tag{1.7}$$

where Δh and ΔS are the enthalpy of migration and entropy change in the system respectively. In the absence of an external electric field gradient, this equation (1.7) represents an equal number of ion jumps both in left and right directions at thermodynamic equilibrium.

As the electric field E, is applied along the x-direction, as shown in figure 1.4, the jump probabilities ($P^{'}$ and $P"$) of the ions in and against the direction of the field are given as follows:

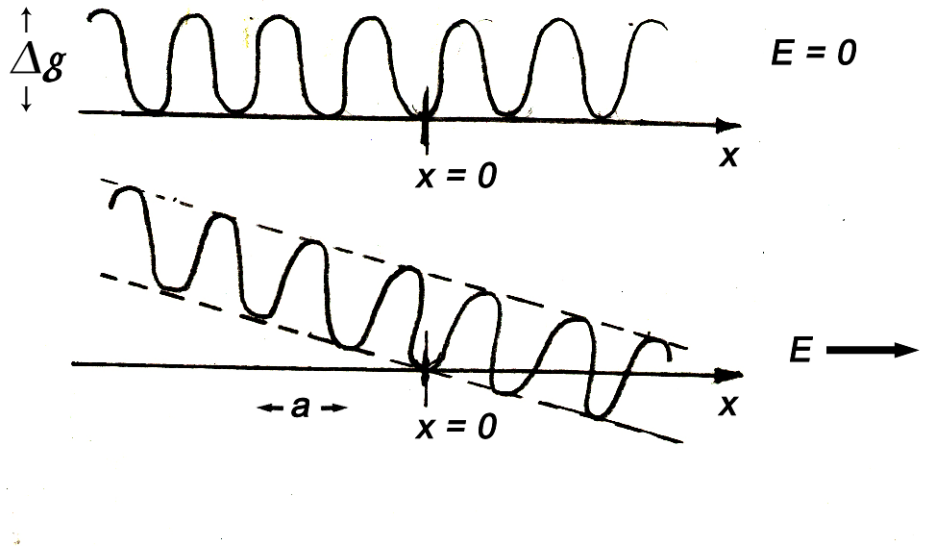

Fig. 1.4 Potential barrier for an ion with and without electric field, E, where a is the interatomic spacing.

$$P^{'} = \upsilon_o \exp\{-[\Delta g - (q a E/2)]/k_B T\} \tag{1.8}$$

and

$$P" = \upsilon_o \exp\{-[\Delta g + (q a E/2)]/k_B T\} \tag{1.9}$$

Hence the number of ions per unit volume moving in the direction of the field is

$$n' = n\left(P' - P''\right)$$
$$\cong n\ \left(q\,a\,E / k_B T\right)P \tag{1.10}$$

where it is assumed that $q\,a\,E << k_B T$. Here n is the number of charge carriers per unit volume. So the current density j, defined as the amount of charge passing through unit area in unit time can be given by

$$j = n'\,q\,a$$
$$= n\ q^2\,a^2\left(P\,E / k_B T\right) \tag{1.11}$$

Hence the ionic conductivity σ can be expressed as

$$\sigma = j / E$$
$$= n\left(a^2\,q^2 / k_B T\right)\upsilon_o \exp\left(-\Delta g / k_B T\right) \tag{1.12}$$

In the case of solids having Schottky defects, one can derive from equation (1.4)

$$\sigma = N\left(a^2\,q^2 / k_B T\right)\upsilon_o \exp\left\{-\left[\left(g_S / 2\right) + \Delta g\right] / k_B T\right\} \tag{1.13}$$

Similarly in case of solids with Frenkel defects,

$$\sigma = \left(N\,N'\right)^{1/2}\left(a^2\,q^2 / k_B T\right)\upsilon_o \exp\left\{-\left[\left(g_f / 2\right) + \Delta g\right] / k_B T\right\} \tag{1.14}$$

However, in case of solid electrolytes, the number of mobile charge carriers is extremely large, therefore the energy of formation of the defects i.e., g_f or g_S, is negligibly small.

Hence for solid electrolytes, these equations are slightly modified and can be generalized to the following Arrhenius type equation

$$\sigma = \sigma_o \exp\left(-\Delta E_a / k_B T\right) \tag{1.15}$$

where σ_o is the pre-exponential factor ($\equiv N\left(a^2 q^2 / k_B T\right)\upsilon_o$, for Schottky defects; $\equiv\left(N N'\right)^{1/2}\left(a^2 q^2 / k_B T\right)\upsilon_o$, for Frenkel defects) and $\Delta E_a \left(\equiv \Delta g\right)$ is the activation energy.

1.4.3 Temperature dependence of ionic conductivity

The ionic transport parameters σ, μ and n in equation 1.1 are function of temperature. Hence for solid electrolyte systems having single mobile ion species, the equation (1.1) can be written as

$$\sigma(T) = n(T)\, eZ\mu(T) \tag{1.16}$$

and the variations of n and μ with temperature can be expressed by following the Arrhenius type equations

$$n(T) = n_o \exp\left(-\Delta E_f / k_B T\right) \tag{1.17}$$

$$\mu(T) = \mu_o \exp\left(-\Delta E_m / k_B T\right) \tag{1.18}$$

where n_o and μ_o are the pre exponential factors and ΔE_f and ΔE_m can be designated as energy of formation and energy of migration respectively for the mobile charge carriers. The energy values $\left(\Delta E_a, \Delta E_f \text{ and } \Delta E_m\right)$ involved in the above thermally activated processes can be related to each other by following energy equation

$$\Delta E_a = \Delta E_f + \Delta E_m \tag{1.19}$$

The j can be expressed in terms of drift velocity, v_d as given below

$$\begin{aligned} j &= n q v_d \\ &= n q v_{do} \exp\left(-\Delta E_d / k_B T\right) \end{aligned} \tag{1.20}$$

where ΔE_d is the activation energy required for ion drift.

1.4.4 Defect chemistry

The role of point defects in transport properties is perhaps among the best atomistically modelled so far [35,36]. The results are commonly represented by the Kroger-Vink notations or Brouwer diagrams [37].

Kroger-Vink notation is a standard form used to describe the point defects. It is represented by the symbol M_y^x; where M represents the defect type, the superscript x represents the effective charge or the relative charge of the defect with respect to the original species and y is the position site. Positive excess charge is marked by a point " • " say $M^\bullet$ and the negative charge by a hyphen " – " or dash " ′ " e.g. $M^{'}$. Considering a Frenkel disordered material M^+X^-, the ionic disorder reaction equation can be written as

$$M_M + V_i \rightleftharpoons M_i^\bullet + V_M^{'} \tag{1.21}$$

where $M_i^\bullet$ is an interstitial cation; $V_M^{'}$ a cation vacancy; M_M a regular cation and V_i a regular interstitial site. Similarly in case of a material MX having Schottky defect, the reaction can be given by

$$M_M + X_X \rightleftharpoons V_M^{'} + V_X^\bullet + MX \tag{1.22}$$

These defect reactions are required to conform to the following conditions:

- A chemical reaction cannot create or loose mass.
- The ratio of cation to anion sites of the host crystal lattice must be preserved.

- The effective charge must be balanced.

1.4.5 Solid electrolytes : a classification

On the basis of the nature of the host matrix and dispersoid, solid electrolyte systems are broadly classified into the following categories:

1.4.5.1 Crystal-crystal composites

They are the most extensively studied dispersed solid electrolyte systems. In these systems the first phase host matrices are moderate ionic solids, like silver halides, copper halides etc.; whereas the second phase dispersoid is either another ionic solid (such as AgCl or AgBr in AgI) or an inert and insulating material (such as Al_2O_3, SiO_2, ZrO_2, fly-ash etc.) [38-42]. In the case of dispersion of insulating and inert second phase material, it has been reported that the smaller the particle size, the larger the conductivity enhancement.

1.4.5.2 Crystal-glass composites

These systems are relatively a new class of composite electrolytes. Ion conducting glasses have several distinct advantages over their crystalline–polycrystalline counterparts. They have (i) continuously variable compositions; (ii) high value of ionic conductivity with isotropic conduction; (iii) practically no grain boundaries; (iv) suitability of fabrication in thin film form etc. The first Ag^+ ion conducting glass: $AgI+Ag_2SeO_4$ was reported by Kunze in 1973 [43]. Since then a large number of glasses with various mobile ion species, namely Ag^+, Li^+, Cu^+, Na^+, F^-, have been developed. These glasses are formed based on the composition ($MX+M_2O+A_xO_y$), where A_xO_y (i.e. B_2O_3, P_2O_5, SiO_2, MoO_3 etc.) is the oxide glass former, M_2O (e.g. Ag_2O, Li_2O, Cu_2O, Na_2O etc.) is the network modifier and MX (e.g. silver halides, alkali halides, copper halides etc.) is the salt [44-47].

1.4.5.3 Glass-polymer composites

Polymer electrolytes have several advantages over other solid electrolytes such as the thin film forming property, good processibility, flexibility, lightweight, elasticity and transparency. However, these systems exhibit less mechanical strength, workability,

time-stability and ionic conductivity etc. at room temperature [48,49]. In order to improve the electrical and mechanical properties, high ion conducting glasses can be dispersed into polymer electrolytes during sample preparation [50-52].

1.4.5.4 Crystal-polymer composites

Another way to improve the electrical and mechanical properties of polymer electrolytes is by dispersing with organic filler (PEO+PMMA) and inorganic filler (Al_2O_3, SiO_2, Nasicon, β–alumina, $LiAlO_2$) into polymer electrolytes [53-56]. There are several crystal polymer composite systems reported in the literature in which the dispersion of fillers has not only improve the mechanical stability of the polymer electrolytes but also significantly enhanced the ionic conductivity. This class of solid electrolytes has attracted considerable attention as compared with glass polymer composites.

1.4.6 Characteristic features

Composite electrolyte systems have several characteristic features. Some of the important features are described below:

1.4.6.1 Concentration of the dispersoid

The conductivity increases with increasing dispersoid concentration and then it decreases after attaining a peak value. The peak is generally sharp, except for a few systems, such as HgI_2+Al_2O_3, AgI+dried Al_2O_3 etc. [57,58]. Furthermore, the appearance of conductivity maximum and the composite system depends on the nature of second phase dispersoid [59]. In some composite systems, the dispersion does not alter or increase the conductivity of the host matrix [51,60].

1.4.6.2 Nature of the dispersoid

For instance, in the systems AgI+Al_2O_3 and LiCl+Al_2O_3, highest conductivity attained with η–Al_2O_3 dispersoid was reported [58,61]. It is reported that, in general, larger conductivity enhancements are found with Al_2O_3 dispersion [59,62]. Other materials such as ferroelectric oxides (viz. $BaTiO_3$, $SrTiO_3$, etc.) having high dielectric constant can also be used as dispersoid [63,64]. Conductivity enhancement was also observed in systems treated with Lewis acid (SbF_5) [65].

1.4.6.3 Particle size of the dispersoid

It has been found that the conductivity of the composite system increases with decreasing particle size [53,59,60]. The particle surface area increases with decreasing particle size [59,66]. Hence porous materials having large surface area, irrespective of the large particle size are reported to exhibit better enhancements in ionic conductivity [39, 67].

1.4.6.4 Conductivity as a function of temperature

The enhancement is highest only at low temperatures. As the temperature increases, the enhancement decreases [68]. This is due to the fact that with increase in temperature, the activation energy for the electrolyte gets lowered as compared to the matrix.

1.4.6.5 Preparation route

An analysis of the various methods used for the preparation of the composite electrolytes shows that the best results can be achieved by mixing the dispersoid with the matrix in its molten state [62,69,70]. This increases the contact surface area and offers more uniform distribution. It has been reported that for composite electrolyte systems prepared by the solution cast method, conductivity enhancement is about one order of magnitude higher than those prepared by conventional methods [71].

1.5 Literature Review

Liang et al. [72,73] in 1969 reported the use of LiI as a solid electrolyte material for the applications in solid state battery systems. LiI is chemically compatible with active anode material lithium and has extremely low ionic conductivity. However, the relatively low ionic conductivity of LiI (10^{-7} $\Omega^{-1}cm^{-1}$ at $25^{o}C$) limits the performance of the solid electrolyte cells. In an attempt to increase the ionic conductivity of LiI, Schlaikjer and Liang [74,75] studied the conduction characteristics of LiI doped with various calcium compounds. However the conductivity was found to decrease with time. In order to overcome this problem, Liang in 1973 [76] tried to stabilize the conductivity of LiI-based solid electrolytes at room temperature by incorporation of Al_2O_3. The maximum increase occurred at 33-45 m/o Al_2O_3 and the conductivity value was found to be about two orders of magnitude higher than that of pure LiI.

Jow and Wagner in 1979 [68] studied the effect of Al_2O_3 particles dispersion in CuCl on conductivity behaviour. It was found that the maximum conductivity enhancement was occurred at lower temperatures and the conductivity value was found to increase by as much as two orders of magnitude. It was also found that the samples containing finer alumina particles show smaller agglomeration and higher conductivities.

In order to confirm the effect of doping, Shahi et al. [58] studied the conduction characteristics of pure and Al_2O_3 dispersed AgI. The addition of undried 30 m/o alumina of 0.06 μm size increased the conductivity by about 3 orders of magnitude, the room temperature value being ~ 6×10^{-4} $\Omega^{-1}cm^{-1}$ as compared to 3×10^{-7} $\Omega^{-1}cm^{-1}$ for pure AgI. Also the larger enhancement was found with finer dispersoids. Further, it was observed that wet dispersoids cause a larger enhancement than the dry ones. This is due to the fact that the dispersion probability in wet condition is more than dry state mixing. It was also proposed that the position of conductivity maximum for a particular system is independent of the dispersoid size; rather it is a sensitive function of the matrix.

Maier [77,78] presented the effect of space charge arising out of possible surface interactions between the matrix and the second phase. This effect results in drawing mobile ions out of the boundary layers and thus increasing the vacancy concentration. The theory developed describes the problem quantitatively very well with experimental results in $AgCl+Al_2O_3$ and $AgCl+SiO_2$ systems.

Fujitsu et al. in 1986 [79] studied the dispersion of Al_2O_3 in $SrCl_2$ and proposed that the enhancement of the ionic conductivity is due to the formation of high ionic conductivity interface layers between $SrCl_2$ and Al_2O_3 particles. The conductivity of the interface layer was found to be ~ 2 orders of magnitude higher than that of pure $SrCl_2$.

Up to 1982, lithium halides were among the first solid electrolytes to be investigated and the main focus was on LiI. Nakamura and Goodenough in 1982 investigated composites of very small particle size Al_2O_3 with lithium bromide monohydrate ($LiBr.H_2O$) [80] and lithium bromide dihydrate ($LiBr.2H_2O$) [81]. $LiBr.H_2O$ shows an electrical conductivity of the order of 1.4×10^{-4} $\Omega^{-1}cm^{-1}$ at 100°C with ΔE_a = 0.59 eV. In the first case, the

conductivity was found to be enhanced by nearly one order of magnitude by Al_2O_3 dispersion, but the activation energy was found to be the same. While in the latter case, very high conductivity value (σ ~ 0.1 $\Omega^{-1}cm^{-1}$) was reported at 130°C with ΔE_a = 0.13 eV. Slade and Thompson [39] reported in 1988, the temperature dependent conductivities for composites of LiBr and $LiBr.H_2O$ with a range of both nonporous and porous dispersed oxides like alumina and silica. Porous alumina can give enhancement when their elementary particle size is very much larger than that required for enhancement by nonporous aluminas. It was also established that surface chemistry plays a significant role in conductivity enhancement. In both the systems, a high surface area of silica does not lead to the same enhancements as are characteristics of aluminas of similar surface area.

Shastry and Rao in 1992 [62] studied the AgI-based composites with a general formula $AgI+M_xO_y$ (M_xO_y = ZrO_2, CeO_2, Fe_2O_3, Sm_2O_3, MoO_3 and WO_3) and observed ~ 2 orders of magnitude enhancement as compared to pure AgI. The thermal stability of AgI in these composites was explained as a consequence of decrease in the Ag^+ ion concentration in AgI due to the migration of silver ions to the interface layer.

Uvarov et al. in 1992 [82] carried out ionic conductivity measurements on $Li_nX+Al_2O_3$ (where n is the valency state of X and X = F^-, Cl^-, Br^-, CO_3^{2-}, SO_4^{2-}, PO_4^{3-}) as well as Li_2SO_4+A (A = Al_2O_3, CeO_2, La_2O_3, Y_2O_3, Yb_2O_3, ZrO_2, $BaTiO_3$) composites prepared by different routes. It was surmised that the particle size of both the dispersoids and the hosts not only influence the ionic conductivity of the host matrix but also affects its bulk properties. Also the preparation route of the composites plays an important role in deciding their properties.

Nagai and Nishino in 1992 [83] reported a novel method to fabricate a composite utilizing porous Al_2O_3 with micropores as a matrix and AgI as a dispersoid. The composites showed the conductivity several to ten times higher than the pure AgI sample prepared by the same starting materials below the β to α phase transition. To confirm the fact that heterojunctions are effective to enhance the ionic conductivity of the system

AgCl+AgI, heterojunctions in the system AgCl+AgI were formed within the thin micropores of porous Al_2O_3 by use of an electrochemical deposition technique [84]. The deposited AgCl and AgI showed enhanced conductivity compared with the reported bulk values. The composite Al_2O_3+AgCl+AgI exhibited enhanced conductivity compared with Al_2O_3+AgCl and Al_2O_3+AgI in a wide range of the composition of the mixture.

Though the composite solid electrolytes were extensively studied, the alkali halide based composites with the exception of lithium salts have not been studied much. Kumar and Shahi in 1994 [85,86] synthesized the composite electrolyte system KCl+Al_2O_3 by conventional as well as by solution casting methods. The samples prepared by solution casting method showed an order of magnitude higher conductivity than those prepared by the conventional method. Also KCl containing dispersed phase Al_2O_3 particles exhibited enhanced conductivity by ~ one order of magnitude higher over its pure phase. Further the dependence of conductivity of KCl+Al_2O_3 composites on the composition and the particle size of Al_2O_3 was reported and it was found to be consistent with the space charge theory of conduction. The conductivity maximum shifted to higher concentrations of Al_2O_3 as the particle size increased. Similar investigations were carried out on NaCl+Al_2O_3 composite system by Kumar and Shahi in 1995 [87]. These investigations indicated that the enhanced ionic conduction in these composites occurs through the migration of Na^+ ion vacancies which are also the dominant charge carriers in pure matrix phase (NaCl).

Brune and Wagner [88] reported a decrease in conductivity of $PbCl_2$ containing dispersion of Al_2O_3 particles. The results were interpreted in terms of the trapping of chloride vacancies at $PbCl_2$+Al_2O_3 interfaces. However, the PbI_2+Al_2O_3 system [89] exhibited an enhanced conductivity. In 1995, Kumar et al. [90] reported a comprehensive study of the three lead halides namely PbX_2+Al_2O_3 (X = Cl, Br, I) systems. The PbI_2+ Al_2O_3 system exhibited enhancement in conductivity, whereas $PbCl_2$+Al_2O_3 and $PbBr_2$+Al_2O_3 showed a decrease in conductivity with respect to that of their matrix values. This behaviour has been attributed to the fact that the Pb^{2+} ion vacancies are almost immobile in $PbCl_2$ and $PbBr_2$, but are as mobile as I^- ion vacancies in PbI_2.

CaF_2 is known to be a good fluoride ion conductor [91]. However, its ambient and moderate temperature conductivities are relatively low. In order to lower the operating temperature of CaF_2, different second heterophases were introduced into it. Wen et al. [92] measured the electrical conductivity of the CaF_2 samples containing 2 and 5 m/o Al_2O_3, Bi_2O_3 or CeO_2 as a second phase and the ionic conductivity was found to be enhanced by up to 3 orders of magnitude. Fujitsu et al. [93] measured the electrical conductivity of CaF_2+Al_2O_3 and BaF_2+Al_2O_3 at a temperature of 500^{o}C up to 40m/o Al_2O_3. The ionic conductivity of both the systems increased by about one to two orders of magnitude. Khandkar et al. [94] prepared two series of CaF_2 electrolytes using Al_2O_3 powders in its two different forms (γ and α) and measured the electrical conductivity in the temperature range of 25-900^{o}C for 5, 10 and 25 m/o Al_2O_3. Rog et al. [95,96] carried out the investigations on CaF_2 doped with Al_2O_3 and SiO_2 inert phases. The conductivity values were increased on dispersion by Al_2O_3 by two orders of magnitude relative to pure CaF_2 and also the conductivities were found to be dependent on the preparation method of the samples. Similarly an increase in conductivity up to four orders of magnitude was observed in CaF_2+SiO_2 composite electrolyte system.

So far, several attempts have been made to enhance the ionic conductivity in polycrystalline solids. The various methods employed, so far, include (i) the addition of aliovalent impurities [97,98], (ii) the opening of the lattice structure by substitution with wrong size ion [99,100], (iii) the optimization of the preparative parameters like the applied load for pelletization, temperature and sintering time etc. [101] and (iv) the dispersion of insulating and chemically inert second phase into the halide matrix resulting into composite solid electrolytes as already discussed.

Although the σ enhancement in case of methods (i) and (ii) is generally limited to a factor of 50 to 100. Yet it has proven to be a powerful tool to tune defect chemistry and ion conducting properties [102]. In the case of two coexisting ion conductors, a redistribution of the mobile ions is expected analogously to the electron redistribution in the case of semiconductor / semiconductor contacts. When a single alkali halide matrix is replaced by a mixed one, a number of possibilities may affect the conductivity behaviour of the matrix. This can happen due to the following reasons:

- mismatch of crystalline structures between the halides leading to distortion / defects at the halide / halide interface;
- difference in ionic (cation and / or anion) sizes resulting in lattice loosening / contraction and
- aliovalent ion substitution, if any.

In order to evaluate the effects of mixed halides on the lattice defect parameters of the silver halides, Cain et al. in 1980 [103] measured the ionic conductivity both of the entire range of mixed AgBr+AgCl single crystals and also of several iodide-doped crystals. For the AgBr+AgCl system, the intrinsic conductivity at a given temperature decreased monotonically from pure AgBr to pure AgCl. However, the results were quite different for the iodide-doped crystals. Small amounts-of iodide caused large increase in the conductivity of AgBr and AgCl, especially in the AgCl. These results were explained by the fact that the elastic strain introduced by the oversized iodide ion and this exerts an appreciable local effect on the Frenkel defect formation.

Shahi et al. in 1981 [104] observed the anomalous increase in conductivity by incorporating Br^- ions in β-AgI and this increase was attributed to purely elastic displacement (lattice distortion) caused by the wrong size of the substituent.

Hoffer et al. in 1981 [105] presented the conductivity data of several Na_2SO_4 solid solutions with cation substitutions. It was found that the conductivity is strongly correlated to the vacancy concentrations, whereas the size and charge of the substituting ions show no effect within the accuracy of the measurements. The maximum of the conductivity was found to be $1.5 \times 10^{-2}\ \Omega^{-1}\ cm^{-1}$ at 500^oC with 7% vacancies, as reported.

Shahi and Wagner introduced the concept that by the substitution of homovalent ion, either the concentration or the mobility of the mobile ions (defects) gets altered and for understanding this phenomenon the studies on AgI+AgBr and KI+KBr were conducted [106-108]. It was found that the substitution of ions having wrong size but the correct charge increases the electrical conductivity. Furthermore, the first order phase transformation temperature in AgI was lowered by the introduction of AgBr into AgI.

The conductivity enhancement was attributed to the lowering of the enthalpies of formation and migration brought about by the resulting lattice strain.

Singh in 1988 [109] carried out the electrical conductivity measurements of Ag_2SO_4 doped with a number of divalent and trivalent impurities at fixed extrinsic vacancy concentration of 7%. The results of impedance analysis showed the largest conductivity of Ag_2SO_4 when doped with $CoSO_4$ and $La_2 (SO_4)_3$ as divalent and trivalent sulphate respectively. The incorporation of a trivalent cation La^{3+} was found to offer higher conductivity compared to divalent cation Co^{2+}, under identical vacancy concentration.

Shahi and Wagner [104] studied the effect of chemical substitution of AgI by AgBr on transport properties and observed the increase in interstitial defects in the AgI lattice. This has also resulted in enhanced covalent phase conductivity with an accompanying reduction in the temperature separating the superionic and covalent phases. In the same direction, Beeken et al. in 1989 [110] prepared the polycrystalline solid solutions of $Ag_3SI_{1-x}Br_x$. It was observed that the room temperature conductivity of Ag_3SI is enhanced with the substitution of bromide for iodide while a corresponding, though smaller, effect is observed in Ag_3SBr as iodide is substituted for bromide.

Various studies [111-113] have revealed that the homovalent ion substitution enhances the ionic conductivity and the enhancement is more pronounced if the mismatch in the size between the host and dopant ions is large. Manoravi and Shahi carried out the same investigations on different mixed crystals and observed the maximum conductivity enhancement by a factor of 25 and 8 in relation to pure KBr and NaBr respectively for the $K_{0.5}Na_{0.5}Br$ solid solution at 500^oC [114]. Similarly maximum conductivity enhancement by factors of 2.8 and 2.4×10^4 with respect to pure LiBr and NaBr respectively was obtained at 400^oC for $Li_{0.7}Na_{0.3}Br$ solid solution [99]. In the light of aliovalent doping, Manoravi and Shahi [115] carried out the investigations of KBr+NaI pseudo binary system. An enhancement in σ by a factor of 500 with respect to pure KBr and a factor of 8 with respect to pure NaI was obtained at 500^oC corresponding to the composition of 70 m/o NaI.

To confirm the conductivity anomaly of AgBr+AgI system, Lauer and Maier carried out the conductivity measurements on AgCl+AgI composites [102, 116]. Distinct anomalies of the ionic conductivity were found in the two phase system AgCl+β–AgI. Two main conclusions were proposed from this study that the conducting interfacial pathways are composed of homo (AgX/AgX) and hetero (AgX/AgX′) contacts, both exhibiting enhanced conductivities as compared to bulk and secondly, both pathways are characterized by vacancy conduction in the relevant space charge layers.

Agrawal et al. [117] reported the ionic mobility, conductivity, number of charge carriers and transference number for annealed and rapidly quenched [x AgI+(1-x) AgCl] mixed systems and then compared these results with those of AgI. The mixed system in all these materials were prepared by melt quench technique for higher Ag^+ ion conductivity. The mobility was found to decrease sharply on phase transformation from the $\beta \rightarrow \alpha$ phase for maximum conducting composition (0.75 AgI+0.25 AgCl). However, a large increase in n is not only compensated for but essentially resulted a net increase in σ.

In the case of sulphate based solid electrolytes which differ from other solid electrolytes in some respect that they are thermodynamically more stable, less expensive and easy to handle. One advantage is that many monovalent and divalent cations have high mobility in their high temperature phases. Hence various researchers have carried out investigations on sulphate based solid electrolytes [118-123].

Hull et al. [124,125] carried out the ionic conductivity measurements on PbF_2 doped with various dopants. Doping with relatively low concentrations of aliovalent cations significantly enhance the ionic conductivity at room temperature. To further investigate the effect of aliovalent substitution, Hull et al. investigated the ionic conductivity measurements of the Ag^+ rich phases in $(AgI)_x+(PbI_2)_{1-x}$; where $2/3 \leq x \leq 4/5$ [126].

1.6 Theoretical Models

Several phenomenological theories have been proposed to understand the ion transport mechanism in composite solid electrolyte systems. No single unified model exists, as yet, which can explain uniquely various experimental results on different composite

electrolyte systems. However, the central feature of the majority of the models, suggested to explain the conductivity enhancement in two phase composite electrolyte systems is the existence of a space charge region (double-layer) at the interface between the host and the dispersoid. Various experimental studies have been directed towards this proposition, namely dependence of conductivity on the dispersoid surface area [59,66,68] and apparent effect of surface hydration [60,68,127] etc. In addition, bulk interactions have also been suggested as a cause of conductivity enhancements in some composite systems [61,128]. Most of these models focus on calculation of the compositional dependence of conductivity. They differ only in the methods of calculation and in the assumptions concerning the distribution of the dispersoid particles in the composite system. Some important models proposed for composite electrolyte systems are discussed below:

1.6.1 Abandoned models

Some of the earlier models, to explain the conductivity behaviour in two-phase mixtures were put forward by Maxwell [129], Raleigh [130], Lichtenecker [131], Landauer [132] and Wagner [133] etc.

Maxwell [129] and Raleigh [130] calculated the conductivity of two phase mixtures in terms of the bulk conductivity of the individual phases. Raleigh assumed that the material of the second phase in the form of spheres or cylinders is embedded in material of the first phase, forming a rectangular array. In this model he assumed the current flow in the mixture is always through the first phase material only. Hence the conductivity of the first phase material always dominates even if the volumes of both phases are equal. This model is applicable only when the volume of the second phase is much less than that of the first phase. However, this model is ideal since such physical arrangements never occur in real systems.

Lichtenecker [131] considered both the phases as nonpassive metallic mixtures and expressed the resistivity, ρ_m, as

$$\rho_m = \rho_1^{x_1} \rho_2^{x_2} \tag{1.23}$$

where ρ_1 and ρ_2 are the resistivities of the first and second phase materials, respectively; x_1 and x_2 their volume fractions. This model is valid only when ρ_1 and ρ_2 are of the same order of magnitude.

Landauer [132] proposed effective medium theory by considering the arrangement of materials in alternate layers. The flow of current is parallel to these layers; hence the conductivity σ_m of the mixture can be expressed by

$$\sigma_m = x_1 \sigma_1 + x_2 \sigma_2 \tag{1.24}$$

where σ_1 and σ_2 are the conductivities of first and second phase materials. This expression is adequate only for passive constituent phases; hence the current can flow straight through the region of low resistance. However, in such a model, the current cannot avoid regions of high resistance, as it will do if the phases are randomly mixed.

Wagner [133] attempted to explain conduction behaviour of bi-phasic metal-semiconductor mixtures on the basis of the existence of an interfacial space charge region at the boundary between the two phases. This space charge region originates from the charge density (or potential) gradient due to the non-passive nature of the different constituent phases at the interface. The total conductivity, σ, of such a bi-phasic system can be expressed as

$$\sigma = 0.19\left(g \in k_B T / q^2\right)\left(V_V / r_A^2\right) q \mu \tag{1.25}$$

where g is a structural factor; $\in$ the dielectric constant of the medium at temperature, T; k_B the Boltzmann constant; V_V the volume fraction of the dispersoid in the mixture; q the fundamental charge; μ the mobility of the charge carrier; and r_A the radius of the dispersoid particle.

Crosbie [134] modified the above expression to explain electrical conduction in a TiO_2+SiO_2 bi-phasic mixture and wrote the equation for the total conductivity of the dispersed mixture as

$$\sigma = \sigma_b \left[1 + 0.83\, g\, |Z| V_V \left(\lambda / r_A\right)^2\right] \tag{1.26}$$

where σ_b is the conductivity of the host; Z the effective charge on the defects created; and λ the thickness of the double-layer called the Debye length, which is given by

$$\lambda = \left[8\pi q^2\, n(\infty) / \varepsilon\, k_B T\right]^{-1/2} \tag{1.27}$$

where $n(\infty)$ is the defect concentration in the bulk. The conductivity of lithium, silver and copper halide systems can be considerably influenced by doping (homovalent and aliovalent). If it is assumed that Al_2O_3 or SiO_2 were soluble in the halides, a few mole percent would be sufficient to saturate the respective lattices with defects. Hence, a classical doping theory can not be used to explain the conductivity behaviour in the composite electrolyte system. Jow and Wagner [68] attempted to explain the conductivity enhancement in the CuCl+Al_2O_3 composite system. As assumed in their model, dissolution of the dispersoid into the bulk lattice creates copper vacancies. Alternative explanation of the conductivity enhancement originates from severe lattice distortion of the phase boundaries. These possibilities were ruled out by XRD results.

The above models failed to explain many experimental outcomes reported for composite electrolyte systems; hence, they were eventually discarded due to the reason that they were originally proposed for electron conducting bi-phasic systems. However, the possible existence of a space charge region, which was ascribed as the major cause for conductivity enhancement proposed by Wagner [133], became the basis for the forthcoming models.

1.6.2 Space charge models

1.6.2.1 Jow and Wagner's model

Kliewer [135] proposed the continuum model for the space charge region near surfaces of Frenkel disordered compounds (e.g. CuCl) to describe the space charge regions surrounding spherical inclusions in matrix material of Frenkel type. In order to explain the conductivity enhancement in a $CuCl+Al_2O_3$ composite electrolyte system, Jow and Wagner [68] extended Kliewer's theory. They assumed that a space charge region is created at the host-dispersoid interface boundary when a dispersoid phase (*A*) is introduced into the electrolyte host matrix (MX). Figure 1.5 (a) shows a dispersoid particle embedded in a host matrix. A space charge layer of thickness λ has been created around the dispersoid particle. Figure 1.5 (b) and (c) show the idealized spherical particle and cross sectional view for analytical calculation. They proposed that the dispersoid has a charge, though the sign is not known, at or near the surface, which is compensated by the formation of oppositely charged defects in the diffused space charge layer. As a result, an excess defect concentration in this region is formed. Figure 1.5 (d) and (e) show the defect concentration profile and excess charge density in the space charge region. Hence, it is assumed that $F_I < F_V$, where F_I and F_V are the free energies of formation of interstitial and vacancy defects, respectively.

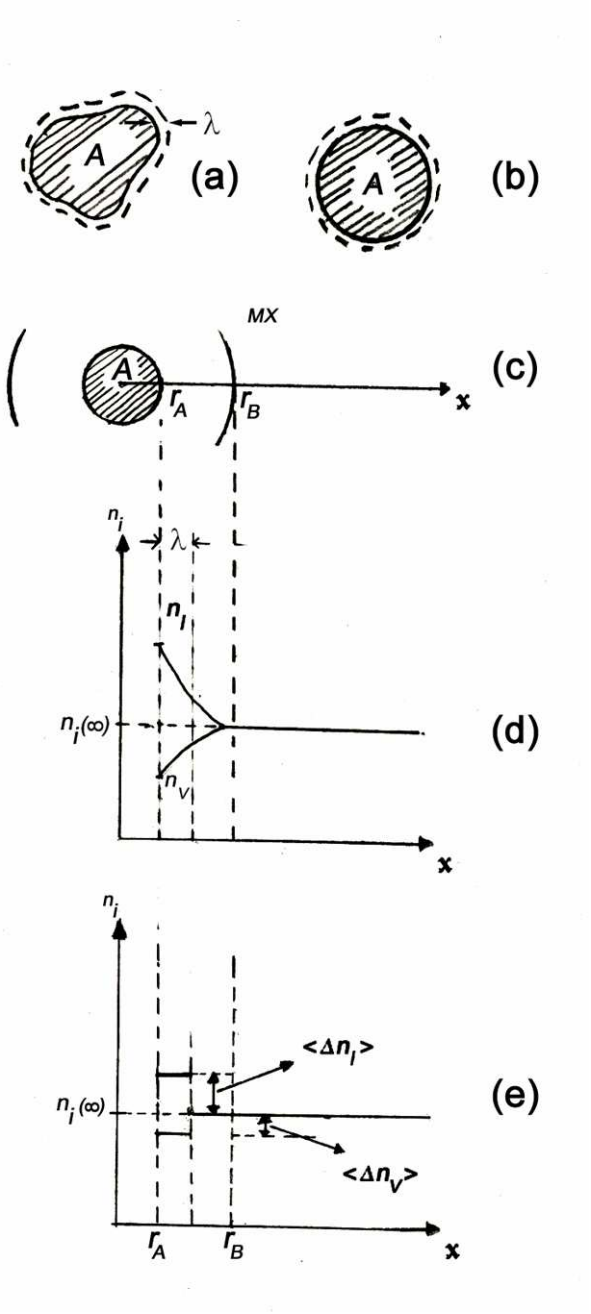

Fig. 1.5 (a) Schematic diagram of a dispersoid particle (*A*) surrounded by a space charge layer of thickness λ embedded in the host matrix (*MX*); (b) an idealized spherical approximation of the dispersoid; (c) a cross-sectional view of *A* of radius r_A, for analytical calculation; (d) defect concentration profile in the space charge region where $F_I << F_V$; (e) average excess charge density, $<\Delta n_i>$, in the space charge region (reference [68]).

Jow and Wagner attributed the space charge effect (σ_{SC}) as the main reason for conductivity enhancement, and hence the expression for total conductivity σ of the composite electrolyte system can be given by

$$\sigma = \sigma_b + \sigma_{SC} \tag{1.28}$$

$$= \sum_i n_i(\infty) q \mu_i + 3 \sum_i q \mu_i \langle \Delta n_i \rangle (\lambda / r_A) [V_V / (1 - V_V)] \tag{1.29}$$

where the conductivity contribution from the space charge region is

$$\sigma_{SC} = \frac{\sum_i q \mu_i \left\{ \int_{r_1}^{r_2} \int_0^{\pi/2} \int_0^{2\pi} [n_i(r) - n_i(\infty)] \, r^2 dr \sin\theta \, d\theta \, d\phi \right\}}{\left\{ \int_{r_1}^{r_2} \int_0^{\pi/2} \int_0^{2\pi} r^2 dr \sin\theta \, d\theta \, d\phi \right\}} \tag{1.30}$$

$$= 3 \sum q \mu_i \langle \Delta n_i \rangle (\lambda / r_A) [V_V / (1 - V_V)] \tag{1.31}$$

The summation runs over all the different defect species. Other notations have their usual meaning. $\langle \Delta n_i \rangle$ is the average excess charge density representing the excess defect concentration near the surface, for which $\lambda << r_A$. Here the conductivity contribution due to the dispersoid is neglected. Moreover, μ and $\langle \Delta n \rangle$ increase with temperature, while λ decreases with temperature. Hence their combined effect is not easy to estimate in this treatment.

This model has qualitatively explained the dependence of conductivity enhancement on (i) temperature, (ii) particle size and (iii) volume fraction of the dispersoid, but with not much of success. Jow and Wagner failed to predict maximum in σ versus V_V experimental plots since the approximation used in their equation for σ_{SC} does not justify its application to composite systems containing high volume fractions of the dispersoid phase. The term $[V_V / (1 - V_V)]$ is an indefinitely increasing term. It also failed to explain the mechanism leading to enrichment of the defect concentration in the space charge region.

1.6.2.2 Pack's model

In order to explain the conductivity enhancement in another composite system HgI_2+Al_2O_3, Pack [57] developed a model and expressed the total conductivity by the following equation

$$\sigma = \sigma_b \left(1 - V_V\right) + G\, S \left(1 - V_V\right)^2 + \sigma_A V_V \tag{1.32}$$

where σ_b and σ_A are the conductivities of the host matrix and dispersoid material respectively, V_V the volume fraction of the dispersoid, S the surface area created by the dispersoid per unit volume of the mixture. $G\ \left(=\sigma_{SC} / \left[S\left(1 - V_V\right)\right]\right)$ is a factor that accounts for the number of excess charges per unit volume of the mixture.

This model not only describes the conductivity enhancement but also accounts for the decrease in conductivity value due to the blocking effect of the dispersoid particles.

1.6.3 Adsorption-desorption model

The most extensive quantitative model has been proposed by Maier [78,102,136-139] who gives a thorough treatment of the redistribution of mobile species at various types of interfaces and its consequences on ionic conduction parallel to the interfaces. He employed the principle of a parallel switching resistor and modified the space charge model by considering the dispersoid phase not as an inactive insulator but as a driving force for the evolution of a space charge region which in turn causes an enrichment in defect concentration at the interfacial boundary. The space charge region was treated as a separate phase which acts as a parallel resistor. The total conductivity of the two phase dispersed solid electrolyte can be expressed as

$$\sigma = \beta_A V_A \sigma_A + \beta_b V_b \sigma_b + \beta_{SC} V_{SC} \sigma_{SC} \tag{1.33}$$

where A, b and SC denote the dispersoid, the bulk (MX) and space charge component respectively. V and σ are the volume fraction and conductivity of the respective phases, and β the parameter describing the deviation from the ideal parallel switching.

Maier discussed a possible mechanism for enrichment of defect concentration at the interface boundary on the basis of defect chemistry of the dispersed solid electrolytes. The second phase dispersoid (A) affects defect equilibrium at the interface boundary. For a host matrix (MX) with Frenkel defects, the metal ions (M^+) will be attracted from or repelled into the MX phase depending on the chemical (charged) species present on the surface of the dispersoid phase (A). The attraction or repulsion processes are discrete and only one of them occurs in a given system under specific conditions. Figure 1.6 (a) and (b) show these phenomena for a Frenkel type $MX+A$ composite system. In the case of attractive interaction, the surface-active dispersoid sucked out the cations from its regular sites and consequently enhanced the vacancy concentration (adsorption process), whereas, in case of repulsive interaction, the dispersoid drives M^+ ions into interstitial sites and enhances the interstitial concentration (desorption process). Therefore an extrinsic conductivity enhancement is assumed in this model as shown in figure 1.6 (c).

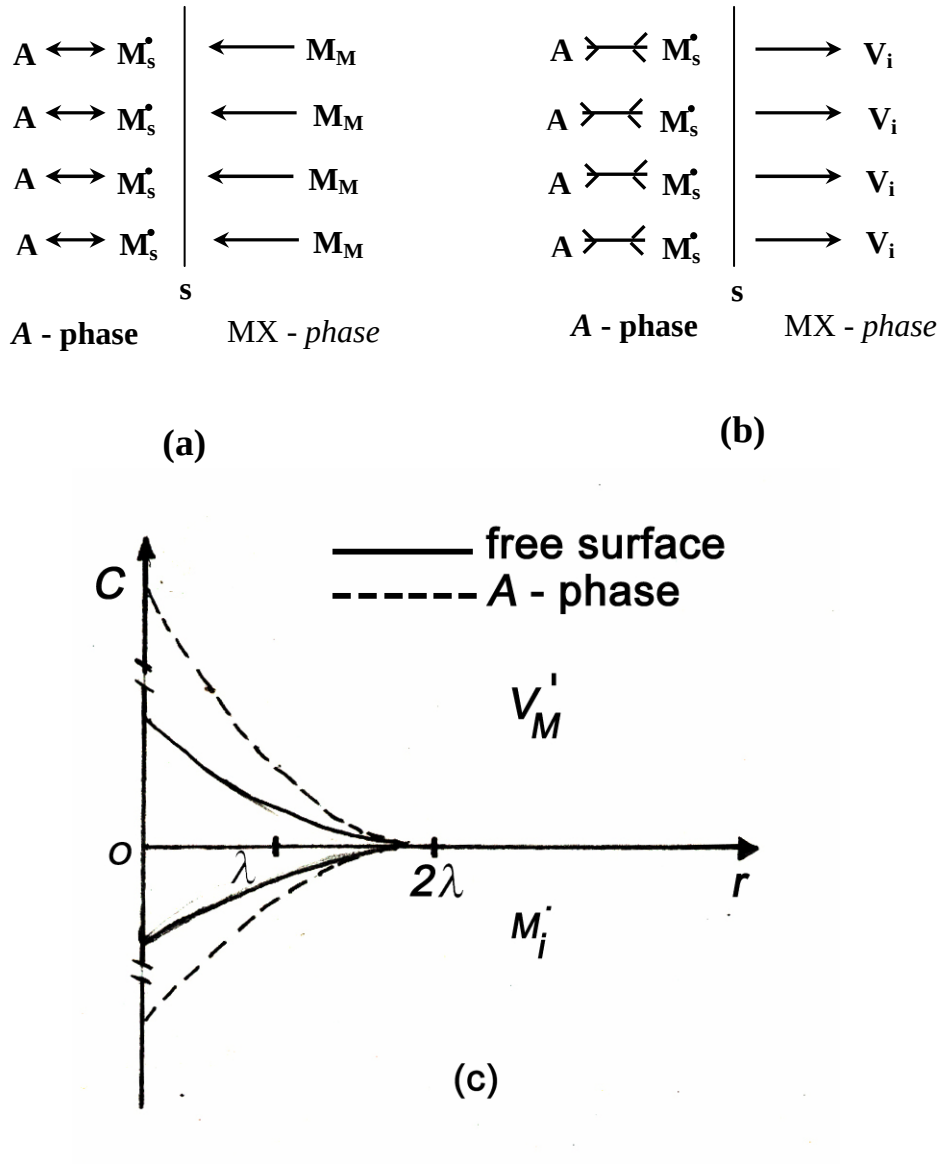

Fig. 1.6 (a) Attraction, (b) repulsion mechanism by the surface of dispersoid *A* and (c) Concentration (C) profiles for the cation vacancies, $V_M^{'}$ and the interstitial cations, M_i (reference [102]).

Using Kroger-Vink notation, these mechanisms can be written as,

For a free surface

$$M_M + V_S \rightleftharpoons M_S^{\bullet} + V_M^{'} \qquad \text{Step 1}$$

$$M_S^{\bullet} + V_i \rightleftharpoons M_i^{\bullet} + V_S \qquad \text{Step 2}$$

and in the presence of dispersoid phase A

$$M_M + V_S \rightleftharpoons M_S^{\bullet} + V_M^{'} \qquad \text{Step 3}$$

$$M_S^{\bullet} + V_A \rightleftharpoons M_A^{\bullet} + V_S \qquad \text{Step 4}$$

$$M_A^{\bullet} + V_i \rightleftharpoons M_i^{\bullet} + V_A \qquad \text{Step 5}$$

where M denotes the cation or its regular site; V, a vacancy; S, surface; I, an interstitial site and "$\bullet$" or "$'$" represent the charge of the defect (positive or negative) relative to the perfect lattice. Here steps 1 and 2 indicate the adsorption process, whereas steps 3 to 5 indicate the desorption process. In the case of a Schottky defect ionic solid *MX+A* composite system, both cation and anion compete for attractive and repulsive interaction of the dispersoid. Consequently these two processes will be non-discrete in nature. Hence it becomes too difficult to predict whether the dispersion of *A* into *MX* will enhance conductivity. The mechanism for the formation of cation and anion vacancy pairs in a Schottky ionic solid *MX+A* composite system can be visualized as

$$M_M + V_S \rightleftharpoons V_M^{'} + M_S^{\bullet}$$

$$X_X + V_S \rightleftharpoons X_S^{'} + V_X^{\bullet}$$

$$\overline{M_M + X_X + 2V_S \rightleftharpoons V_M^{'} + V_X^{\bullet} + M_S^{\bullet} + X_S^{'}}$$

Employing the principle of parallel switching, Maier calculated the conductivity contribution from the space charge region by integrating equation (1.30) in one dimensional Cartesian coordinates using an exponential variation of the defect concentration and wrote the equation for conductivity enhancement as

$$\sigma_{SC} = q\,\mu_V \left(c_{VS}\, c_{Vb}\right)^{1/2} \tag{1.34}$$

where μ_V is the mobility of vacancies; c_{VS} and c_{Vb} are the concentration at the surface and bulk, respectively. Here dispersoid particles are assumed to be spherical and surrounded by a spherical space charge region of thickness 2λ. The volume fraction of

the space charge region can be obtained by subtracting the volume of the inner sphere from that of the outer sphere and is given by

$$V_{sc} = 3(2\lambda / r_A)V_A \tag{1.35}$$

Neglecting the conductivity of the insulating dispersoid phase, Maier expressed the total conductivity as

$$\begin{aligned}\sigma &= (1 - V_A)\sigma_b + \beta_{SC}\, V_{SC}\, \sigma_{SC} \\ &= (1 - V_A)\sigma_b + 3q\,\beta_{SC}(2\lambda / r_A)V_A\, \mu_V\, (c_{VS}\, c_{Vb})^{1/2}\end{aligned} \tag{1.36}$$

By adjusting the ideal parallel switching parameter, β_{SC}, in the range 0.2-0.7 depending upon distribution topology, it has been seen that the above equation (1.36) could explain the following experimental results: (i) larger conductivity enhancement at low temperatures, (ii) particle size dependence, (iii) effect of wet dispersoid etc., for various solid electrolyte systems fairly well. The attractive feature of Maier's model is that it highlights the mechanism responsible for enrichment of surface defects in the space charge region. Although Maier's model explains many characteristic features of composite electrolyte systems well, it failed on several points such as: occurrence of maximum in σ versus V_A plots; the assumption of an oversimplified distribution topology being characterized by a β-factor; the assumption of spatially constant values for mobility; the dielectric constant and the molar volume; neglecting the structural changes, polarization effect, elastic effects etc.

1.6.4 Percolation model

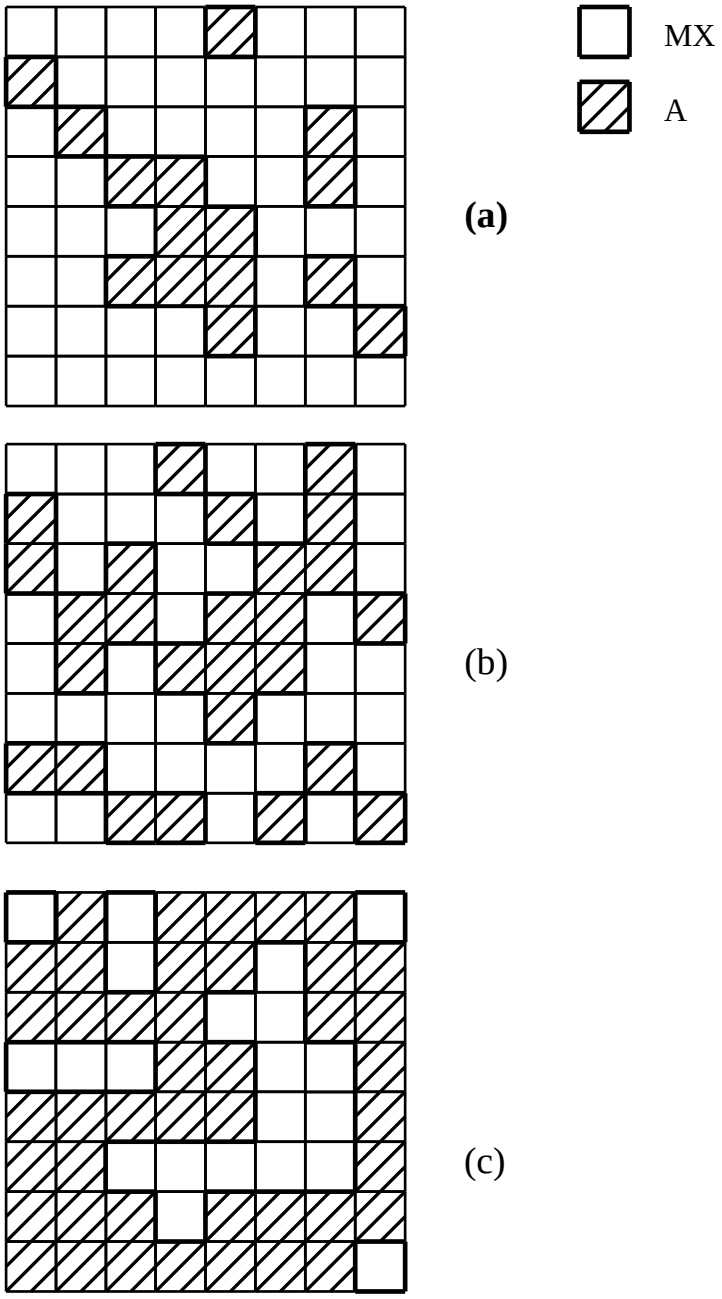

Fig. 1.7 Two phase mixtures on a square lattice for different concentration, p, of dispersoid *A* [142]. The highly conducting layers are marked by bold lines (a) $p < p_c^{'}$, (b) $p = p_c^{'}$, onset of interface percolation and (c) p > $p_c^{''}$ for disruption of conducting paths.

The models of Jow, Wagner and Maier could not account for the typical conductivity variation with composition in most of the composite electrolyte systems. The variation is marked by initial increase in conductivity with increasing concentration of the dispersoid phase followed by rapid decrease. Bunde, Dieterich and coworkers [140-142] attempted to explain this behaviour through their percolation model. They assumed a two-dimensional percolation network as shown in figure 1.7 in which insulating dispersoid and conducting host grains of identical size and shape are randomly distributed. An interfacial high conducting path is formed, as shown by the dark boundary line in the figure. Monte Carlo simulations for conduction in such a three-dimensional array identified two percolation threshold concentrations, $p_c^{'}$ and $p_c^{''}$.

$p_c^{'}$ ($0 < p_c^{'} < 0.5$) corresponds to the onset of interface percolation and $p_c^{''}$ ($0.5 < p_c^{''} < 1$) to conductor insulator transition, where conductivity may approach to zero. Maximum enhancement in conductivity, σ, with concentration of dispersoid, p, is found to be between $p_c^{'}$ and $p_c^{''}$. This model accounts for effects for the physical nature (i.e. size and shape) of the dispersoid and bulk conductivity of the host-matrix in conductivity enhancement.

1.7 Scope of the present work

From the foregoing discussions, it can be seen that the development of composite electrolytes took place in several systems. Silver-based halides either in single matrix or mixed matrix form, are the well studied materials, so far. The primary reason for developing silver-based materials is that they exhibit higher ionic conductivity even at room temperature. Likewise, other metallic halides (such as copper halides, etc.) were also investigated for battery applications. However, these metallic halides suffer from stability criteria for operation over a wide temperature range.

Though alkali halides are very important members for solid electrolytes technology, the conductivity that could be obtained with these halides is limited to a value relatively low compared to that of metallic halides. However, the thermal stability of alkali halides over a wide temperature range is a merit in the electrolyte applications. So far, most of the

investigations in the family of alkali halides are confined to the development of lithium and sodium halide based electrolytes. To the best of author's knowledge, not much of works have been reported, so far, on KCl-based electrolytes from the point of view of their application and understanding of the conductivity enhancement mechanisms. Therefore, there has been a need to develop composite solid electrolytes with suitable modifications either at the halide base and / or nature of dispersoid. The present thesis deals with "Ion transport properties of some mixed halide based oxide dispersed composite electrolyte systems". In order to fulfill the objective, suitable halides were chosen to demonstrate the characteristics. The investigations started with KCl-based matrix dispersed with Zirconia (ZrO_2) powder.

The reason for choosing the KCl-based matrix is primarily due to the fact that it does not undergo phase transformation before melting, thereby accommodating the effect of wide variation of temperature on transport characteristics viz. conductivity (σ) and ionic mobility (μ). ZrO_2 was taken as a dispersoid in the majority of the present studies. This is due to the fact that in general, alumina is used as dispersoid for which systems were well studied and reported by other researchers. However, to the best of author's knowledge, no systematic studies on ZrO_2-dispersed composite electrolytes are reported in the literature. In order to demonstrate the superiority of mixed matrix base for the oxide dispersion as compared to the case of single halide matrix and the resulting oxide dispersion characteristics-both in mixed and single matrices, a number of electrolytes in the following systems (i) $(KCl)_{1-x}+(ZrO_2)_x$; (ii) $[(KCl)_{1-x}+(NaCl)_x]_{1-y}+(ZrO_2)_y$; (iii) $[(KCl)_{1-x}+(CuCl)_x]_{1-y}+(SnO_2)_y$; (iv) $[(BaCl_2)_{1-x}+(KCl)_x]_{1-y}+(ZrO_2)_y$ and (v) $[(KCl)_{1-x}+(KI)_x]_{1-y}+(ZrO_2)_y$, were prepared, characterized and studied for their transport characteristics. The detailed studies are presented in the subsequent chapters.

Chapter II

Experimental procedures

Overview

This chapter describes the materials and the methods used for the preparation of composite electrolyte systems. The samples were prepared in the form of cylindrical pellets following powder compaction and solid state sintering process. The samples were characterized by Scanning electron microscopy (SEM), X-ray diffraction (XRD) and Thermal analyses (TG, DTA). The samples were electroded with silver paste for conductivity measurements which were carried out using Impedance spectroscopy technique. The ionic mobility (μ) and the ionic transference number (t_i) were determined for the composite electrolyte samples using Transient ionic current (TIC) technique and Hebb–Wagner's polarization method, respectively.

2.1 Raw materials

In the present study, the raw materials used were KCl (purity>99%, E Merck), Zirconia powder (particle size ~ 1μm, purity>99%, C S Zircon), $BaCl_2$ (purity>99%, Qualigens), NaCl (purity>99%, Qualigens), CuCl (purity>99%, sd fine) and KI (purity>99%, sd fine). All these materials were used without any further purification.

2.2 Sample preparation

This section is divided into the following subsections:

2.2.1 Powder preparation

Powders of following five different systems were prepared:

Single matrix based

(i) $(KCl)_{1-x}+(ZrO_2)_x$

Mixed matrix based

(ii) $[(KCl)_{1-x}+(NaCl)_x]_{1-y}+ (ZrO_2)_y$

(iii) $[(KCl)_{1-x}+(CuCl)_x]_{1-y}+(SnO_2)_y$

(iv) $[(BaCl_2)_{1-x}+(KCl)_x]_{1-y}+(ZrO_2)_y$

(v) $[(KCl)_{1-x} + (KI)_x]_{1-y} + (ZrO_2)_y$

The powders in the required compositions were weighed. The mixed halide matrices were prepared by melt quench technique in which a homogeneous mixture of the mixed halide powders was melted in suitable temperature ranges and then the melt was air quenched to room temperature. The chunks so obtained were ground using a mortar and pestle. The oxide dispersion in the matrix (both in single and mixed) was carried out in a wet medium (acetone). The wet mixing process is effective in two ways: (i) uniform mixing and (ii) avoidance of agglomeration of oxide powders. The composite solid electrolytes of interest were prepared with the highest conducting composition of the mixed matrix powder.

2.2.2 Pellet fabrication

The powders of mixed matrix and oxide dispersed one were compacted in a hydraulic press at an applied load of about 200 kN (or a pressure level of 240 Kg/cm^2) to form cylindrical pellets of 20 mm diameter and 3 mm thickness.

2.2.3 Sintering the samples

The green pellets were then sintered in a muffle furnace at suitable temperature ranges for the soaking period of about 5 hours in air with a heating and cooling rate of about 10^oC / min. The sintering process is very critical for the microstructural development in the samples which in turn has a strong bearing with the transport characteristics of the samples.

2.3 Characterization of the materials

2.3.1 Microstructural investigation

The size and morphology of the powders were determined by SEM (JEOL, 840A and LEO, 435 VP). The primary objective of the microstructural study was to visualize the morphological features of grain formation and the dispersoid-matrix interfaces confirming the possible development of percolation paths for the conductivity enhancement. Grain sizes were also measured directly from the micrographs of the samples.

2.3.2 Thermal analyses (TG/DTG, DTA)

The samples were subjected to thermal analyses using TG / DTA to determine the phase transformations and to assess the possibility of compound formation, if any, due to sintering process. The analyses were carried out in the temperature range of 20ºC to 1000ºC at a heating rate of 5ºC / min, using the analyzer (Perkin-Elmer, Model: Pyris-Diamond) taking alumina as reference sample.

2.3.3 Phase identification

The new phases form, if any, due to sintering the samples were analyzed and identified by X-ray powder diffraction recorded at room temperature using X-ray diffractometers: (i) Rigaku, Model D max IIIc and (ii) Phillips, Model PW 1140/09, employing CuK_{α} radiation at moderate scanning speed in both the meters. The diffraction data of the samples were analyzed with reference to standard base of powder diffraction files provided by the International Centre for Diffraction Data – ICDD (formerly known as JCPDS).

2.4 Transport characteristics

The mechanism of high ionic conduction in solid electrolytes is governed by a number of ionic transport parameters viz. (i) ionic conductivity (σ), (ii) mobility (μ), (iii) mobile ion concentration (n), (iv) ionic transference number (t_i) and (v) activation energies involved in various processes. In order to characterize the ion transport behaviour in solid electrolytes, it is imperative to have quantitative information of these basic transport parameters. A wide variety of experimental techniques is employed to determine these parameters [143]. Some of the widely used techniques are:

- Impedance spectroscopy (IS) for measurement of electrical conductivity (σ) [144];
- Transient ionic current (TIC) technique for measurement of charge mobility (μ) [145,146];
- Wagner's polarization method for measurement of ionic transference number (t_i) [147].

From the measured values of μ and σ, the n is determined from the equation $\sigma(T) = n(T) eZ\, \mu(T)$

IS, TIC and Wagner's methods can be explained as below:

2.4.1 Impedance spectroscopy (IS)

2.4.1.1 Introduction

Several direct current (dc) methods are available for the determination of the electrical conductivity [148]. Each method depends on the type of conductor (i.e. ionic, electronic or mixed). The simple two-point dc method is of limited use since there are usually large voltage drops across the interfaces between the non-metallic conductor and electrodes. A common method to eliminate this effect is to apply the four-probe technique [149] as shown in figure 2.1.

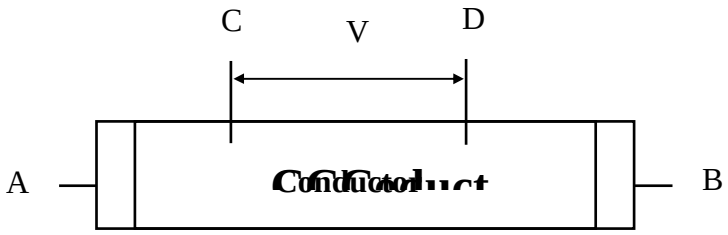

Fig. 2.1 Configuration of four probe technique.

In this configuration, the current (I) is passed between A and B electrodes and the resulting voltage drop $V = I\,R$ (R being the resistance offered between the C and D) is measured between the probes C and D which are separated by a distance L.

Therefore the conductivity is

$$\sigma = \frac{jL}{V}$$

This technique is commonly used for semiconductors measurements. But this method has a limitation in measuring the ionic conductivity, as the electrodes used in the measurements should be of reversible in nature. Another prerequisite is that the internal resistance of the voltmeter must be much larger than the resistance between the probes C and D. This method demands rather complicated sample preparation. This measurement provides the total conductivity values, with no information about any morphological

related features which are often present in polycrystalline materials having grains and grain boundaries.

The alternating current (ac) method has been developed since 1970s and has been boosted by the rapid developments of microelectronics and computers. Impedance spectroscopy (IS) is a powerful ac measurement technique [150,151], which has been applied quite successfully to determine a number of important characteristics such as bulk resistivity in the case of single crystals and contribution of grain and grain boundary resistivities in poly crystalline solid electrolytes. This technique involves the measurements of impedance data (resistance vs. reactance) of the samples as a function of frequency and plotting the data in a complex plane.

2.4.1.2 Theory

If a monochromatic signal having angular frequency of ω, given by

$$V(t) = V_m \, Sin \, (\omega t) \tag{2.1}$$

is applied to a cell, a steady current expressed as

$$I(t) = I_m \, Sin \, (\omega t + \theta) \tag{2.2}$$

can be measured, where θ is the phase difference between current and voltage. In the case of a purely resistive component, θ will be zero.

As the Impedance

$$Z(\omega) = Z' + Z'' \tag{2.3}$$

is a vector quantity, it may be plotted on plane with either rectangular or planar co-ordinates. A representation of such a plot is shown in figure 2.2.

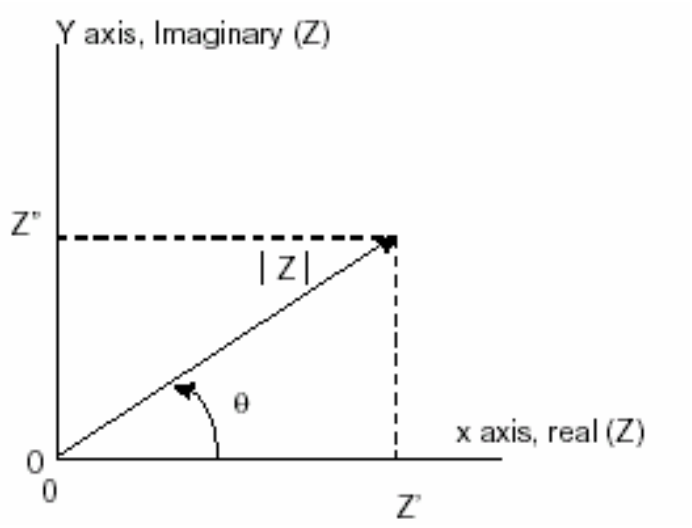

Fig. 2.2 Impedance Z plotted as rectangular and polar Co-ordinates.

In the above figure, the rectangular co-ordinates are;

$$\mathrm{Re}(Z) = Z' = |Z| Cos(\theta) \tag{2.4}$$

and

$$\mathrm{Im}(Z) = Z'' = |Z| Sin(\theta) \tag{2.5}$$

with the associated phase angle of

$$\theta = \tan^{-1}\left(Z'' / Z'\right) \tag{2.6}$$

giving a modulus of

$$|Z| = \left[(Z')^2 + (Z'')^2\right]^{1/2} \tag{2.7}$$

From this an Argand diagram can be drawn in polar form allowing, Z to be expressed as

$$Z(\omega) = |Z| \exp(j\theta) \tag{2.8}$$

The complex ionic situations are modelled with a more simple electronic (circuit) representation and the analogies are often drawn in the form of equivalent circuits where an equivalent circuit is made to represent the IS spectrum produced.

The equivalent circuit gives '*RC*' element which is characterized by a relaxation time, $\tau\ (=RC)$. Alternatively RC can be expressed in terms of $\omega_{\max}$ (= the frequency at which the loss is maximum) as

$$\omega_{\max} RC = 1 \tag{2.9}$$

The value of R directly yields the dc resistance. The cell (electrode/ion conductor/electrode) function, which involves essentially charge carriers, is described by the suitable combinations of R and C. The equivalent circuit consisting of R and C in series and the corresponding impedance plot is shown in figure 2.3 (a) and (b).

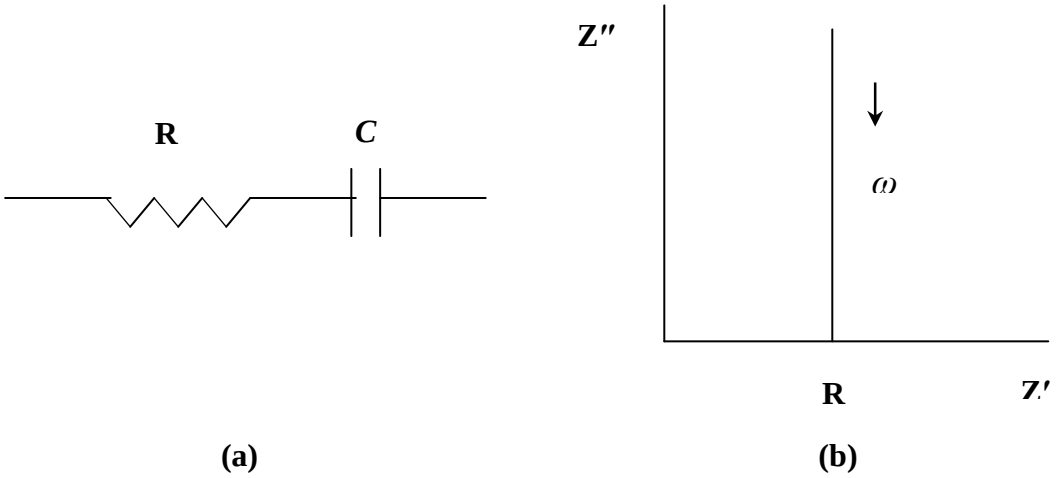

Fig. 2.3 (a) Series combination of R and C, (b) Impedance plot for the equivalent circuit.

The impedance of the circuit is given by

$$Z = R + \frac{1}{i\omega C} = R - \frac{i}{\omega C} \tag{2.10}$$

where $Z' = R,\ \ Z'' = \frac{1}{\omega C}$

When imaginary part is plotted against the real part, the above combination gives a vertical spike in the Z^* complex plane as shown in figure 2.3 (b) because Z' is of fixed value R and Z'' decreases with the increasing ω.

In the case of parallel combination of R and C, as shown in figure 2.4 (a),

$$Z = \left(\frac{1}{R} + i\omega C\right)^{-1} \tag{2.11}$$

$$= \frac{R}{1+(\omega RC)^2} - R\frac{i\omega RC}{1+(\omega RC)^2}$$

The data when plotted lies in a semicircle in the complex Z^* plane, as shown in figure 2.4 (b).

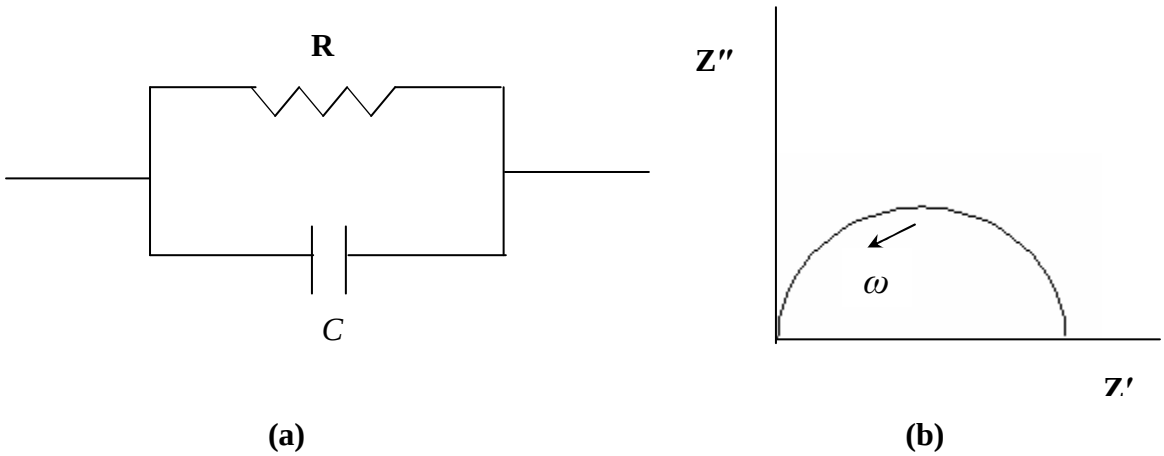

Fig. 2.4 (a) Parallel combination of R and C, (b) Impedance plot.

A typical IS spectrum for a polycrystalline solid electrolyte consists of a series of semi-circles. Each semi-circle represents a separate process. A simple equivalent circuit model that could be used to represent electrode-electrolyte system consists of three parallel RC circuits representing grain, grain boundaries and electrodes, connected in series. The values of the components are obtained from the intercepts of respective arcs on the Z' axis and the frequencies at which the arcs show a maximum height. Thus the values of dc resistivities can be obtained from ac measurements.

In the present study, the measurements were performed using LCR meter (HP, Model 4274A) in the frequency range of 100 Hz to 100 kHz. For the measurements, the samples were electroded with silver paste.

2.4.2 Transient ionic current technique

Ionic mobilities (μ) of the samples at room temperature and at higher temperatures were measured using transient ionic current (TIC) technique, originally suggested by Watanabe et al. [145] and Chandra et al. [146]. In the TIC method, the sample is sandwiched between two blocking electrodes as shown in figure 2.5 and polarized by applying a constant dc voltage for sufficiently long time to ensure that a state of complete polarization has been attained.

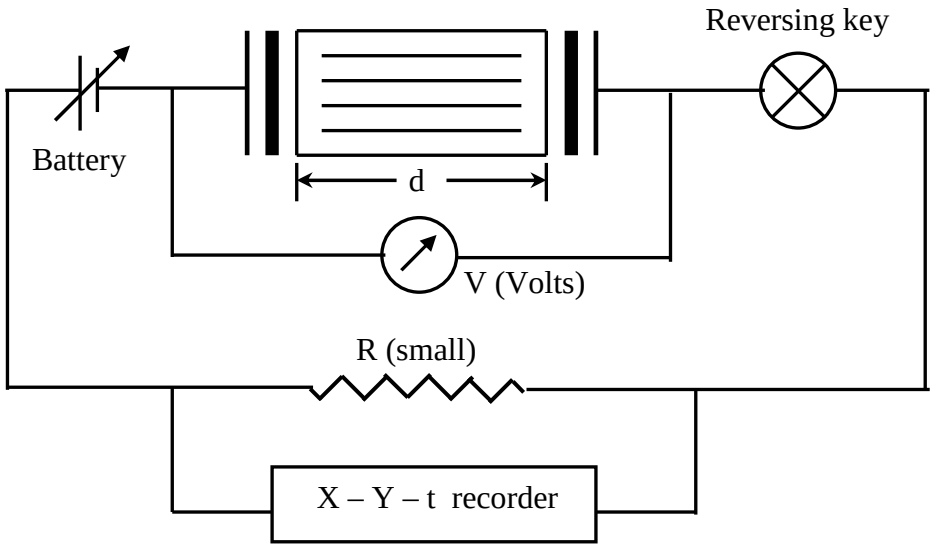

Fig. 2.5 Schematic circuit diagram for transient ionic current measurements.

Thus the mobile ions remain blocked at the respective electrolyte-electrode interfaces. The polarity of the applied potential is then reversed and the current is monitored with respect to time using X-Y-t recorder. The instant the polarity is reversed, the polarized ion clouds start travelling in the bulk towards the electrode of opposite polarity. This results in a flow of current through an external circuit. The moment the polarizing / blocking ion cloud reaches the other end of the sample, a peak occurs in the current vs. time plot. If more than one ionic species were mobile in the system, a number of peaks appear in TIC plot when suitable blocking electrodes are used. Each individual peak corresponds to one type of mobile ionic species. The position of the peak on the time axis directly measures the time of flight t of the mobile ion species to cross the thickness d of the sample. Hence the ionic mobility μ can be determined using the following expression:

$\mu = d^2 / (tV)$, where V is the applied constant dc potential.

2.4.3 Transference ionic number determination

Transference ionic number (t_i) of mobile species is an important factor in establishing the suitability of a conductor as an electrolyte. High ionic conductivity and an ionic transference number close to unity over wide cell operating conditions are some of the criteria which must be fulfilled by a material to be a good electrolyte. Many materials are mixed conductors and even a small electronic conductivity can limit the use of a material as an electrolyte. The t_i can be expressed as

$$t_i = \sigma_i / (\sigma_i + \sigma_e)$$

and the associated equations are given below :

$$\sigma_T = (\sigma_i + \sigma_e)$$

and

$$t_e = \sigma_e / \sigma_T$$

where t_e is referred as the electronic transference number. For a purely ionic conductor, t_i =1 and for electronic conductors, t_e = 1. For mixed conductors, the t_i may have any values from 0 to 1.

Several different techniques are available for separating the ionic and electronic contributions to the total conductivity in solid electrolytes. The most common techniques are described below [152,153]:

- Electrolysis – Tubandt's method
- Electrochemical potential measurements
- Polarization cell – Wagner's method

2.4.3.1 Tubandt's electrolysis method

This dc electrolysis method is based on Faraday's law of electrolysis. The change in mass (or volume) due to the ionic movement is measured when a certain charge is passed through the sample. This method can furnish information about both cation and anion transference numbers at the same time.

Transference number measurement by this method [154] has the advantage that relatively simple measuring systems may be used. However, the transference number calculated from this method may be significantly erroneous for a number of reasons. For example, at high temperatures, problems may arise from loss of weight by evaporation or from diffusion of the protective electrolyte into the material being studied. The use of a protective electrolyte may also cause blocking of current carriers (i.e. if an electrolyte with t_i = 1 is placed in series with a conductor which exhibits both electronic and ionic conduction, the ionic electrolyte may block the electronic charge carriers and thus alter the ionic transference number of the material).

2.4.3.2 Electrochemical potential measurement

The ionic transference number of electrolyte may also be determined from emf measurements [155,156] on the cells with ionic conductor sandwiched between different

reversible electrodes with different chemical potentials. Because of the chemical potential gradient, the cations migrate towards the cathode and the anions towards the anode.

The major limitation of this technique is the selection of appropriate electrodes having its compatibility with the electrolyte as it may cause internal or external current leakage paths. The net effect of the current leakage paths is to produce a mass transfer through the electrolyte via an ionic current. Polarization of the electrodes will occur if the ionic current is large enough to disturb local thermodynamic equilibrium and produce an undefined chemical potential of the electrodes at the electrode-electrolyte interfaces.

2.4.3.3 Wagner's polarization method

This is a most convenient and widely used method suggested by Wagner [157] to measure ionic / electronic transference number in solid electrolytes. This technique [158-160] involves placing the sample between a reversible and irreversible electrode. A constant dc voltage is applied across the sample as shown in figure 2.6 and the resulting current is monitored as a function of time with the help of an X–Y–t recorder.

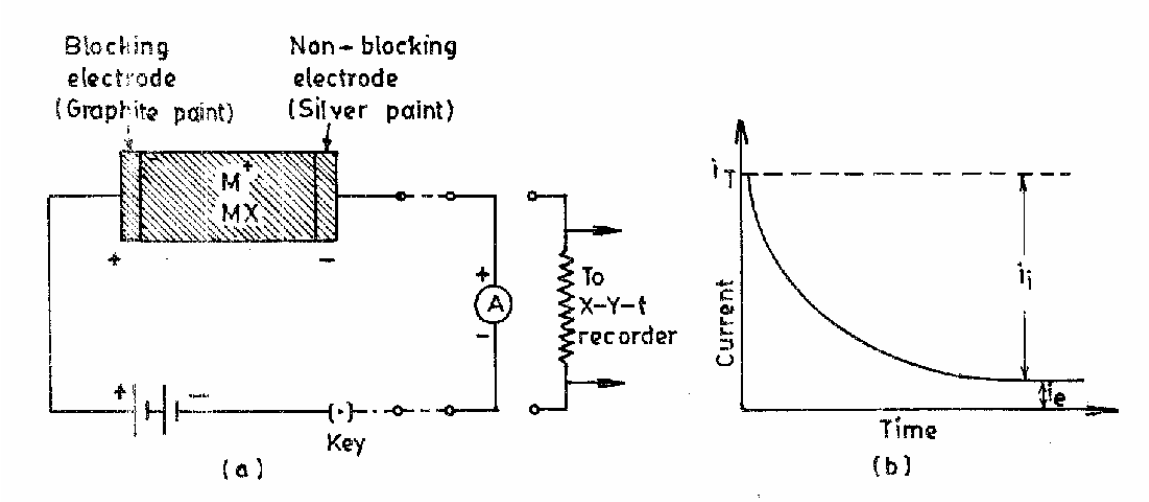

Fig. 2.6 (a) Schematic circuit diagram for the ionic transference number measurements, and (b) Variation of total current (i_T) with time.

A typical current versus time plot is shown in figure 2.6 (b). Initially the current is due to the movement of ions across the sample. After some time, the current decays to a steady state. The remaining part of the total current is due to the movement of electrons or holes across the sample, as ion concentration gradient becomes equal throughout the sample.

Chapter III

Microstructural features and transport characteristics of $(KCl)_{1-x}+(ZrO_2)_x$ system

Overview

The present chapter deals with the preparation, characterization and transport characteristics (namely conductivity (σ) and mobility (μ)) of ZrO_2 dispersed KCl based solid electrolytes. The temperature dependent carrier concentrations (n) were estimated from the σ and μ values at corresponding temperatures. The main objective of the present work is to find which factor (μ or n) dominates the conductivity behaviour.

3.1 Experimental

The samples in the form of cylindrical pellets were prepared in the system $(KCl)_{1-x}+(ZrO_2)_x$ by varying x (mol%) from 0.0 to 1.0 by powder compaction followed by the solid state sintering process. The pellets were sintered in the temperature range 650–850^oC for 5 hours in a muffle furnace. The electrical resistivity of the samples was measured for all the compositions. The temperature dependent impedance spectra were studied for both the base matrix (KCl) and the samples having maximum conducting composition in the temperature range of 100^o-500^{o}C at an interval of 20^{o}C. The activation energies for the ionic transport were determined from the temperature dependent conductivity plot ($\log\sigma$ vs. $1/T$). The ionic mobilities at room temperature and at higher temperatures in the range of 300- 460^{o}C in steps of 20^{o}C, were also studied.

3.2 Results and Discussion

3.2.1 XRD analyses

The X–ray diffraction patterns were obtained for the sintered samples in the system $(KCl)_{1-x}+(ZrO_2)_x$, where x = 0.0 to 1.0. The patterns corresponding to x = 0, 0.5, 0.7 and 1 are presented in figure 3.1. As can be examined from the figure 3.1 that the composite electrolyte system essentially consists of KCl and ZrO_2 as separate phases without showing any evidence of new chemical compound / phase formation due to sintering. However, the relative intensities of the KCl and ZrO_2 peaks vary with the composition of the electrolyte system.

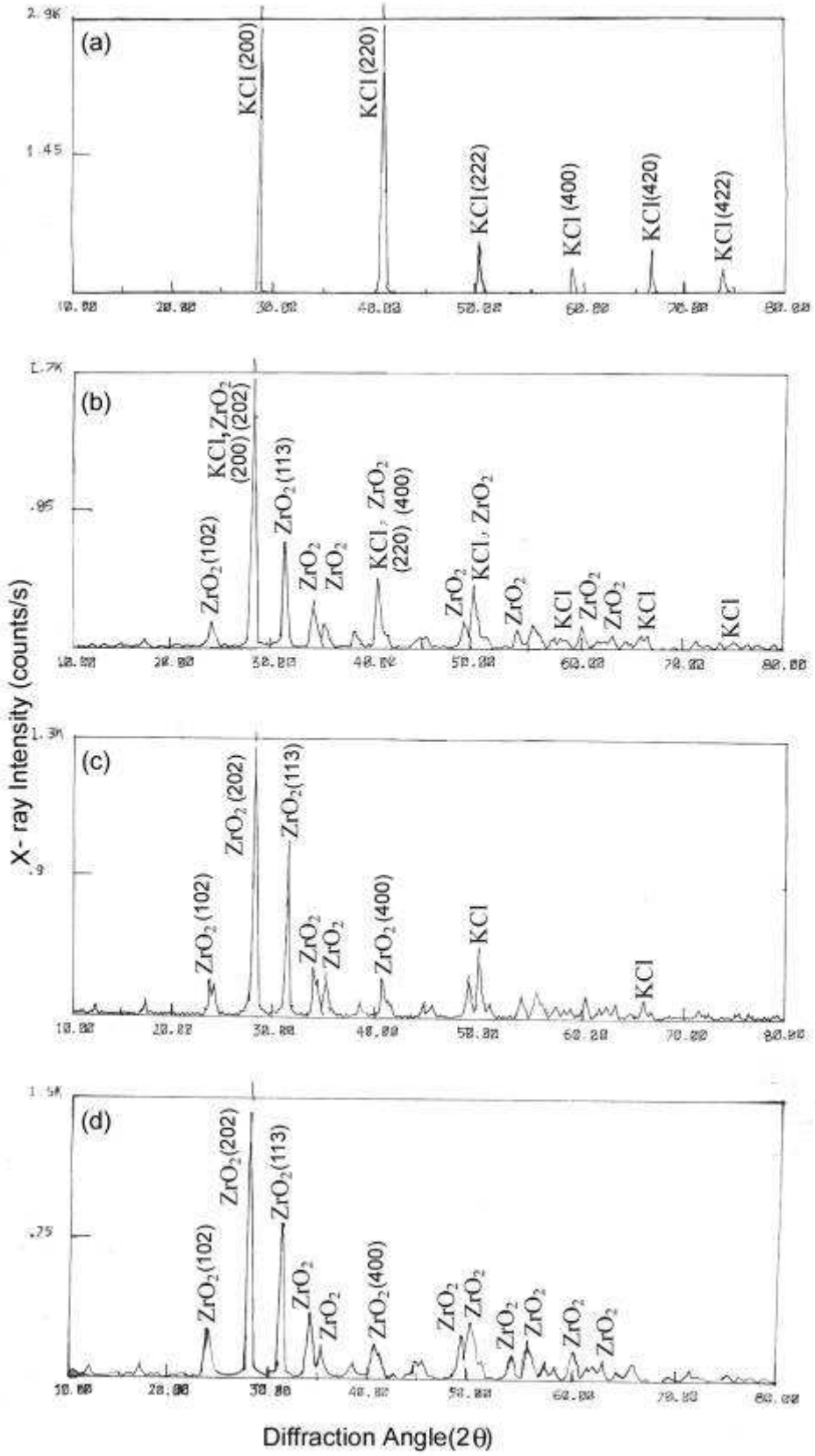

Fig. 3.1 The X-ray diffraction patterns for (a) KCl; (b) $(KCl)_{0.5}+(ZrO_2)_{0.5}$; (c) $(KCl)_{0.3}+(ZrO_2)_{0.7}$ and (d) ZrO_2 sintered samples.

3.2.2 SEM micrographs

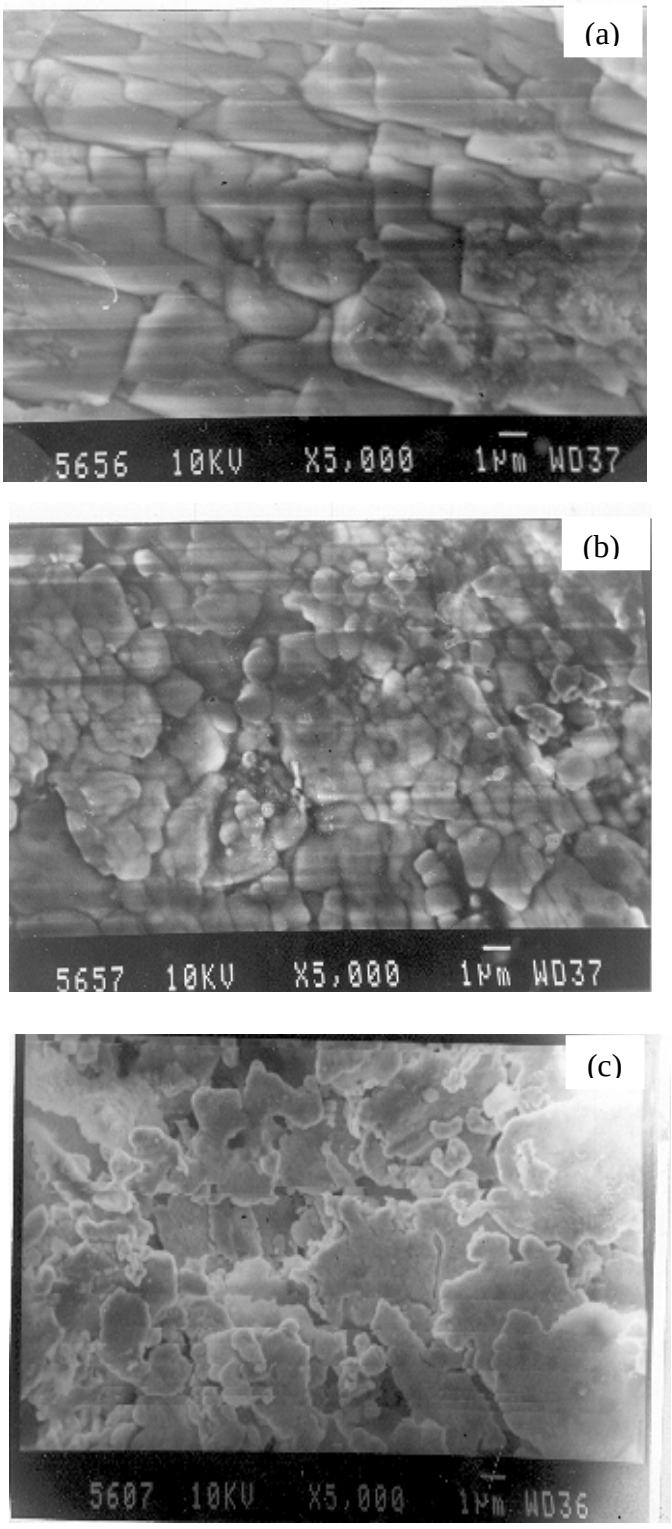

Fig. 3.2 SEM micrographs of (a) KCl, (b) KCl+10 m/o ZrO_2, and (c) KCl+30 m/o ZrO_2 composite electrolyte samples.

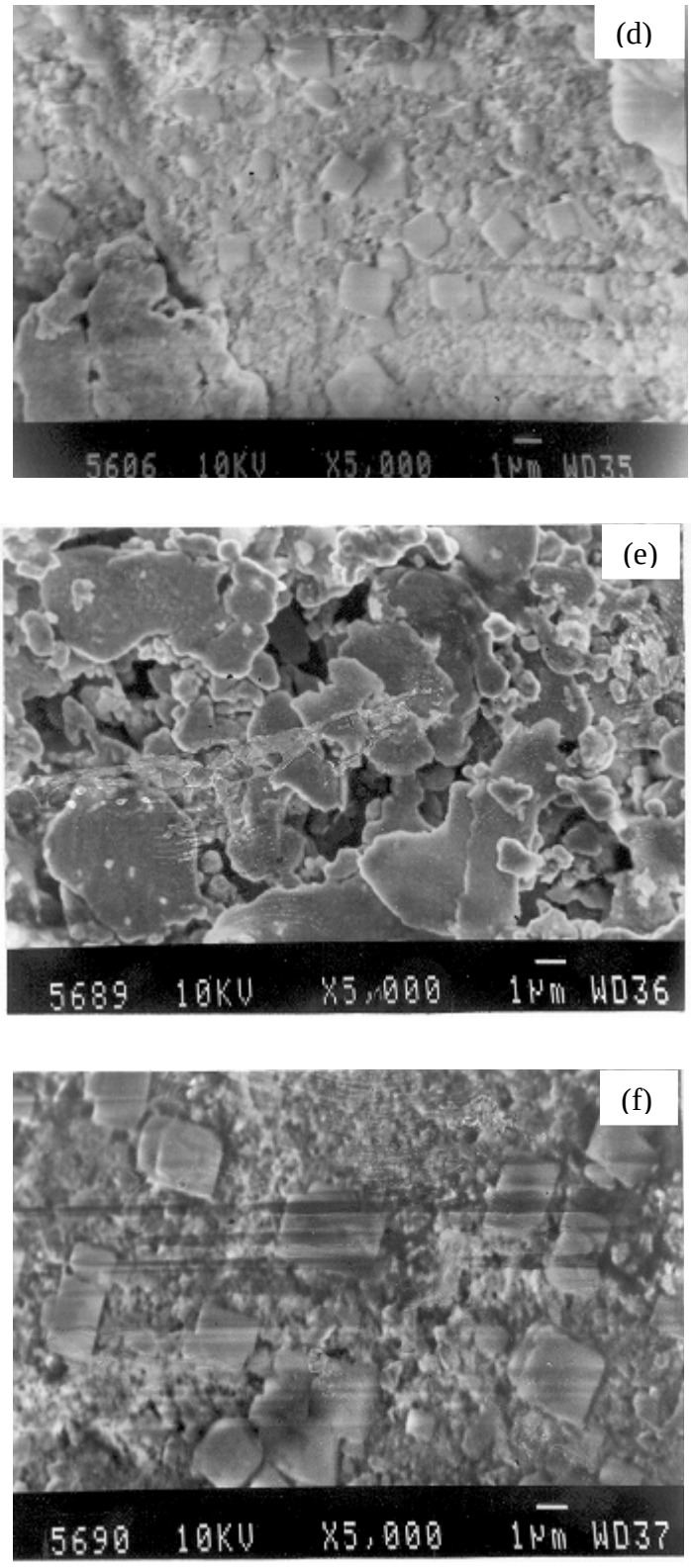

Fig. 3.2 SEM micrographs of (d) KCl+50 m/o ZrO_2, (e) KCl+70 m/o ZrO_2 and (f) KCl+80 m/o ZrO_2 composite electrolyte samples.

The microstructural observations were made on all the samples and the micrographs corresponding to x = 0, 0.1, 0.3, 0.5, 0.7, 0.8 are presented in figure 3.2. As can be seen from the micrographs, the evidence of grain formation due to sintering is clear with an indication of the oxide dispersion in the base matrix. Uniformity in grain size is more in the pure KCl samples.

An important aspect of the microstructural features in figure 3.2 is examining the degree of interconnecting interfaces formed due to intimate contact between the dispersoid and the halide matrix. On careful examination of the microstructures of the samples shown in figure 3.2, it can be seen that such interconnecting interface regions are significantly higher for the sample corresponding to x = 0.7 explaining the reason for obtaining the conductivity enhancement in this composition.

It is imperative to mention at this point that various researchers [82, 140, 141] have proposed that the microstructural development resulting in interconnecting interface is the key factor to explain the conductivity enhancement in composite solid electrolytes.

3.2.3 Electrical conductivity

The impedance spectra of the samples (x = 0.1 to 0.8) at room temperature obtained by plotting imaginary part, Z_{Im} against the real part, Z_{Real} of complex impedance measured at different frequencies are shown in figure 3.3. The plots mostly resembled semicircular curves. The dc resistances of the samples were estimated by extrapolating the curves to both low and high frequency regions following the semicircular trend. The bulk dc conductivities of the samples were derived from the estimated values of their dc resistances.

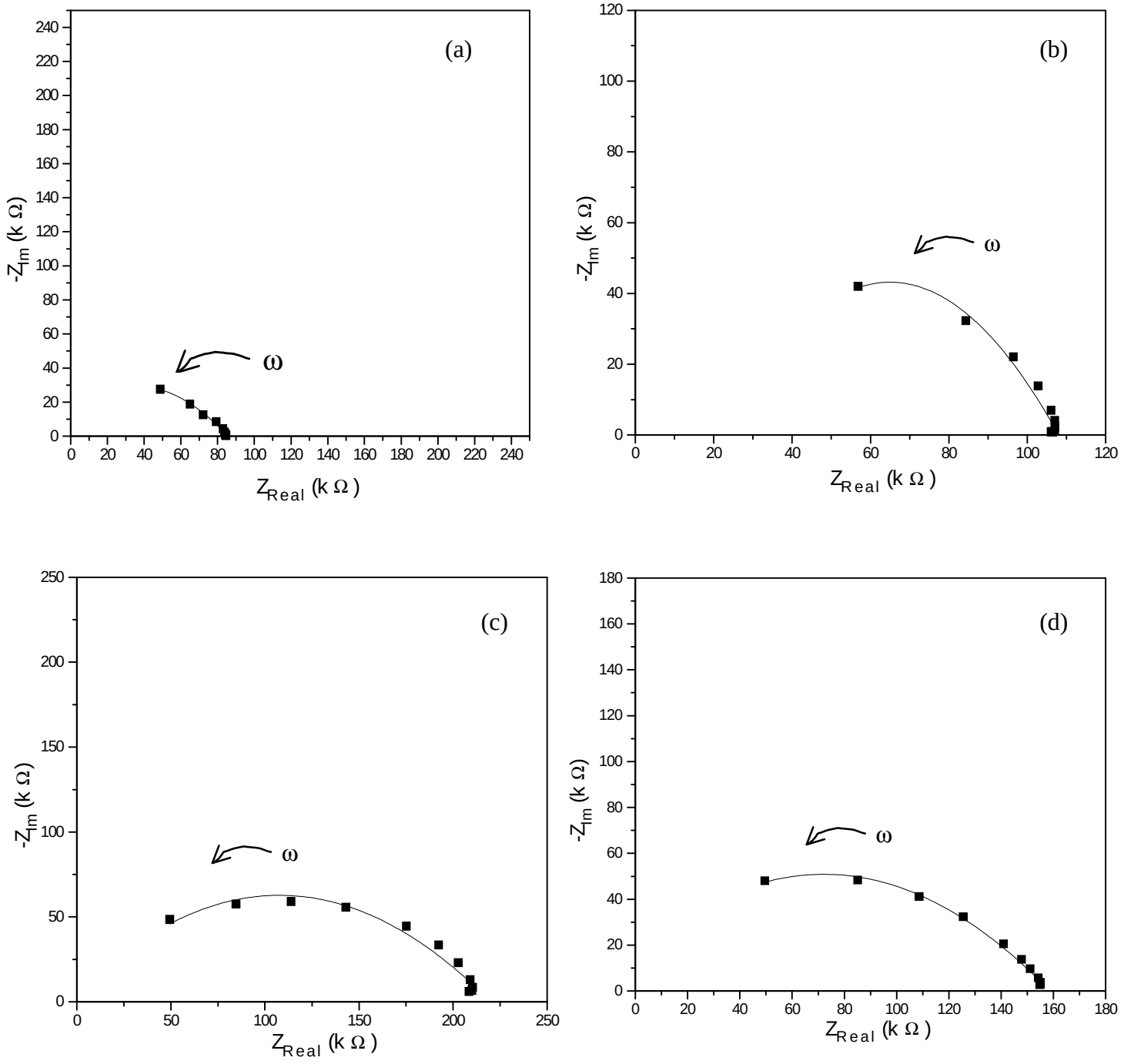

Fig. 3.3 Impedance spectra of the composite $(KCl)_{1-x}+(ZrO_2)_x$ with (a) 0.1 m/o ZrO_2; (b) 0.2 m/o ZrO_2; (c) 0.3 m/o ZrO_2 and (d) 0.4 m/o ZrO_2 at room temperature.

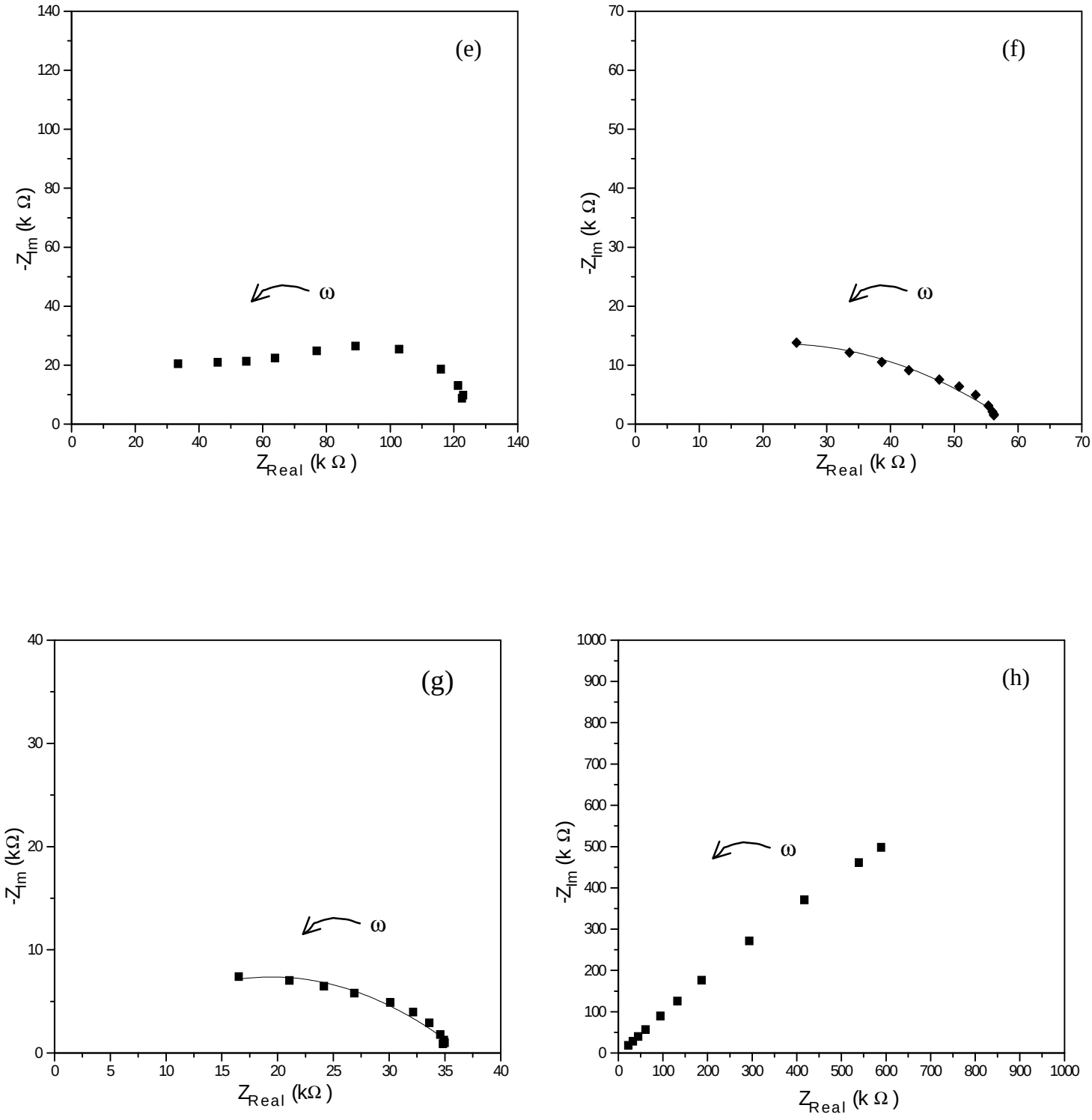

Fig. 3.3 The room temperature impedance spectra of the composite $(KCl)_{1-x}+(ZrO_2)_x$ with (e) 0.5 m/o ZrO_2; (f) 0.6 m/o ZrO_2; (g) 0.7 m/o ZrO_2 and (h) 0.8 m/o ZrO_2.

Figure 3.4 shows the variation of room temperature conductivity (σ) as a function of dispersoid (ZrO_2) concentration (m/o). It can be seen from the figure 3.4 that within the ZrO_2 concentration range of 0 to 40 m/o, the conductivity value passes through a maximum at around 10 m/o of ZrO_2 and at this composition the conductivity value has been estimated to be 1.19×10^{-6} $\Omega^{-1}cm^{-1}$ (about 500 times the base matrix value 0.24×10^{-8} $\Omega^{-1}cm^{-1}$).

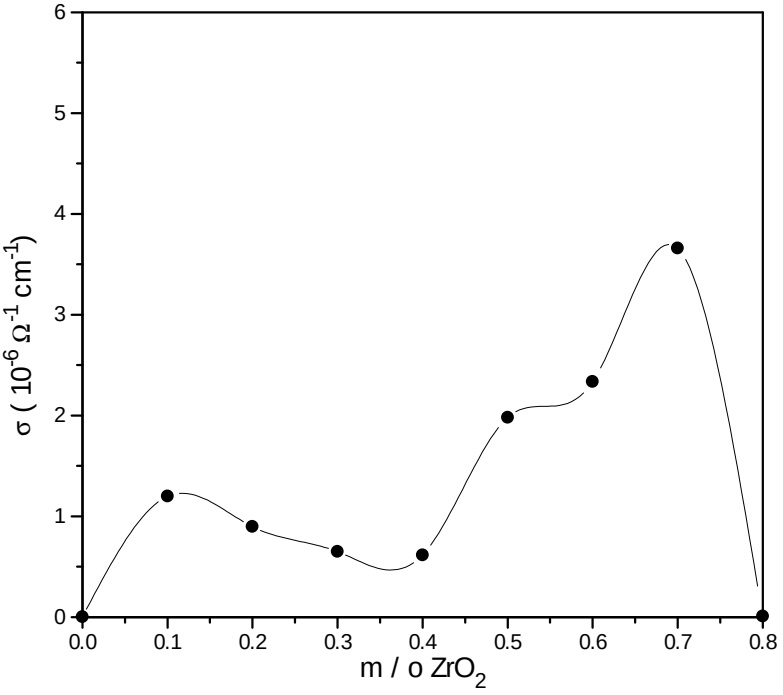

Fig. 3.4 Composition dependence of conductivity for $(KCl)_{1-x}+(ZrO_2)_x$; $0.0 \leq x \leq 0.8$ system at room temperature.

The occurrence of appreciable conductivity enhancement lies in the range of 40 m/o and 100 m/o in which the highest conductivity was found at about 70 m/o ZrO_2 dispersion. The conductivity value at this composition (x = 0.7) has been estimated to be 3.66×10^{-6} $\Omega^{-1}cm^{-1}$ which is about three orders of magnitude compared to that of the base matrix conductivity. The conductivity enhancement can be attributed to the change in the carrier concentration at or near the interface region (region of space charge formation) and / or the increase in ionic mobility.

3.2.4 Conductivity as a function of temperature

Expressing explicitly the temperature dependence, the ionic conductivity can be written as

$$\sigma(T) = n_o \exp\left(-\Delta E_f / 2 k_B T\right) q \mu_o \exp\left(-\Delta E_m / k_B T\right) \quad (3.1)$$

where $\Delta E_f / 2$ is the activation energy required for the formation of one cation vacancy in the intrinsic region assuming the defects are of purely Schottky type and ΔE_m the activation energy for migration of the cation. As the conductivity is very sensitive to the temperature change, the temperature dependent conductivity study was also carried out for $(KCl)_{0.3}+(ZrO_2)_{0.7}$ system in the temperature range of 100 to 500°C and the results are plotted in log σ vs. $1/T$ (figure 3.5).

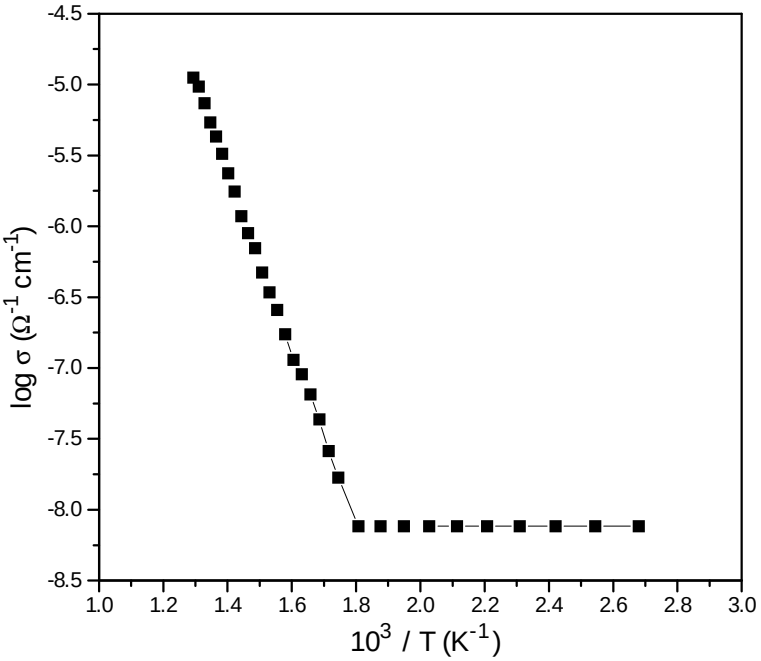

Fig. 3.5 log σ versus $1/T$ plot for $(KCl)_{0.3}+(ZrO_2)_{0.7}$ composition.

It can be seen from the plot that due to the increase in temperature from 300^{o}C to 500^{o}C, the conductivity enhancement to about 11.20×10^{-6} Ω^{-1}cm^{-1} is resulted. The conductivity remains almost constant over the temperature range up to about 300^{o}C. This temperature range is regarded as extrinsic region in view of the operating temperature of the material. The increase in $\sigma(T)$ over this temperature range (i.e. up to ~ 300^{o}C), which is nominal, is due to the restricted increase in ionic mobility with temperature owing to the increasing probability of scattering that the ions experience with the increase in temperature. In the temperature range of 300^{o}C to 500^{o}C, the conductivity increase is quite significant. The enhanced σ value was estimated as 11.20×10^{-6} Ω^{-1}cm^{-1} which is 4667 times that of room temperature matrix conductivity value. This increase can be attributed to the combined effect of increasing vacancy concentration with increase in temperature and the ionic mobility enhancement.

This temperature range can be regarded as intrinsic region in view of the operating temperature range of the material. The scattering centers may be impurities present in the material and the grain boundaries in the sintered samples.

In order to compare the temperature dependent conductivity behaviour of $(KCl)_{0.3}$+$(ZrO_2)_{0.7}$ with that of base matrix KCl, the log σ versus $1/T$ plots of the measured conductivity values in the temperature range of 300^{o} to 500^{o}C are presented in figure 3.6.

From the plots, the average activation energies for KCl and the highly conducting $(KCl)_{0.3}$+$(ZrO_2)_{0.7}$ samples have been estimated to be 0.35 eV and 0.54 eV respectively. The difference in the activation energy values is attributed to (i) the nature of the plots, (ii) difference in the relative contributions of the ionic mobility and the carrier concentration.

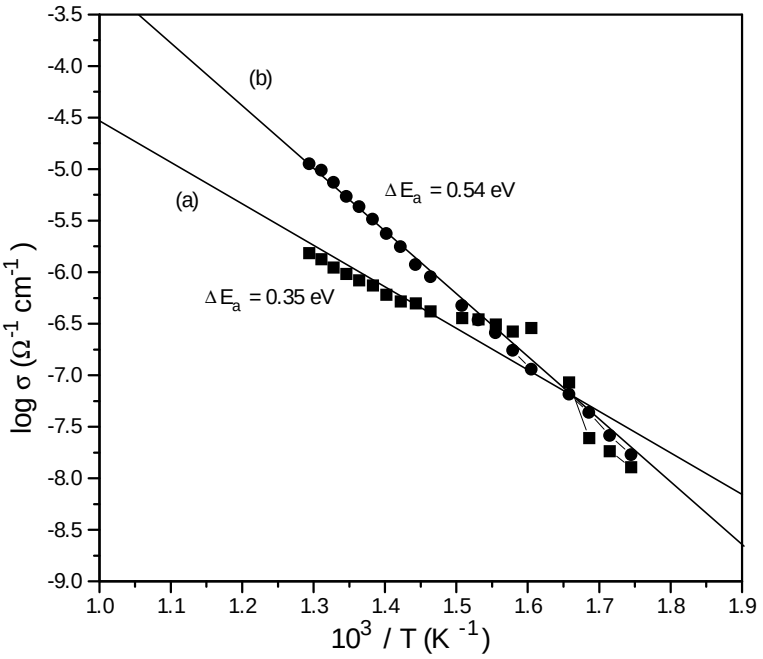

Fig. 3.6 The variation of conductivity (σ) as a function of inverse temperature $(1/T)$ for (a) KCl and (b) $(KCl)_{0.3}+(ZrO_2)_{0.7}$ sintered samples.

The enhanced conductivity for the electrolyte composition $(KCl)_{0.3}+(ZrO_2)_{0.7}$ can further be explained from its microstructural features (figure 3.2 (e)) in which the presence of interconnecting interfacial regions were observed. The requirement of interconnecting interfacial regions for satisfying the percolation theory has thus been achieved in the present study.

3.2.5 Ionic mobility determination

Figure 3.7 shows the variation of transient ionic current at room temperature with time through the $(KCl)_{0.3}+(ZrO_2)_{0.7}$ samples.

From this trace, the μ has been estimated to be 20.8×10^{-2} cm^2 / V sec. It is pointed out that KCl sample has mobility of 5.7×10^{-2} cm^2 / V sec. Therefore it can be inferred that the oxide dispersion (70 m/o) in KCl has enhanced the mobility by about 3.5 times that of KCl value.

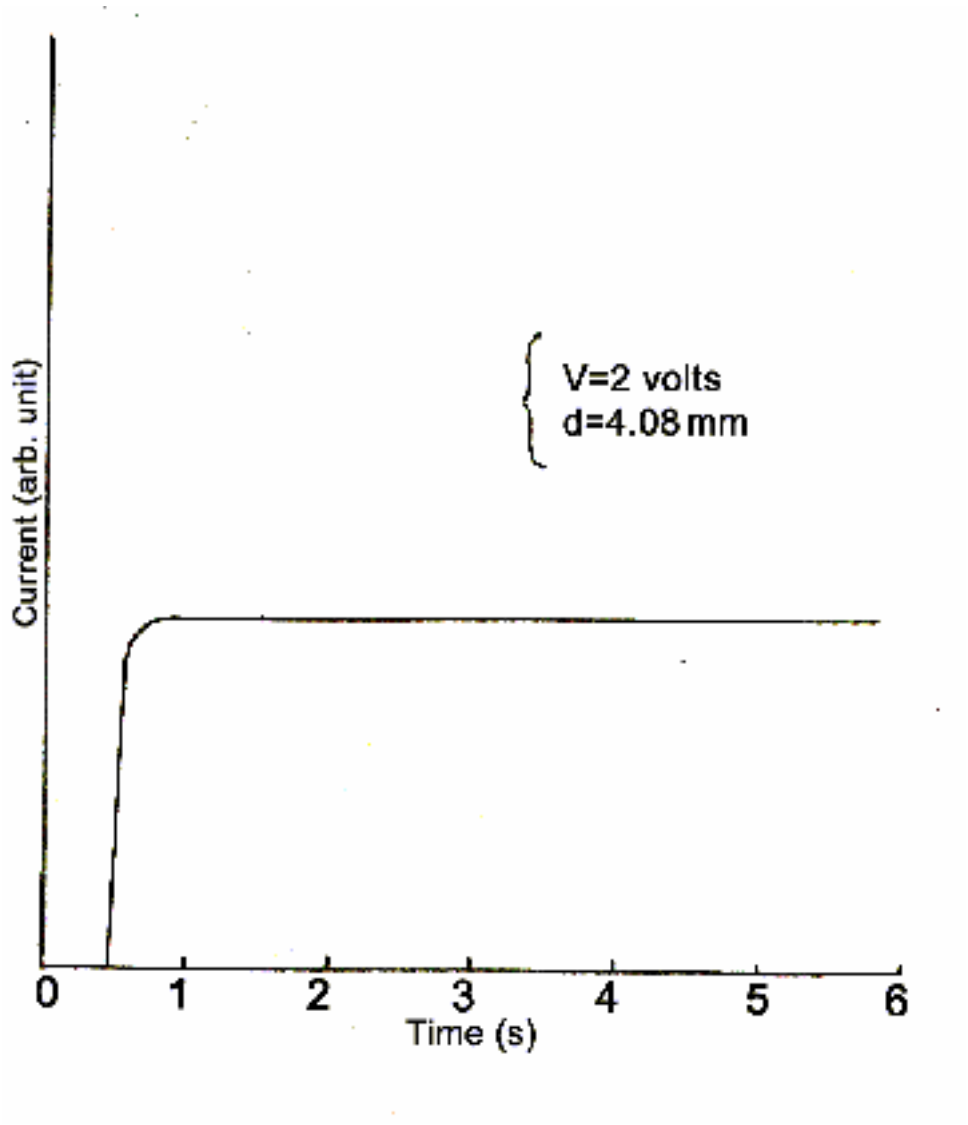

Fig. 3.7 Transient ionic current vs. time plot obtained for ionic mobility measurement of the $(KCl)_{0.3}+(ZrO_2)_{0.7}$ composition at room temperature.

The transient ionic current variations as a function of time were recorded at various temperatures and one such typical plot at 400^{o}C is shown in figure 3.8.

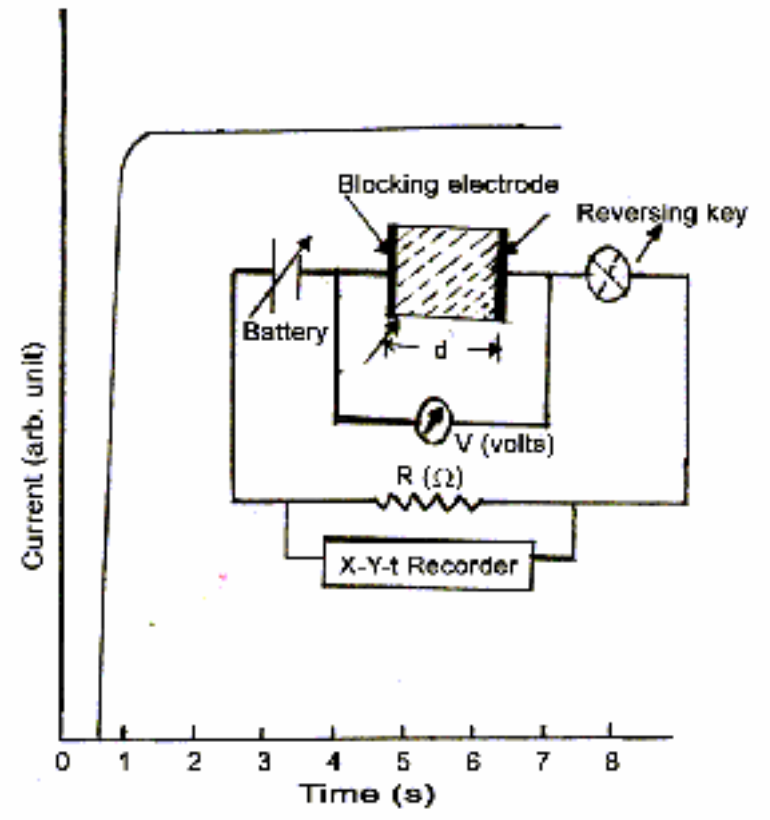

Fig. 3.8 Typical TIC plot for μ-measurements at 400^{o}C. Inset : Schematic experimental circuit for TIC measurement.

The temperature dependent mobility values for the samples having highly conducting composition are plotted in terms of log μ versus $1/T$ in figure 3.9.

.

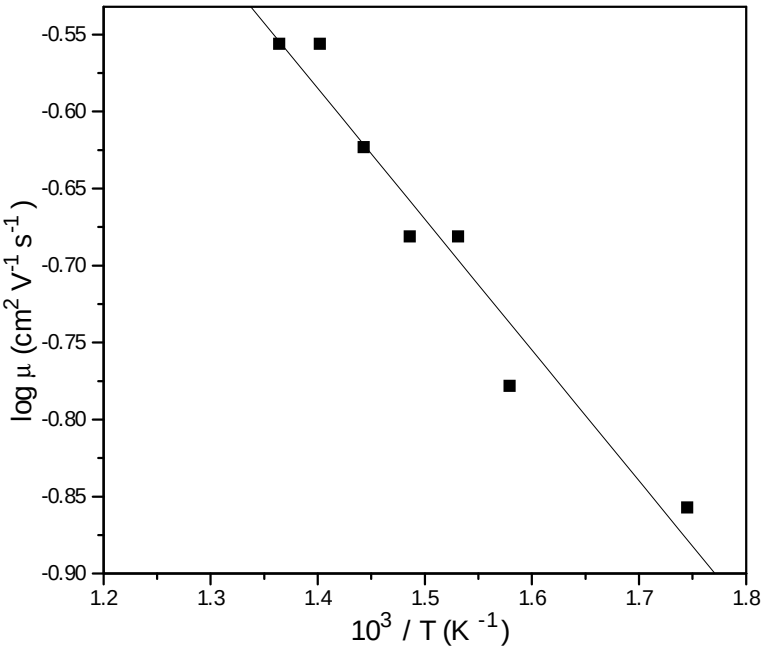

Fig. 3.9 log μ versus $1/T$ plot for the highly conducting composition $(KCl)_{0.3}+(ZrO_2)_{0.7}$.

An average linear variation of $\mu(T)$ values over the temperature range 300°C to 460°C was found. As the mobility is expressed by the equation:

$$\mu = \mu_o \exp\left(-\Delta E_m / k_B T\right) \tag{3.2}$$

the activation energy (ΔE_m) for K^+ ion migration was calculated from the slope of log μ versus $1/T$ curve (figure 3.9) and value was found to be ΔE_m = 0.06 eV which is significantly small. The mobility enhancement that has been resulted due to the temperature increase from 300° to 460° C, is very small ($\mu_{T=460^oC}$ = 1.4 $\mu_{T=300^oC}$). This is perhaps due to the obstructions of the ionic movements with the impurities, distortion in regular interionic spacing etc.

3.2.6 Charge carrier concentration

The temperature dependent n values were calculated from the σ and μ values measured at corresponding temperatures and are given in Table 3.1. The plot of log n vs. $1/T$ is made in figure 3.10.

Table 3.1 Ionic mobility, conductivity and charge concentration of $(KCl)_{0.3}+ (ZrO_2)_{0.7}$ at various temperatures.

Temperature (^oC)	**$10^3/T$ (K^{-1})**	**μ ($cm^2 V^{-1}s^{-1}$)**	**σ ($\Omega^{-1}cm^{-1}$)**	**n (cm^{-3})**
300	1.745	1.38×10^{-1}	1.6×10^{-8}	7.24×10^{11}
360	1.579	1.66×10^{-1}	1.73×10^{-7}	6.51×10^{12}
380	1.531	2.08×10^{-1}	3.41×10^{-7}	1.02×10^{13}
400	1.486	2.08×10^{-1}	7.02×10^{-7}	2.10×10^{13}
420	1.443	2.37×10^{-1}	1.18×10^{-6}	3.11×10^{13}
440	1.402	2.77×10^{-1}	2.36×10^{-6}	5.32×10^{13}
460	1.364	2.77×10^{-1}	4.30×10^{-6}	9.70×10^{13}

It can be seen from the plot that by increasing the temperature from 300^o to 460^oC, an increase in n value to 9.63×10^{13} cm^{-3} was resulted.

Assuming the defects that are produced due to thermal energy in the intrinsic region are of purely Schottky type, defect concentration (n) can be expressed as

$$n = n_o \exp\left(-\Delta E_f / 2k_B T\right) \tag{3.3}$$

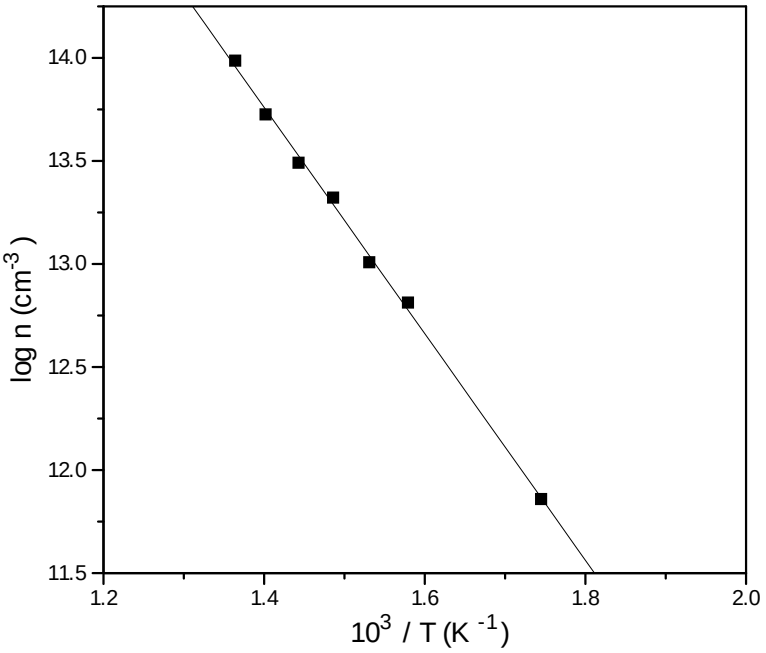

Fig. 3.10 log n versus $1/T$ plot for the $(KCl)_{0.3}+(ZrO_2)_{0.7}$ composition.

The activation energy for the formation of one cation vacancy was estimated from the graph (figure 3.10) and the value was found to be 0.48 eV. The mobility enhancement over the temperature range studied was found to be less significant. As the overall conductivity of the material depends upon both n and μ as given by equation (3.1), the resultant conductivity enhancement can be explained due to the large increase in the carrier concentration.

Chapter IV

Preparation, characterization and ionic conductivity measurements of cation conducting systems

Overview

Among the various techniques employed so far to enhance the ionic conductivity of composite electrolyte systems, one of the techniques is the opening of the lattice structure by substitution with wrong size ion (cation / anion). This chapter describes the preparation and ionic conductivity measurements of mixed halide based composite electrolyte systems $[(KCl)_{1-x}+(NaCl)_x]_{1-y}+(ZrO_2)_y$ and $[(KCl)_{1-x}+(CuCl)_x]_{1-y}+(SnO_2)_y$, where y is the mole fraction of the dispersoids.

4.1 Experimental

The constituent powders in the required compositions were weighed. The mixed halide matrices were prepared by melt quench technique. The chunks so obtained were ground. The oxide dispersion in the matrix was carried out in a wet medium (acetone). The homogeneous mixtures so obtained were pelletized at a load of 10 tons in the form of cylindrical pellets having diameter of 20 mm and thickness of about 3 mm. The pellets were then sintered in a muffle furnace at temperatures ranging between 250^{o}C and 650^{o}C for the soaking period of 5 hrs.

4.2 Results and Discussion

4.2.1 Electrical conductivity of $(KCl)_{1-x}+(NaCl)_x$ system

Figure 4.1 shows the variation of room temperature conductivity (σ) vs. composition (x) of the mixed matrix $(KCl)_{1-x}+(NaCl)_x$ $(0 \leq x \leq 0.4)$. It can be seen that the σ becomes maximum (about 50 times that of the base matrix KCl value), at x = 0.1.

The following gives an explanation of the composition dependent conductivity behaviour and the appearance of a maximum. It is appropriate to consider the lattice distortion caused by the incorporation of the guest ion having different size (wrong size with respect to the regular lattice ion size) into the lattice of the host material. The lattice distortion would be larger, in general, if the guest ions are of much larger or smaller size than the corresponding host ion and therefore, the host lattice may be forced to expand or contract by the ionic substitution.

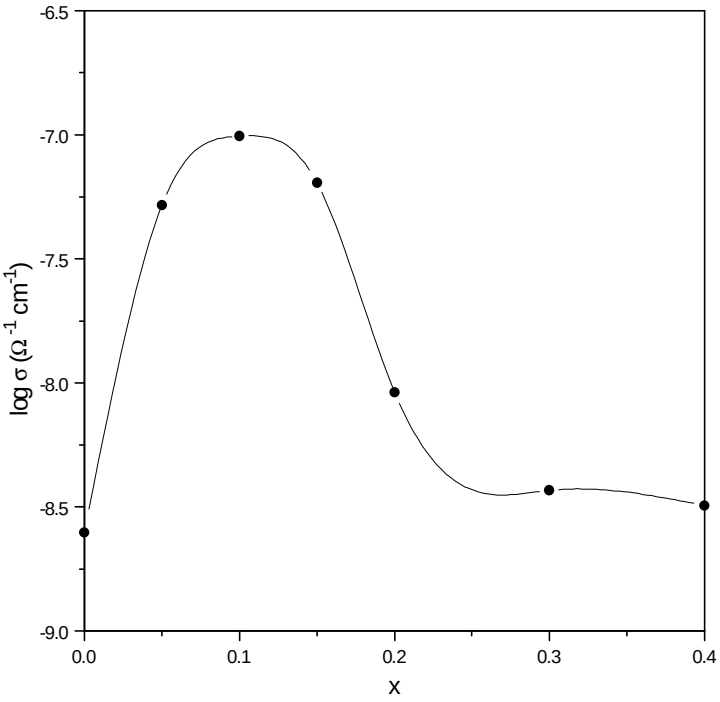

Fig. 4.1 The room temperature conductivity variation of mixed halide matrix $[(KCl)_{1-x}+(NaCl)_x]$ as a function of x ($0.0 \leq x \leq 0.4$).

In either of these cases the host lattice is subjected to a strain whose magnitude depends on a factor $f = \left|1 - r_h / r_g\right|$, where r_g and r_h are the ionic radii of the guest and the host ions respectively. The net result of such a strain is apparently lattice loosening leading to a decrease in the melting point of the mixed matrix. This also decreases the enthalpy of formation of defects (Δh_f), which leads to the generation of more number of defects contributing to σ enhancement. The substitutions with larger values of f are then expected to cause more lattice distortion resulting in appreciable increase in σ. In the present system, the lattice distortion is appreciable (f = 0.3103) causing the conductivity enhancement.

As KCl and NaCl both possess rock salt structure, the substitution of KCl by NaCl cause the possible defect reaction

$$\underset{KCl}{NaCl} \Rightarrow Na_K^x + Cl_{Cl}^x$$

As the cations are isovalent, the ionic size difference of K^+ and Na^+ essentially plays the major role for the conductivity enhancement. The ionic radii of the Na^+ and K^+ are 0.95 and 1.33Å respectively, according to Pauling crystal radius (in Å) data. Therefore the substitution by wrong size ions (Na^+) lowers the melting temperature and this is in agreement with the phase diagram of the system KCl+NaCl. Since the formation and the migration enthalpies are correlated to the melting temperature of the solid, the effect of substitution within the limited composition of the mixed matrix, is to increase the concentration as well as mobilities of the defects leading to increased ionic conductivity.

4.2.2 Electrical conductivity of $[(KCl)_{0.9}+(NaCl)_{0.1}]_{1-y}+(ZrO_2)_y$ system

The dc conductivities (σ) of the samples in the system $[(KCl)_{0.9}+(NaCl)_{0.1}]_{1-y}+(ZrO_2)_y$ were determined from respective complex impedance data plots. These σ values were then plotted as a function of composition y as shown in figure 4.2.

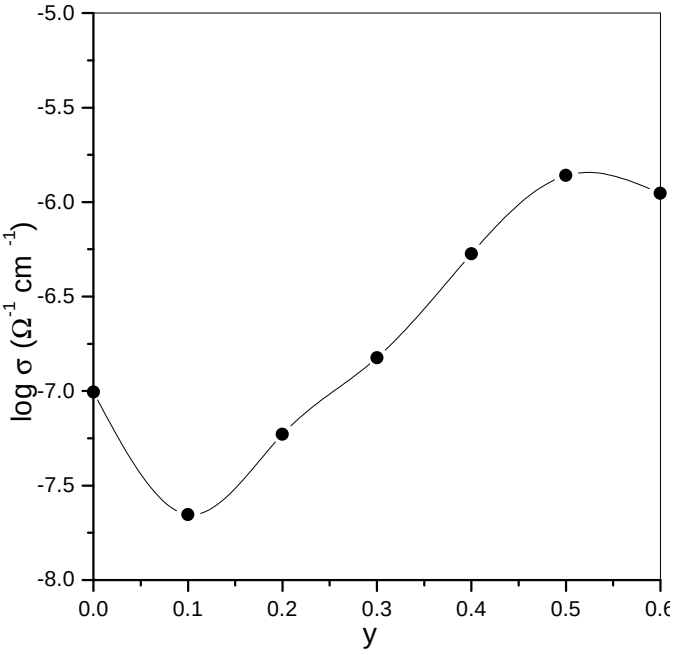

Fig. 4.2 The composition dependence of the conductivity for $[(KCl)_{0.9}+(NaCl)_{0.1}]_{1-y}+(ZrO_2)_y$ system at room temperature as a function of y ($0.0 \leq y \leq 0.6$).

It can be seen from the plot that the conductivity enhancement of about one order of magnitude was found to occur at 50 m/o ZrO_2.This enhancement could be attributed to the formation of space charge layer at the host-dispersoid interfaces.

4.2.3 Conductivity as a function of temperature

The temperature dependent impedance data at different frequencies were collected for the maximum conducting composition $[(KCl)_{0.9}+(NaCl)_{0.1}]_{0.5}+(ZrO_2)_{0.5}$ in the temperature range of 250°-450°C. The dc conductivities, which were derived from the complex impedance plots at different temperatures, were plotted in figure 4.3 as a function of temperature in the form of log σ vs. $1/T$.

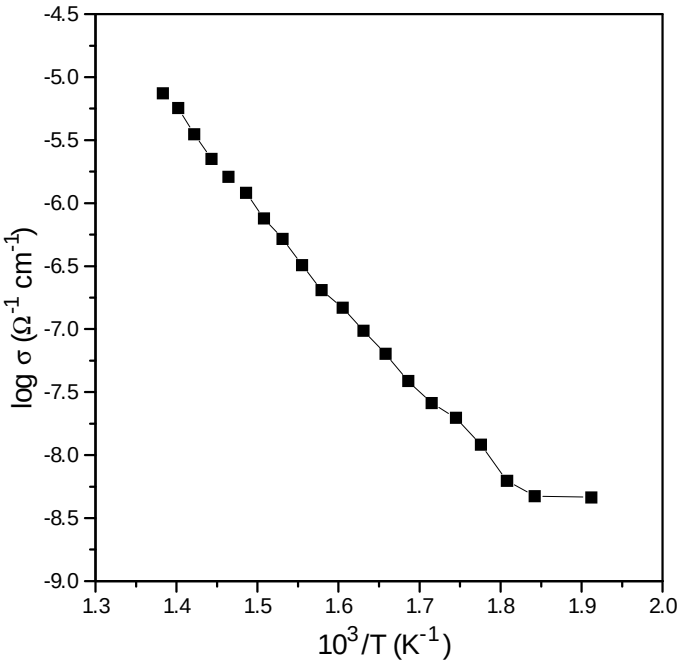

Fig. 4.3 The variation of conductivity as a function of inverse temperature for $[(KCl)_{0.9}+(NaCl)_{0.1}]_{0.5}+(ZrO_2)_{0.5}$ sample.

It can be seen from the plot that by increasing temperature from 250°C to 450°C, the σ increases from 0.00461×10^{-6} $\Omega^{-1}cm^{-1}$ (at 250°C) to about 7.45×10^{-6} $\Omega^{-1}cm^{-1}$ (at 450°C) yielding the activation energy for ion transport ΔE_a = 0.57 eV. This ΔE_a value is found

to be comparable with other reported electrolyte systems such as PbX_2+Al_2O_3 (where X = Cl, Br, I), KCl+ZrO_2 and AgX based systems [90, 161,162].

4.2.4 SEM micrographs

The microstructural studies were carried out for the [$(KCl)_{0.9}$+$(NaCl)_{0.1}$] mixed matrix and ([$(KCl)_{0.9}$+$(NaCl)_{0.1}$]$_{1-y}$+$(ZrO_2)_y$; $0 \leq y \leq 0.5$) composite electrolyte systems. The micrographs are shown in figure 4.4. From the micrograph 4.4(a), the evidence of grain formation is clear. The grain sizes are found to vary from 2μm to about 9μm. However, the majority of the grains are in the range of 2μm to 4μm and there are a fewer number of larger grains which are in the size of 5μm to 9μm. The presence of ZrO_2 particles is clear from the micrographs of all the composite samples, as shown in figure 4.4(b) – 4.4(f). On examination of the micrographs the relative increase in dispersoid phase content in the samples is evident. From the observation of the micrographs it may be commented that ZrO_2 particles have not undergone coarsening on sintering the composite electrolyte samples. It is difficult to comment on the quantitative development of interfacial paths validating the percolation theory. However, the continuity of interfaces is relatively more in the case of ([$(KCl)_{0.9}$+$(NaCl)_{0.1}$]$_{0.5}$+$(ZrO_2)_{0.5}$) samples as can be seen in the figure 4.4 (f).

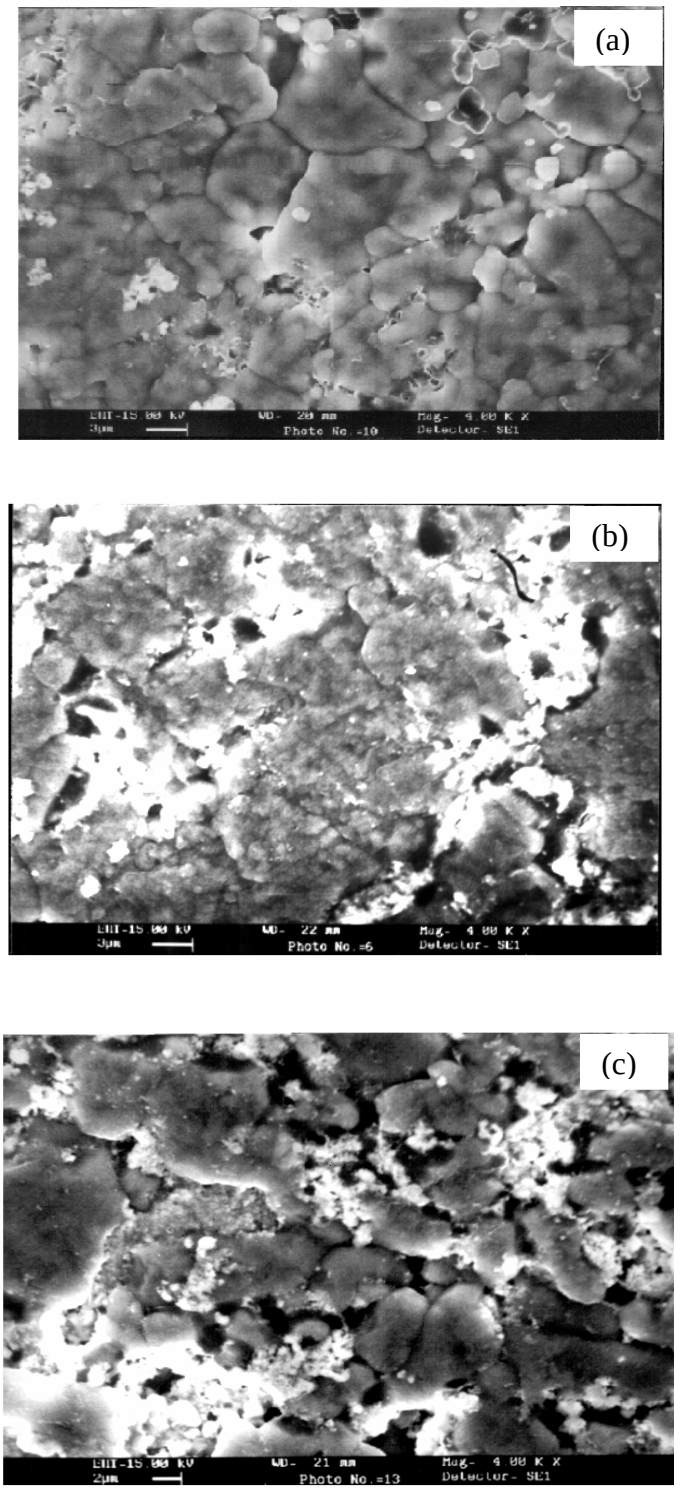

Fig. 4.4 The SEM micrographs of (a) the mixed halide matrix composition $(KCl)_{0.9}+(NaCl)_{0.1}$, (b) composite electrolyte $[(KCl)_{0.9}+(NaCl)_{0.1}]_{0.9}+(ZrO_2)_{0.1}$ and (c) composite electrolyte $[(KCl)_{0.9}+(NaCl)_{0.1}]_{0.8}+(ZrO_2)_{0.2}$.

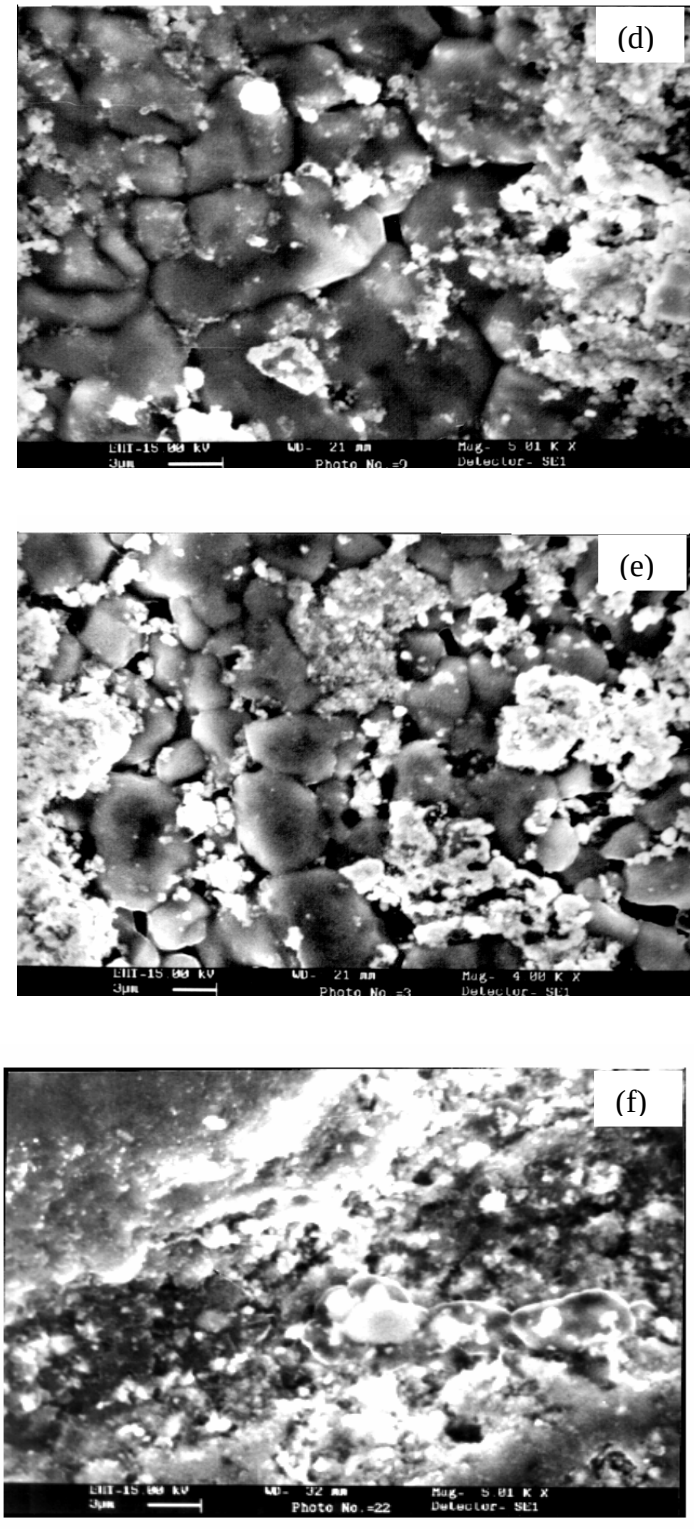

Fig. 4.4 The SEM micrographs of composite electrolyte $[(KCl)_{0.9}+(NaCl)_{0.1}]_{1-y}+(ZrO_2)_y$ with y equal to (d) 0.3, (e) 0.4 and (f) 0.5.

4.2.5 XRD analyses

The X-ray diffraction analyses of mixed halide system and oxide dispersed composite electrolytes were conducted. In the present case, the patterns corresponding to highest conducting compositions both for matrix and composite electrolytes are given in figure 4.5 (a) & (b). In both the cases, the scanning was done between 5^o and 120^o.

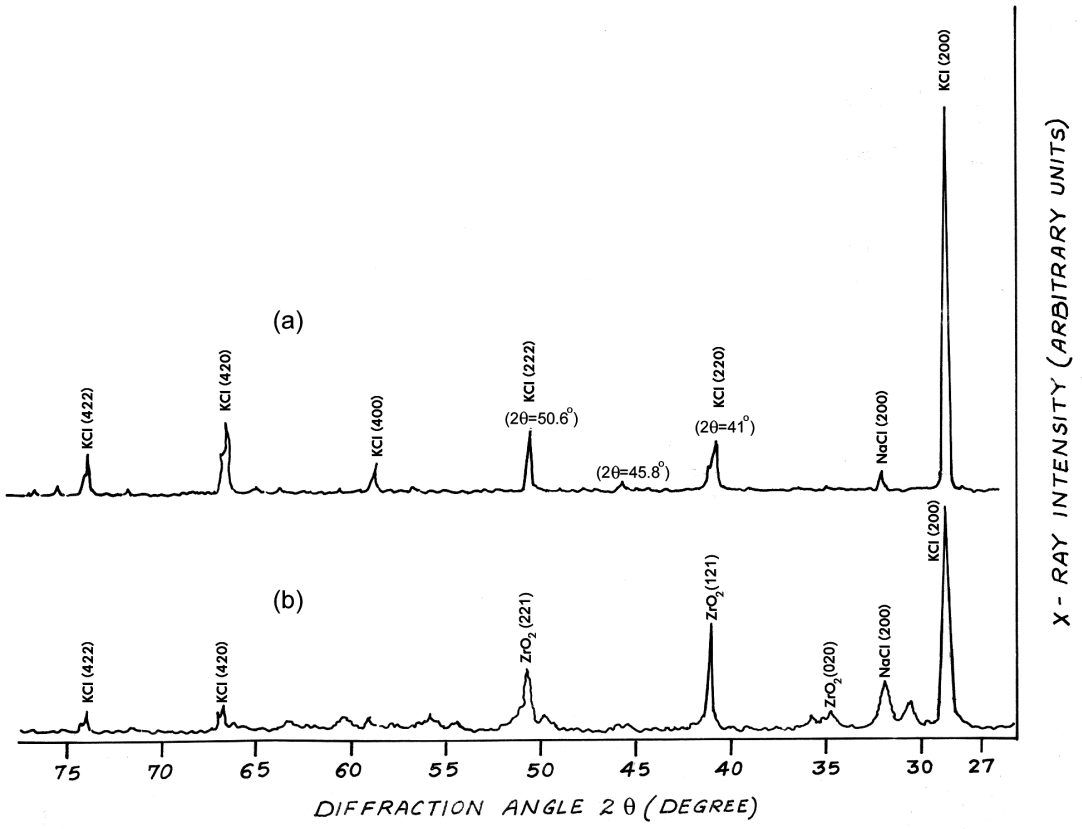

Fig. 4.5 The X-ray diffraction patterns for (a) mixed halide matrix $(KCl)_{0.9}+(NaCl)_{0.1}$ and (b) composite electrolyte $[(KCl)_{0.9}+(NaCl)_{0.1}]_{0.5}+(ZrO_2)_{0.5}$ sintered samples.

The patterns were recorded using a strip chart recorder. The relevant portions of the patterns showing high intensity peaks are given in the figure 4.5. The patterns were analyzed and the peaks were identified using JCPDS data file. One can see from the patterns (figure 4.5) that the peaks corresponding to mixed matrix material are retained with reduced intensities in the pattern of the composite electrolyte. The intensity reduction is attributed to the difference in weight fraction of mixed matrix in the

composite electrolyte. The additional peaks that are present in the pattern (b) correspond to ZrO_2 material. Therefore the XRD results confirm the presence of oxide material as a separate unreacted phase. This fact was further indicated by thermal analyses also.

4.2.6. Thermal analyses

The samples of high conducting matrix and composite electrolyte were analyzed by using TG & DTA and the thermal traces are shown in figures 4.6 & 4.7. The TG plot (figure 4.6) shows the thermal stability of the matrix up to the temperature 780^{o}C and then the reduction of mass corresponding to the melting of the material, takes place. The melting temperature of the matrix material as can be seen is very close to that of pure KCl. This is due to the fact that the material is KCl-rich. However, the DTA trace is found to be quite uniform except there are minor endothermic peaks at 728^{o}C and 745^{o}C temperatures. The peak corresponding to 745^{o}C, is relatively larger compared to 728^{o}C peak and this is perhaps due to the appearance of the liquid phase of the material.

The DTG trace confirms the melting of the matrix material well below the temperature of 826^{o}C. The material that has been formed is more or less uniform with minute quantities of unreacted components. This is due to the fact that as the mass changes from the starting value 10.41mg to the final value 0.01mg, the TG trace is quite smooth after the melting process.

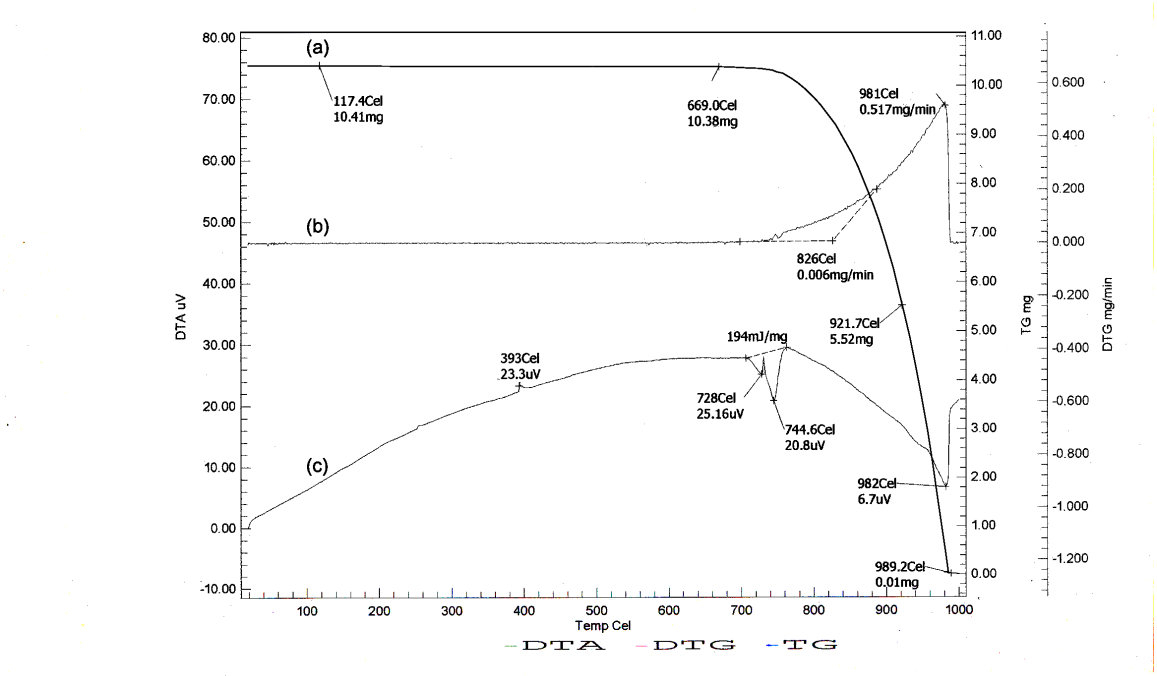

Fig. 4.6 Typical (a) TG, (b) DTG and (c) DTA curves simultaneously recorded for the mixed matrix $(KCl)_{0.9}+(NaCl)_{0.1}$.

Figure 4.7 shows the thermal analyses of the composite $[(KCl)_{0.9}+(NaCl)_{0.1}]_{0.5}+[ZrO_2]_{0.5}$. It can be noticed that the residual mass of the thermal run is 6.18 mg which is the estimated quantity of ZrO_2 in 10.11mg initial sample powder. This observation supports the XRD results that the ZrO_2 presents in the composite electrolyte as a separate phase. The relative reduction of mass from the starting temperature to near the melting point in TG study is more for composite electrolyte as compared to matrix system. This may be due to the partial sublimation of oxides. However, the melting process starts at around the same temperature as was found in the mixed matrix. The DTG trace confirmed the melting well below 814^{o}C.

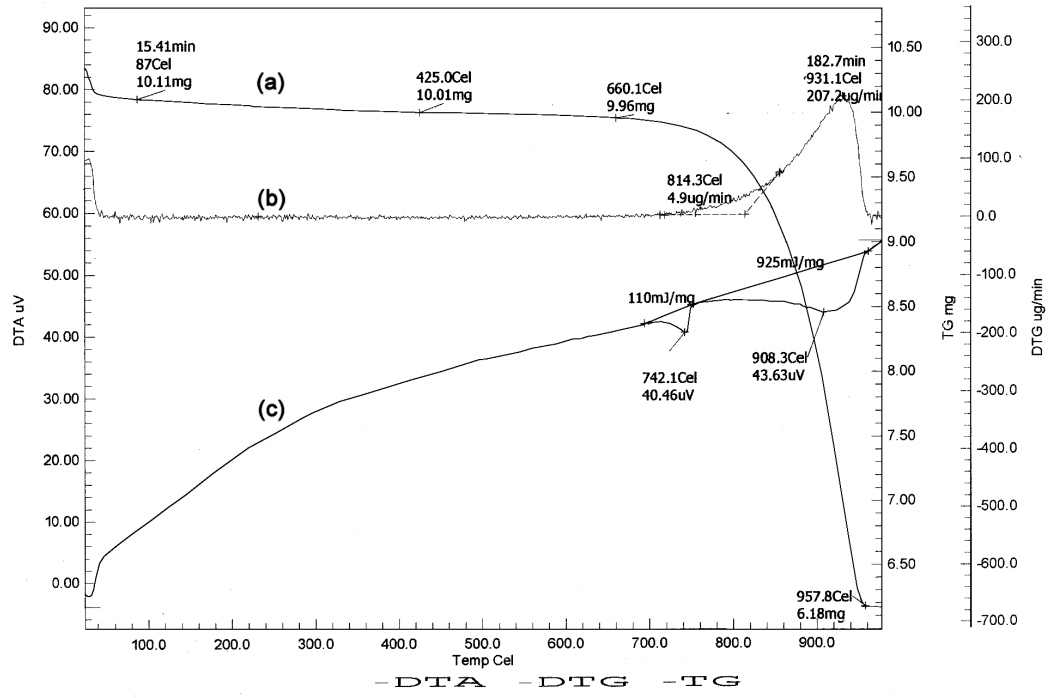

Fig. 4.7 (a) TG, (b) DTG and (c) DTA profiles of the composite electrolyte $[(KCl)_{0.9}+(NaCl)_{0.1}]_{0.5}+(ZrO_2)_{0.5}$ in the temperature range of 20^o to 1000^oC.

The DTA trace in the composite is almost identical to that of mixed matrix till the melting process. The minute endothermic peaks at 742^oC temperature and 908^oC temperature are less sharper than that of the matrix indicating the involvement of less quantity of the matrix material.

4.2.7 Conductivity due to finer dispersoid particles

In order to observe the effect of particle size of the dispersoid on the conductivity behaviour of composite electrolytes, an attempt was made to disperse the matrix $(KCl)_{0.9}+(NaCl)_{0.1}$ with very fine (size is 20-50 nm) ZrO_2 particles.

4.2.7.1 $[(KCl)_{0.9}+(NaCl)_{0.1}]_{1-y}+(ZrO_2)_y$ system

The dc conductivities (σ) of the samples in the system $[(KCl)_{0.9}+(NaCl)_{0.1}]_{1-y}+(ZrO_2)_y$; $0 \leq y \leq 0.5$ were determined from respective complex impedance data plots. These σ values were then plotted as a function of composition y in figure 4.8.

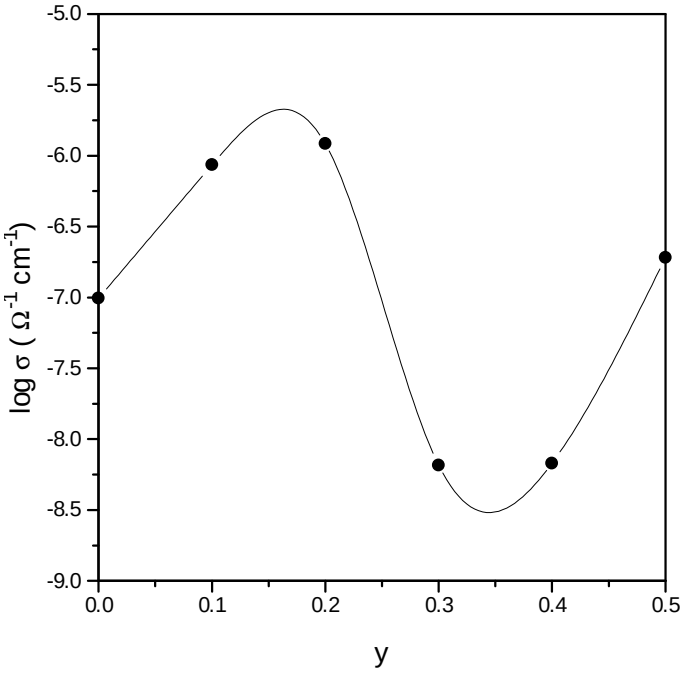

Fig. 4.8 The room temperature conductivity of the composite electrolyte $[(KCl)_{0.9}+(NaCl)_{0.1}]_{1-y}+(ZrO_2)_y$ as a function of y ($0.0 \leq y \leq 0.5$).

The conductivity variation with composition shows the conductivity maximum at around 20 m/o dispersoid. The room temperature σ value at this composition was found to be 1.22×10^{-6} $\Omega^{-1}cm^{-1}$ which is slightly lower than the maximum conductivity value obtained with micron size powder. The insensitivity of the particle size contrasts with the well-established composite theories that state an almost inverse relationship between the conductivity and the particle size. The observation interestingly indicates that although a certain minimum particle size is required to obtain a noticeable conductivity enhancement, the size factor perhaps become ineffective beyond some critical particle

size. The conductivity maximum with finer particle is attained at lower oxide composition than the case of micron size particle dispersion presented in section 4.2.2. This feature can be attributed to the fact that as the second-phase particle size decreases, the matrix-particle interface area increases. Ideally it is assumed that all the particles are separately contributing to the interface formation required for the space charge layer leading to conductivity enhancement. However, this is not the case in actual practice, because the particles being finer have a strong tendency to undergo agglomeration and remain in that state.

4.2.7.2 SEM micrographs

The SEM micrographs were taken for the composite electrolyte $[(KCl)_{0.9}+(NaCl)_{0.1}]_{1-y}+(ZrO_2)_y$ and the micrographs corresponding to y = 0.1, 0.2, 0.4 and 0.5 are given in figure 4.9.

In all the micrographs, contrast difference across the micrographs ensures the presence of oxides in the microstructural developments. However, as can be seen from the micrographs that the grain structure in the materials for y = 0.2 is more clear with an almost continuous layer of dispersoid at the grain boundaries. The presence of dispersoid particles on the grain surfaces is also there. The increase in the dispersoid content is also evident from the micrographs 4.9 (c) and (d). Due to the excess dispersoid quantity, the blocking effect results.

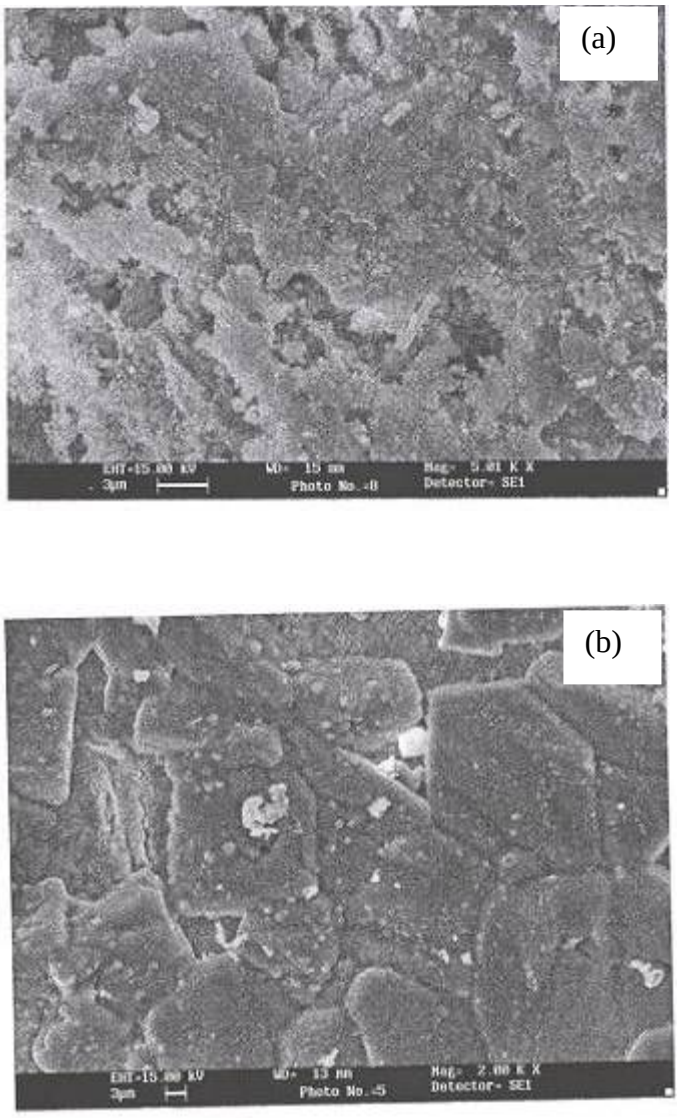

Fig. 4.9 The SEM micrographs of $[(KCl)_{0.9}+(NaCl)_{0.1}]_{1-y}+(ZrO_2)_y$ composite with y equal to (a) 0.1 and (b) 0.2.

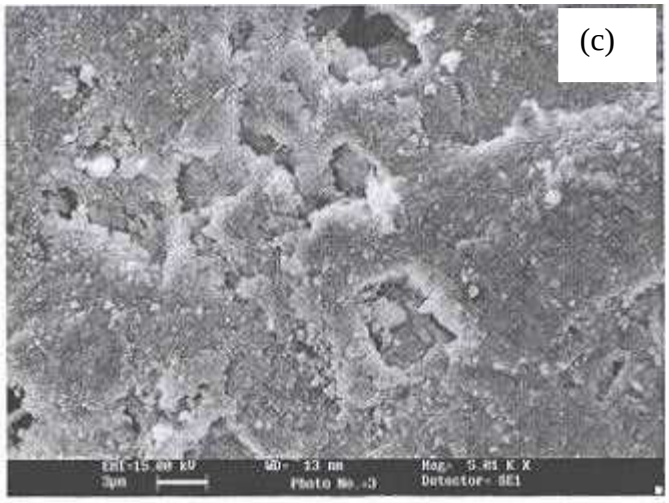

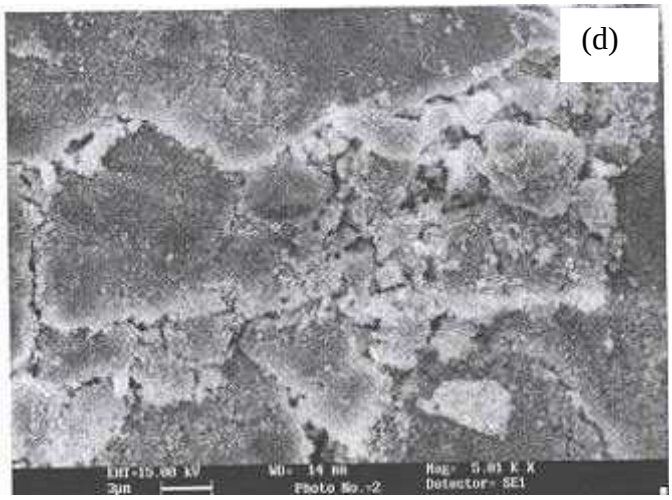

Fig. 4.9 The SEM micrographs of $[(KCl)_{0.9}+(NaCl)_{0.1}]_{1-y}+(ZrO_2)_y$ composite with y equal to (c) 0.4 and (d) 0.5.

4.2.8 Electrical conductivity of $(KCl)_{1-x}+(CuCl)_x$

Figure 4.10 represent the different impedance spectra of the mixed halide matrix $(KCl)_{1-x}+(CuCl)_x$; $0.1 \leq x \leq 0.6$. The dc resistances determined by extrapolating the impedance plots to the real axis and the dc conductivities were calculated.

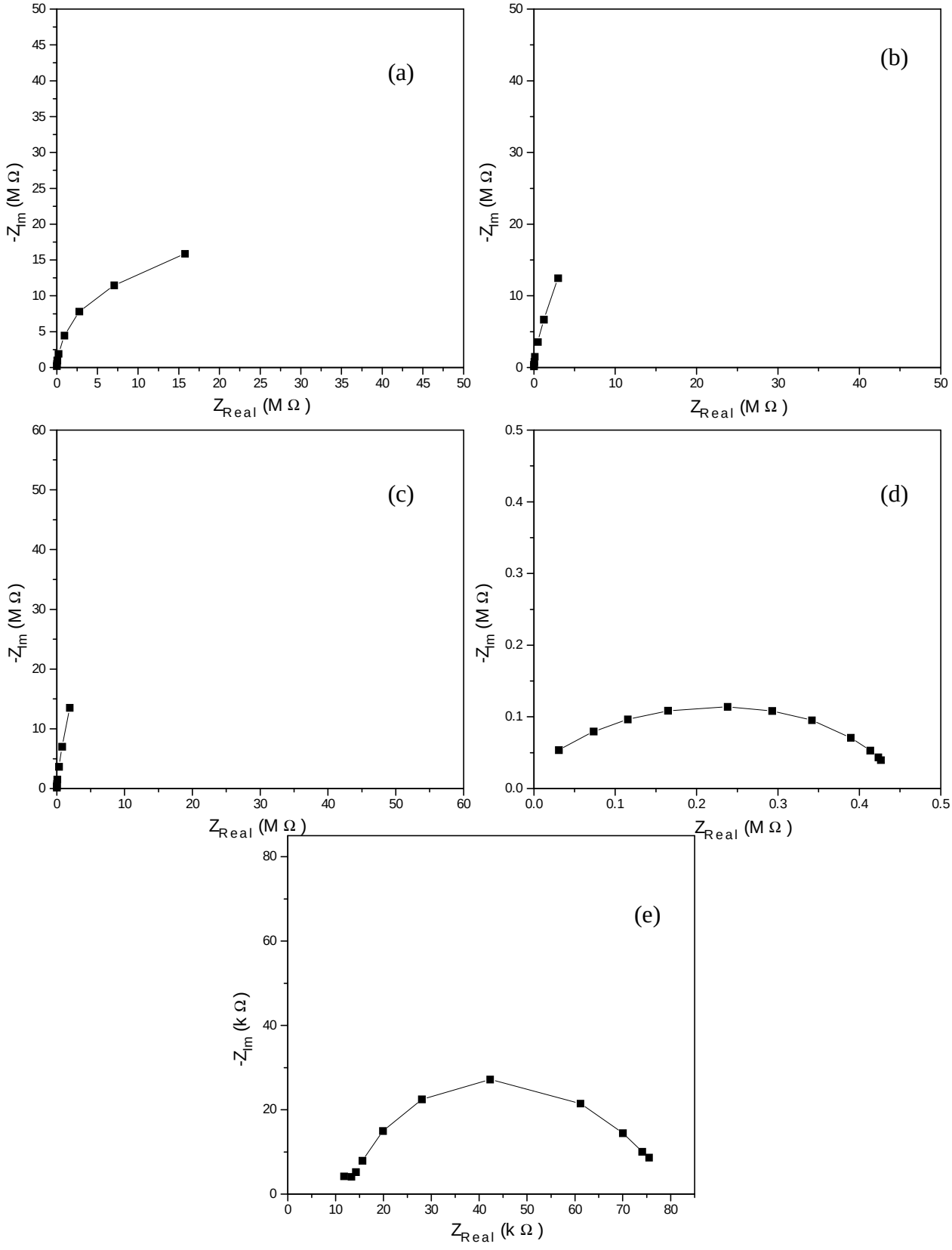

Fig. 4.10 The room temperature impedance spectra of the mixed matrix $(KCl)_{1-x}+(CuCl)_x$, when x is equal to (a) 0.1, (b) 0.2, (c) 0.3, (d) 0.4 and (e) 0.5.

Figure 4.11 shows the plot of log σ versus x for the $(KCl)_{1-x}+(CuCl)_x$ system at room temperature.

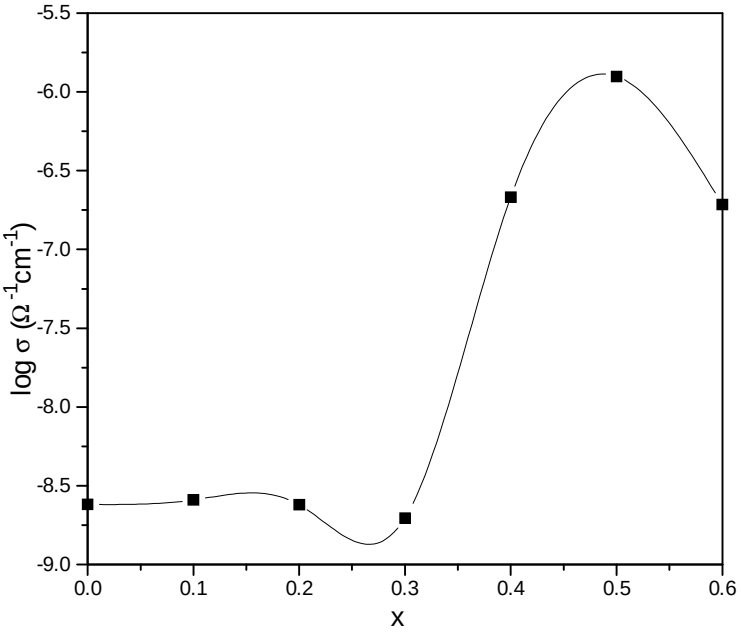

Fig. 4.11 Variation of log σ with x in the mixed halide matrix $(KCl)_{1-x}+(CuCl)_x$ at room temperature.

From the figure 4.11, it can be seen that the conductivity enhancement occurs at the composition $(KCl)_{0.5}+(CuCl)_{0.5}$ and the conductivity becomes about 500 times that of the base matrix KCl. Therefore the matrix with $(KCl)_{0.5}+(CuCl)_{0.5}$ was used as the base matrix for further preparation of the oxide dispersed composite electrolytes with varying oxide concentrations.

4.2.9 Electrical conductivity of $[(KCl)_{0.5}+(CuCl)_{0.5}]_{1-y}+(SnO_2)_y$

The samples in the system $[(KCl)_{0.5}+(CuCl)_{0.5}]_{1-y}+(SnO_2)_y$ were prepared and the conductivity (σ) variation with composition of SnO_2 was studied.

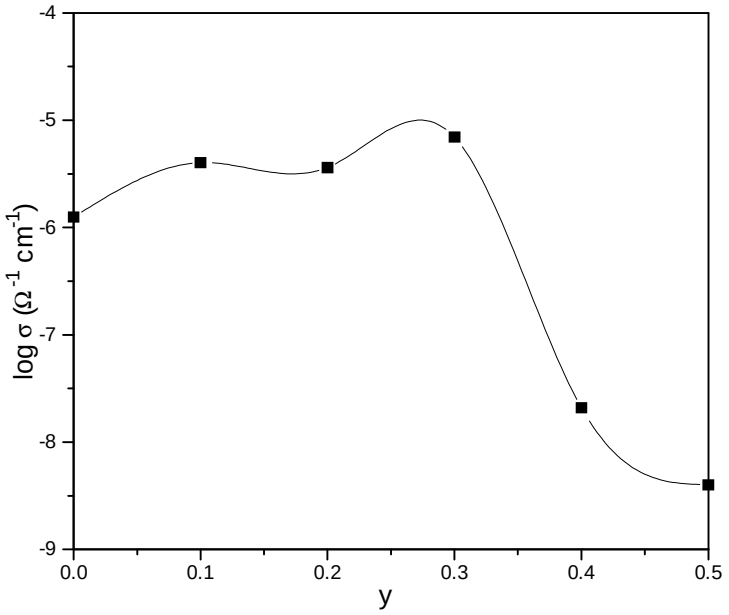

Fig. 4.12 log σ versus y plot at room temperature for composite electrolyte system $[(KCl)_{0.5}+(CuCl)_{0.5}]_{1-y}+(SnO_2)_y$ prepared using solid state sintering route.

The results are plotted in figure 4.12 from which it can be seen that with 30 m/o SnO_2 dispersion in $(KCl)_{0.5}+(CuCl)_{0.5}$ mixed matrix results in highest enhancement in conductivity which is about six times than that of the base matrix $(KCl)_{0.5}+(CuCl)_{0.5}$, giving thereby an overall conductivity enhancement of about 3000 times compared with the base KCl value.

Chapter V

Preparation, characterization and ionic conductivity measurements of anion conducting systems

Overview

This chapter presents the preparation, characterization and ionic transport characteristics of $[(BaCl_2)_{1-x}+(KCl)_x]_{1-y}+(ZrO_2)_y$ system. Such system has been considered to show the simultaneous effect of substitution of aliovalent ions and wrong size ion on the mixed matrix conductivity. However, the system acts as an anionic conductor. The present chapter also deals with the preparation and electrical resistivity measurements of $[(KCl)_{1-x}+(KI)_x]_{1-y}+(ZrO_2)_y$ to consider the anionic substitution.

5.1 Experimental

The homogeneous powder mixtures of the system $(BaCl_2)_{1-x}+(KCl)_x$ were melted in the temperature range of 700°C–1000°C and quenched to the room temperature in air. The solids thus obtained were ground and then pressed at a load of 200 kN to prepare the samples in the form of cylindrical pellets of 2 cm in diameter and 3 mm in thickness. The green pellets were sintered in a muffle furnace in the temperature range of 500°–700°C for 5 hrs. The ZrO_2 particles were dispersed in the highly conducting matrix composition. The conductivity behaviour of the dispersed electrolytes was studied as a function of ZrO_2 content. The composite of maximum conductivity was characterized by SEM and XRD.

The ionic mobilities (μ) and the ionic transference number (t_i) were determined for the maximum conducting composite electrolyte at room temperature. In order to investigate the temperature dependent transport characteristics of the material, the variations of σ and μ with temperature were also studied.

The mixed matrix $(KCl)_{1-x}+(KI)_x$ was considered to observe the effect of the size difference of the anions Cl^- and I^-. The preparation route of this system was same as for the previous system. The composite samples were sintered in a muffle furnace in the temperature range of 350°–700°C for 5 hrs. The dc resistivity measurements were carried out.

5.2 Results and discussion

5.2.1 Electrical conductivity of $(BaCl_2)_{1-x}+(KCl)_x$

Figure 5.1 shows the variation of conductivity (σ) vs. composition (x) of the matrix $(BaCl_2)_{1-x}+(KCl)_x$ $(0 \leq x \leq 0.5)$ at room temperature. It can be seen from the figure 5.1, that σ becomes maximum at x = 0.1. However, the increase is nominal.

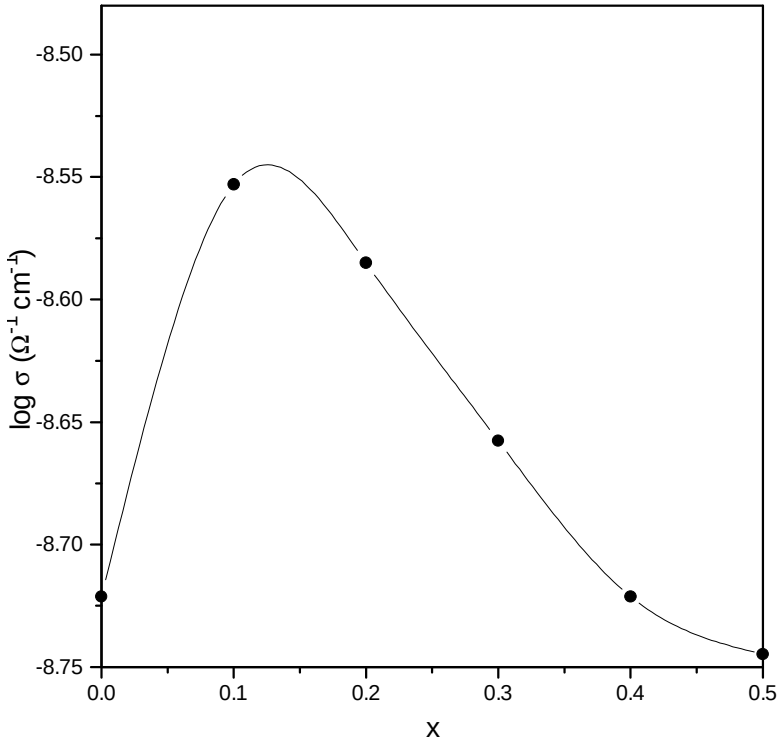

Fig. 5.1 The room temperature conductivity of $[(BaCl_2)_{1-x}+(KCl)_x]$ as a function of x ($0.0 \leq x \leq 0.5$).

The following gives an explanation of the composition dependent conductivity behaviour and the arise of maximum. On substituting the host lattice ion by guest ion, the lattice distortion takes place, which is characterized by the factor $f = \left|1 - r_h / r_g\right|$ where r_h and r_g are the ionic radii of the host and guest ions respectively. In the present case, the magnitude of this factor (~ 0.014) is negligibly small. Therefore the effect of lattice distortion towards the conductivity enhancement is insignificant. The conductivity increase could be attributed to the net charge transfer across the interface of the bi-phasic mixture.

Further, it is worth mentioning a brief account of the bulk defect structures of KCl, $BaCl_2$ and at the interfaces of KCl+$BaCl_2$. The crystallographic structures of KCl and $BaCl_2$ are rock salt and fluorite respectively. Therefore, the predominant bulk defects are of

Schottky and Frenkel types in KCl and $BaCl_2$ crystals respectively. In $BaCl_2$, Ba^{2+} ions form FCC structure and the tetrahedral voids are occupied by Cl^- ions. The structure of KCl is cubic with the anions arranged in cubic close packing with all the interstitial octahedral sites occupied by the cations. On adding KCl into $BaCl_2$, the following defect reaction is possible:

$$2KCl \xrightarrow{BaCl_2} K_{Ba}^{\prime} + K_i^{\bullet} + 2Cl_{Cl}^{\times}$$

On the other hand, if the $BaCl_2$ addition is made into KCl the possible defect reactions satisfying the preservation of the regular site ratios of the host crystal, would be as follows :

$$BaCl_2 \xrightarrow{2KCl} Ba_K^{\bullet} + V_K^{\prime} + 2Cl_{Cl}^{\times} \qquad \text{and}$$

$$BaCl_2 \xrightarrow{KCl} Ba_K^{\bullet} + Cl_i^{\prime} + Cl_{Cl}^{\times}$$

In view of the fact that K^+ ion is smaller (smaller than Ba^{2+} ion size) the replacement of Ba^{2+} site by K^+ would be relatively easy provided the required thermodynamics and kinetic properties of point defects are satisfied. Therefore an appreciable effect on defect mobility as reflected by the above defect reaction may be the likely cause of the conductivity enhancement in the $BaCl_2$+KCl mixed matrix.

5.2.2 Electrical conductivity of $[(BaCl_2)_{0.9}+(KCl)_{0.1}]_{1-y}+(ZrO_2)_y$

The conductivities (σ) of the samples in the system $[(BaCl_2)_{0.9}+(KCl)_{0.1}]_{1-y}+(ZrO_2)_y$ were determined from their complex impedance plots. The σ values were plotted as a function of composition y in figure 5.2.

From the plot, it can be seen that a significant conductivity enhancement (almost two orders of magnitude) occurs at about 50 m/o ZrO_2. This enhancement is attributed to the maximum percolation pathways at 50 m/o ZrO_2. The pathways are developed due to the

formation of space charge layer at the interface between matrix and dispersoid. The indication of such interface formation was found by microstructural investigation of the sample.

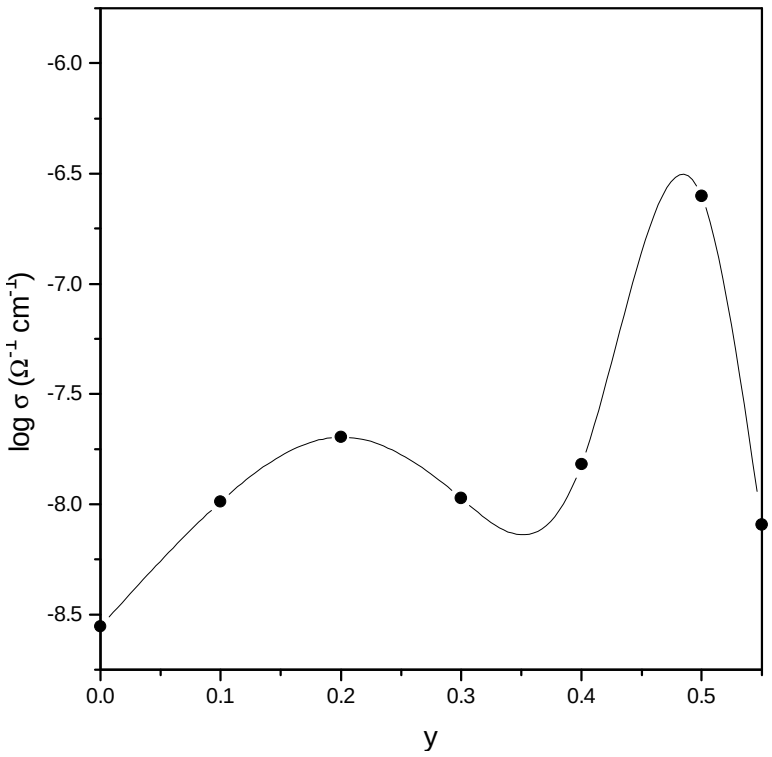

Fig. 5.2 Variation of the room temperature conductivity of composite electrolyte $[(BaCl_2)_{0.9}+(KCl)_{0.1}]_{1-y}+(ZrO_2)_y$ as a function of y ($0.0 \leq y \leq 0.55$).

As the defects in KCl and $BaCl_2$ are of different types (Schottky type in KCl and Frenkel type in $BaCl_2$), a difference in diffusivities (be they ionic or vacancy) will result at the interfaces $BaCl_2$+KCl. For $BaCl_2$, KCl or the matrix $BaCl_2$+KCl in contact with ZrO_2 which being oxide; is normally nucleophilic, the characteristic defect inducing process responsible for the increased vacancy concentration as compared to the bulk can be written as

$$V_A + K_K \Leftrightarrow K_A^{\bullet} + V_K^{'}$$

$$V_A + Ba_{Ba} \Leftrightarrow Ba_A^{\bullet\bullet} + V_{Ba}^{''}$$

and

$$V_A + K_{Ba}^{'} + K_i^{\bullet} \Leftrightarrow K_A^{\bullet} + K_{Ba}^{'}$$

respectively. V_A denotes a free active surface site which is responsible for the K^+ / Ba^{2+} cation adsorption. $V_K^{'}$ and $V_{Ba}^{''}$ are the potassium and barium vacancies formed in the space charge region. While the adsorption process from the halide components KCl and $BaCl_2$ separately creates potassium and barium vacancies respectively in the space charge region; the adsorption process from the mixed matrix will make the oxide / halide interface positive and as a result $K_{Ba}^{'}$ may get bound near the interface in the space charge region.

5.2.3 Conductivity as a function of temperature

As the ionic conductivity is a very sensitive function of temperature, the temperature dependent conductivity was also studied. The study was carried out for $[(BaCl_2)_{0.9}+(KCl)_{0.1}]_{0.5}+(ZrO_2)_{0.5}$ sample in the temperature range of 100^o–300^oC. The conductivities were plotted as a function of temperature in the form of $\log \sigma$ vs. $1/T$, in figure 5.3.

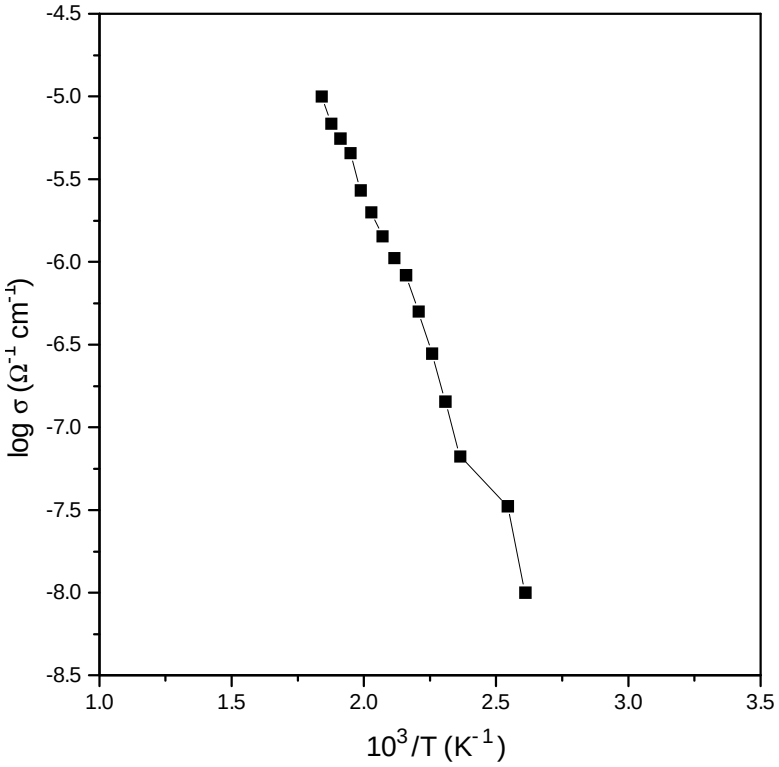

Fig. 5.3 Variation of the conductivity with temperature in $[(BaCl_2)_{0.9}+(KCl)_{0.1}]_{0.5}+(ZrO_2)_{0.5}$ sample.

From the plot, it can be seen that the σ increases from 0.01 x 10^{-6} $\Omega^{-1}cm^{-1}$ (at 100^{o}C) to about 10 x 10^{-6} $\Omega^{-1}cm^{-1}$ (at 270^{o}C) yielding the activation energy for ion transport ΔE_a = 0.34 eV. This value is found to be comparable with that of other reported electrolyte systems [90, 161,162].

5.2.4 XRD analyses

The XRD analyses of sintered KCl, $BaCl_2$, matrix $(BaCl_2)_{0.9}+(KCl)_{0.1}$ and composite electrolyte $[(BaCl_2)_{0.9}+(KCl)_{0.1}]_{0.5}+(ZrO_2)_{0.5}$ samples were carried out. The patterns are presented in figure 5.4. It is evident from the figure 5.4 (c) that for the matrix, the major peaks are either of $BaCl_2$ or KCl. There is no strong evidence of compound formation between $BaCl_2$ and KCl. It can be seen that most of the high intensity peaks of the matrix remain in their angular position, when compared with the patterns of KCl and $BaCl_2$ given in figure 5.4 (a) and 5.4 (b) respectively. However, a slight shift was observed in case of a few peaks. This shift may be attributed to the lattice distortion which is very

limited as there is no appreciable size difference between the Ba^{2+} and K^{+} ions. In the pattern given in figure 5.4 (d), the presence of ZrO_2 was found while $BaCl_2$ and KCl peaks are found to remain in their position with intensity reduction as compared to those seen in the matrix pattern (figure 5.4 (c)). However, in the composite electrolyte, a few unidentified peaks were also observed. This may be due to the nonavailability of matching peak data in the JCPDS file.

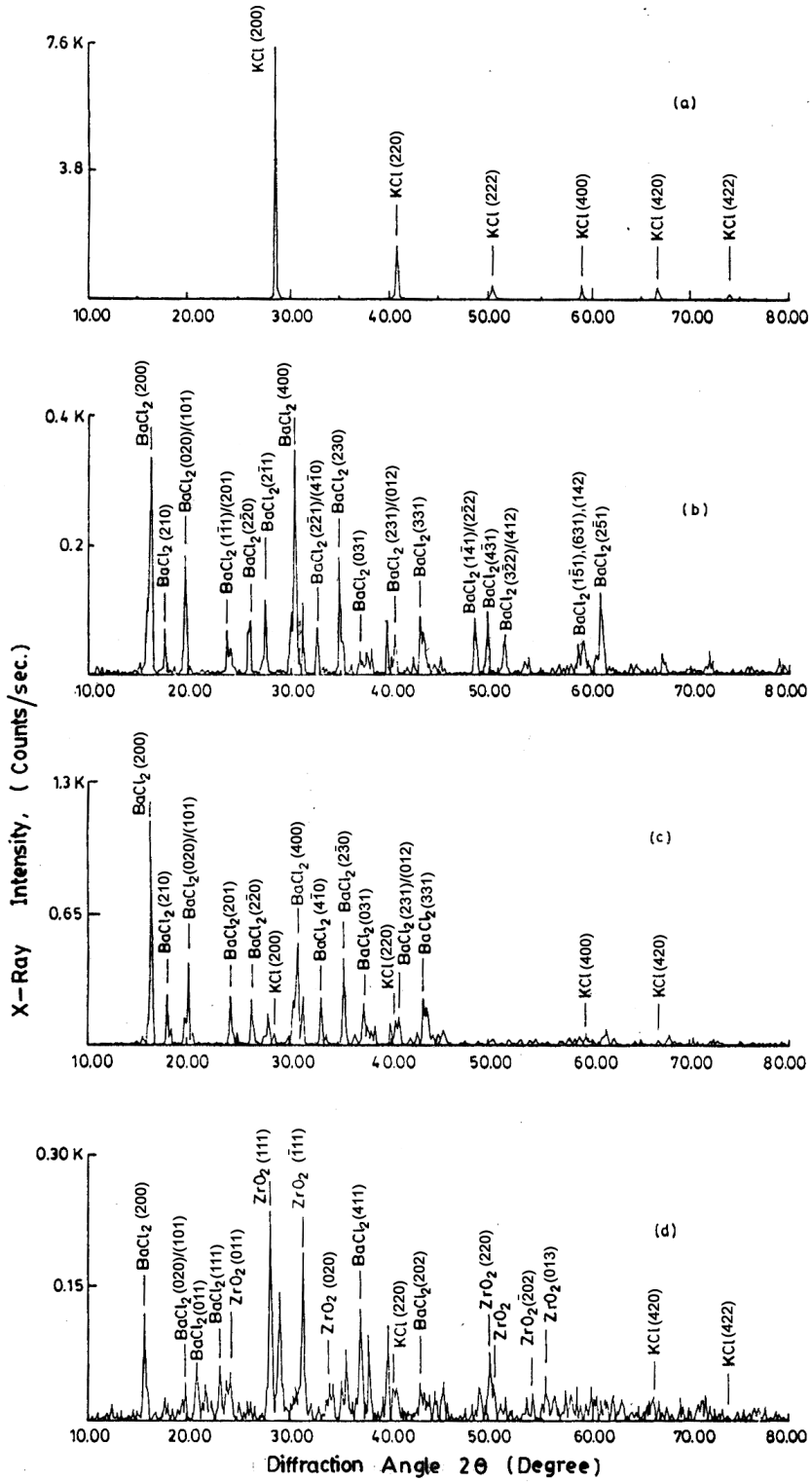

Fig. 5.4 XRD patterns of (a) KCl; (b) $BaCl_2$; (c) $(BaCl_2)_{0.9}$+$(KCl)_{0.1}$ and (d) $[(BaCl_2)_{0.9}+(KCl)_{0.1}]_{0.5}+(ZrO_2)_{0.5}$.

5.2.5 SEM micrograph

The microstructural investigation was carried out for the composite electrolyte $[(BaCl_2)_{0.9}+(KCl)_{0.1}]_{0.5}+(ZrO_2)_{0.5}$ sample. The micrograph is shown in figure 5.5. From the micrograph, the evidence of grain formation due to sintering is clear. The micrograph suggests that the system is a composite, wherein ZrO_2 particles are dispersed in the grains of matrix. As can be seen from the micrograph that the interconnecting interface regions are quite significant. Thus the microstructural evidence of the sample supports the development of higher percolation pathways in it.

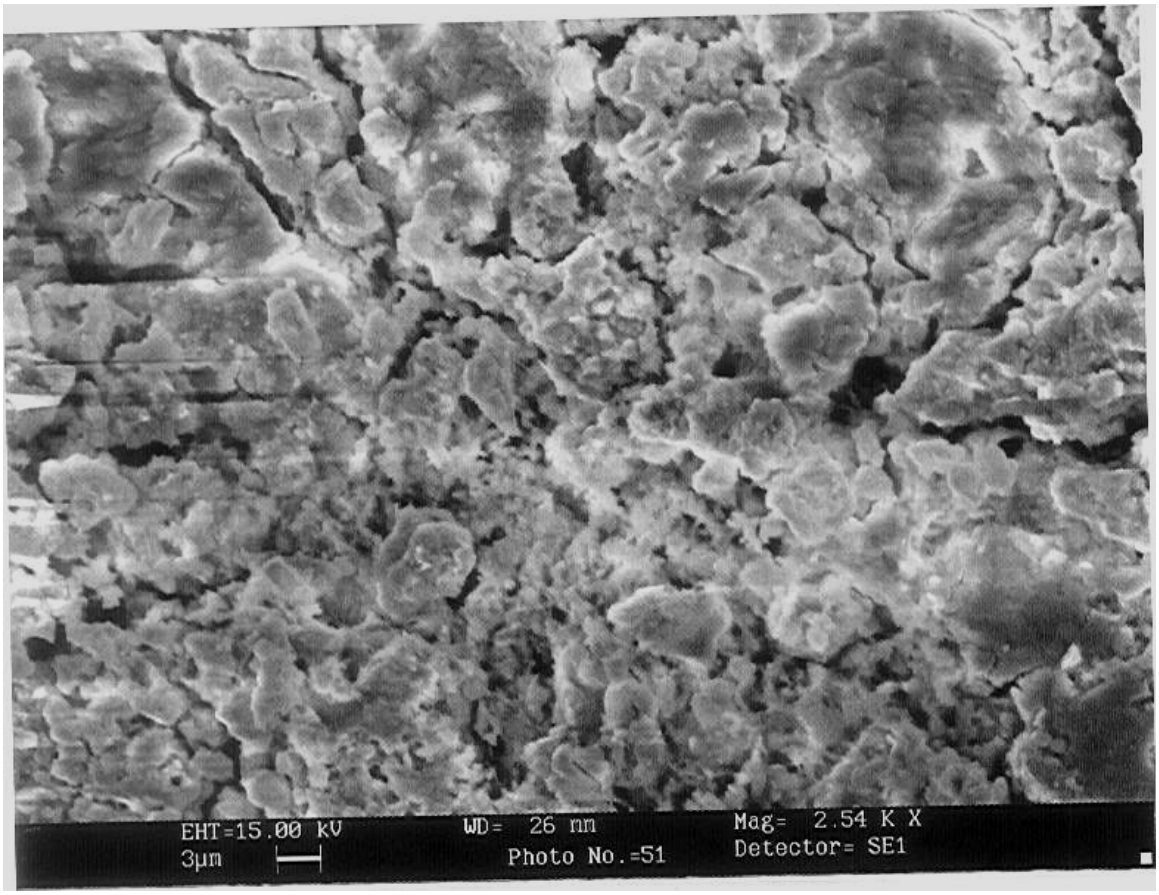

Fig. 5.5 SEM micrograph of $[(BaCl_2)_{0.9}+(KCl)_{0.1}]_{0.5}+(ZrO_2)_{0.5}$ sintered sample.

5.2.6 Ionic mobility determination

In order to estimate the conductivity contribution due to the ionic mobility (μ) factor, the ionic mobilities of the composite electrolyte $[(BaCl_2)_{0.9}+(KCl)_{0.1}]_{0.5}+(ZrO_2)_{0.5}$ were determined at different temperatures. The mobility values were estimated using d = 3.08 mm and V = 1.95 V. Some of the mobility values e.g. 0.185, 0.230, 0.328 and 0.383 $cm^2\ V^{-1}s^{-1}$ determined at 25°C, 100°C, 250°C and 300°C respectively are given here as typical data. A transient ionic current profile at a typical temperature of 250°C is presented in figure 5.6 from which the t has been estimated as 0.17s.

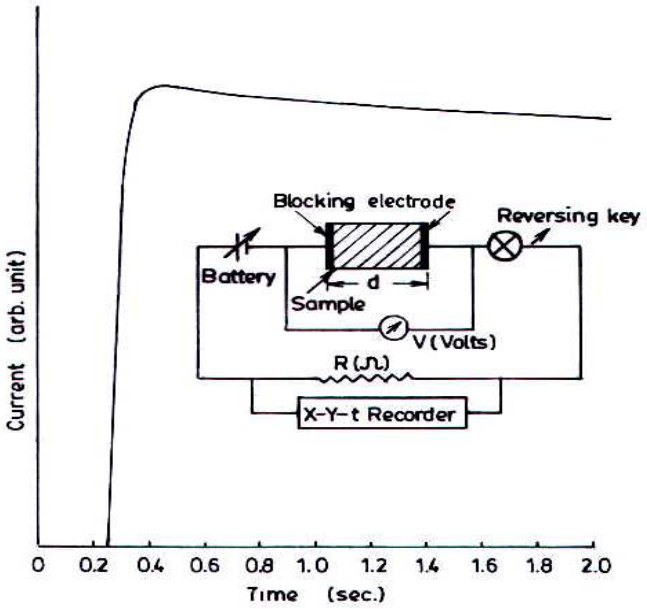

Fig. 5.6 Typical TIC plot of the composite electrolyte $[(BaCl_2)_{0.9}+(KCl)_{0.1}]_{0.5}+(ZrO_2)_{0.5}$ at 250°C. Inset : Schematic experimental circuit for TIC measurement.

From the μ values, it can be seen that the mobility at 300°C becomes just two times the room temperature value, confirming the contribution of the mobility to the conductivity, is limited. Therefore the conductivity variation with temperature is due to a combined effect of the mobility and the carrier concentration enhancements.

5.2.7 Ionic transference number determination

In order to ascertain the extent of the ionic and electronic contributions to the total conductivity, a measurement of the ionic transference number (t_i) was made. A profile showing the time dependent ionic current at room temperature for $[(BaCl_2)_{0.9}+(KCl)_{0.1}]_{0.5}+(ZrO_2)_{0.5}$ is shown in figure 5.7.

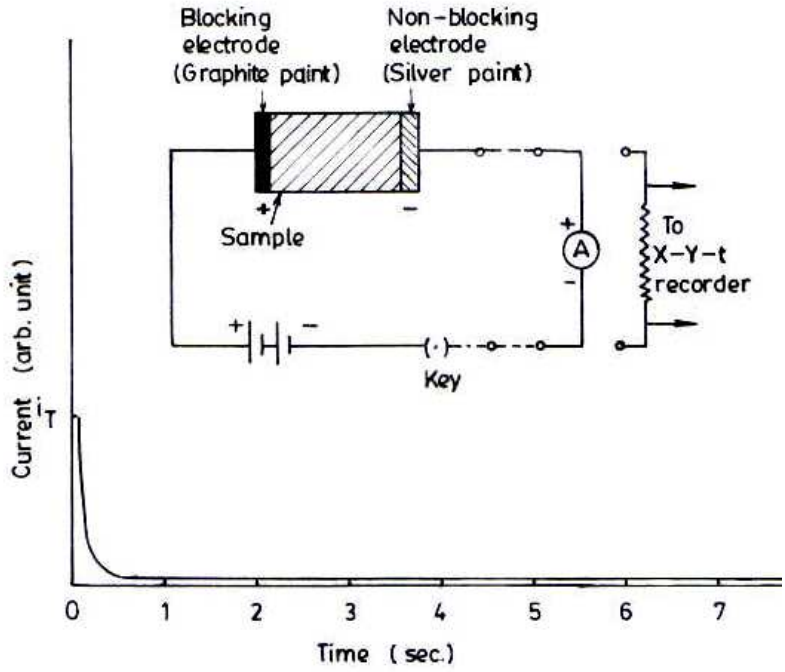

Fig. 5.7 Time dependent current response of the composite electrolyte $[(BaCl_2)_{0.9}+(KCl)_{0.1}]_{0.5}+(ZrO_2)_{0.5}$. Inset: Schematic experimental circuit diagram for the transference ion number study.

The current value decreased to a negligibly small value. Therefore, it can be concluded that the contribution to conductivity is predominantly due to the ions and from the plot the transference number has been estimated as $t_i \approx 0.964$ at room temperature.

5.2.8 Electrical conductivity of $(KCl)_{1-x}+(KI)_x$

Figure 5.8 shows the variation of room temperature conductivity (σ) vs. composition x of the matrix $(KCl)_{1-x}+(KI)_x$, where $0.0 \leq x \leq 0.5$. From the figure 5.8, it is evident that the conductivity enhancement of ~ 2 orders of magnitude was found to occur for $(KCl)_{0.6}+(KI)_{0.4}$ composition when compared with the base matrix (KCl) conductivity.

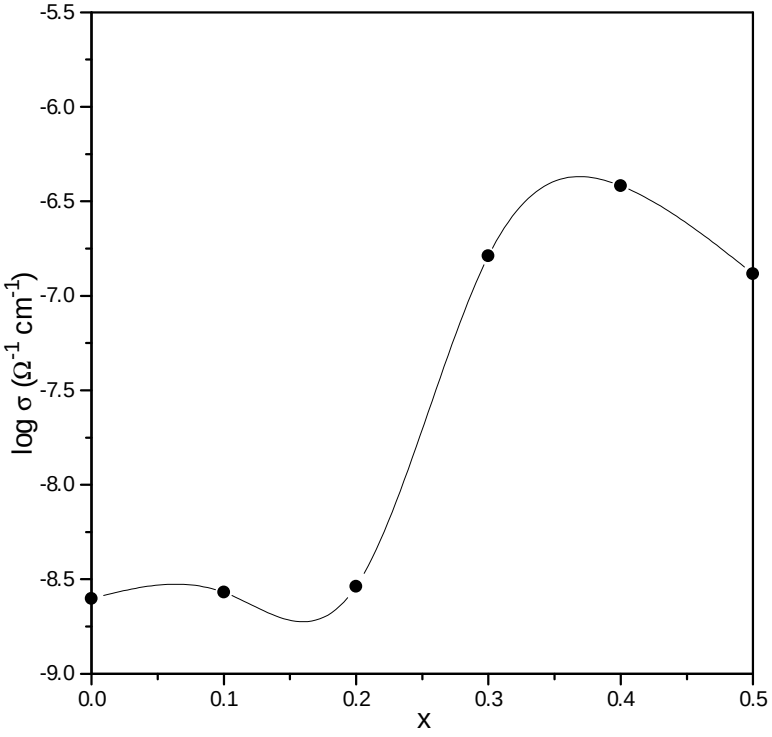

Fig. 5.8 The room temperature conductivity of mixed matrix $(KCl)_{1-x}+(KI)_x$ as a function of x ($0.0 \leq x \leq 0.5$).

The conductivity enhancement could be explained in terms of the lattice distortion caused by the incorporation of the guest ion I^- having different size (wrong size with respect to the regular lattice ion size Cl^-) into the lattice of the host material. In the present case, the magnitude of this factor $f = \left|1 - r_h / r_g\right|$ is quite appreciable (~0.189) and hence the lattice distortion could be considered as the possible cause for the conductivity enhancement.

5.2.9 Electrical Conductivity of $[(KCl)_{0.6}+(KI)_{0.4}]_{1-y}+(ZrO_2)_y$

Figure 5.9 shows the typical impedance spectra of the samples in the system $[(KCl)_{0.6}+(KI)_{0.4}]_{1-y}+(ZrO_2)_y$ where $0.1 \leq y \leq 0.4$.

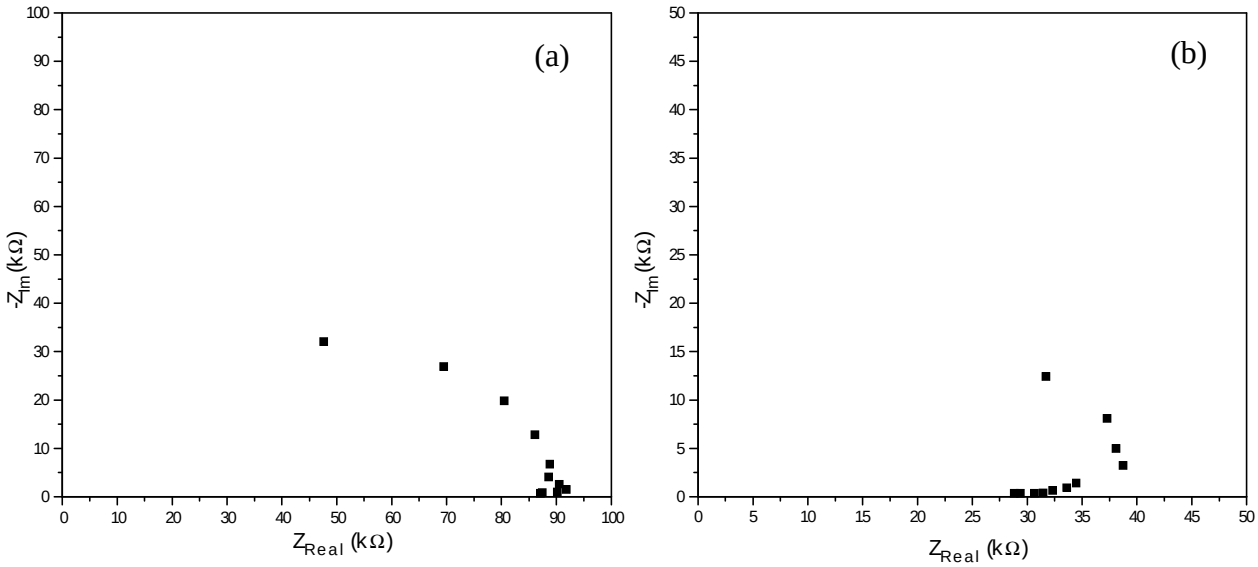

Fig. 5.9 Impedance Spectra of the composite $[(KCl)_{0.6}+(KI)_{0.4}]_{1-y}+(ZrO_2)_y$ with (a) 0.1 m/o ZrO_2 and (b) 0.2 m/o ZrO_2 at room temperature.

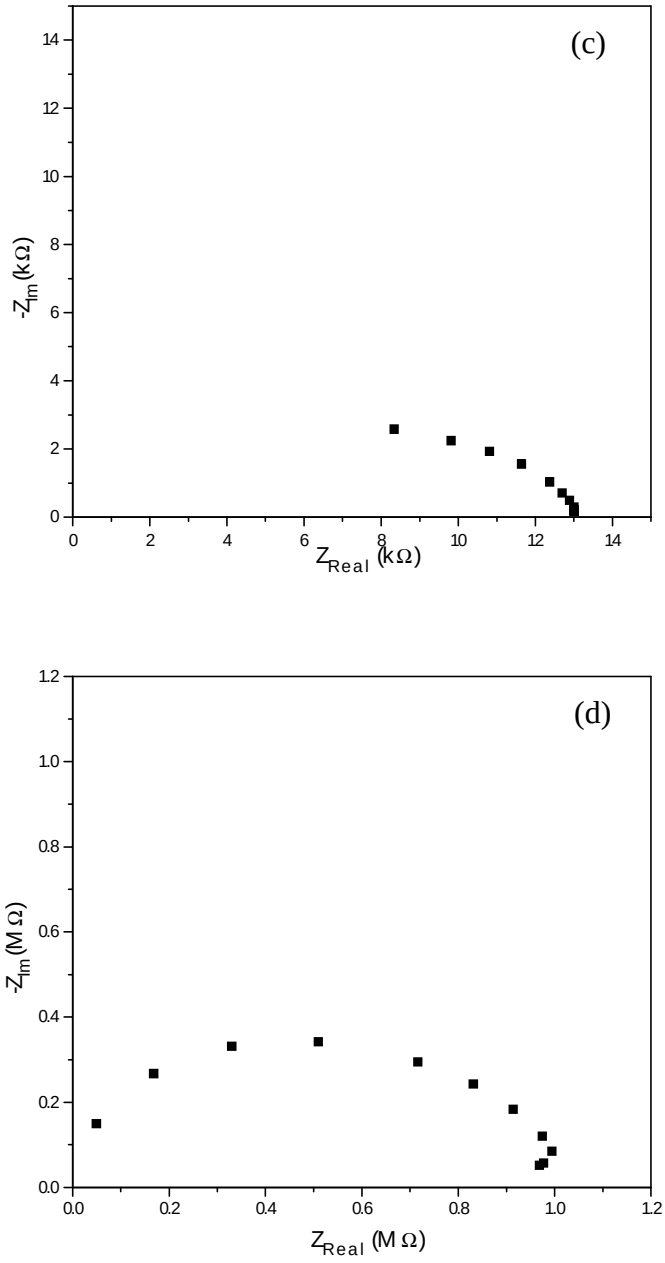

Fig. 5.9 The room temperature impedance spectra of the composite $[(KCl)_{0.6}+(KI)_{0.4}]_{1-y}+(ZrO_2)_y$ with (c) 0.3 m/o ZrO_2 and (d) 0.4 m/o ZrO_2.

From the impedance spectra obtained in the form of semicircles, dc resistances of the samples were obtained by extrapolating the semicircular curves to zero reactance value

(at ω = 0). From the resistance values, the dc conductivities (σ) were calculated. The σ values so obtained were plotted as a function of composition y in figure 5.10.

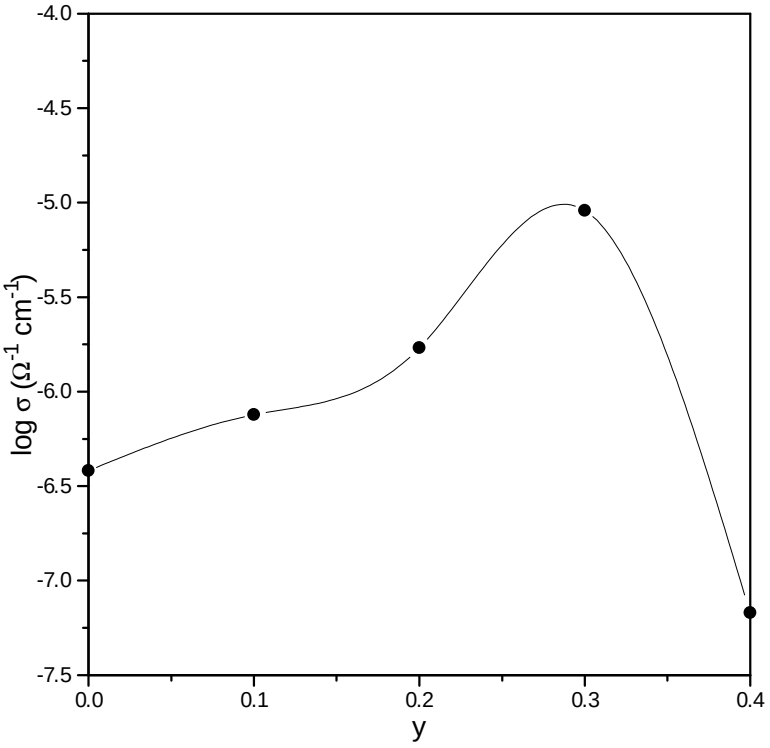

Fig. 5.10 Variation of the room temperature conductivity of composite electrolyte $[(KCl)_{0.6}+(KI)_{0.4}]_{1-y}+(ZrO_2)_y$ as a function of y ($0.0 \leq y \leq 0.4$).

From the plot, it can be seen that a significant conductivity enhancement (~25 times the base matrix value) occurs at about 30 m/o ZrO_2. The pathways are developed due to the formation of space charge layer at the interface between matrix and dispersoid.

Chapter VI

Discussion, conclusion and scope of future work

6.1 Discussion

The composite solid electrolytes were prepared in five different systems as described in the previous chapters, characterized and their ionic transport properties were reported. The primary objective was to study the ionic conductivity behaviour of the electrolytes prepared. There are several ways of increasing the conductivity in the composite solid electrolyte. The choice of base matrix and its modification plays an important role in conductivity value. The conductivity of composite solid electrolyte with a single halide matrix as base, can be enhanced by replacing the single matrix with mixed matrix. Therefore, the single halide matrix and the mixed halide matrix bases were considered for oxide dispersion. The objective of the present thesis has been demonstrated by developing either KCl-based matrix or KCl substituted (partially) mixed matrix dispersed with ZrO_2 powder, in all the cases, except in one case where SnO_2 was used as dispersoid. Initially oxide (ZrO_2) dispersed single matrix (KCl) was studied. Subsequently mixed matrices were developed in a number of systems for oxide dispersion. The systems were so chosen that the conductivity in a system is accomplished preferentially by a particular type of ion (cation / anion). The data obtained in the present study are further discussed in a more cohesive and coherent manner as given below:

6.1.1 XRD analyses

The primary objective of the XRD analyses of the samples was to detect new compound formation, if any, for the preparation of mixed halide matrix and oxide dispersion thereon, resulting in composite solid electrolytes. The mixed matrices and the composites along with the constituents were analyzed and the patterns were presented. On analysis of the patterns concerning a system, it can be seen that the mixed halide matrix and composite electrolyte patterns consist of those of constituting component halides and

oxides. As can be seen from figure 3.1 (a) & (d), the angular positions of some of the peaks of KCl and ZrO_2 are almost same, the peaks of these materials at these positions appear to be overlapping, as seen in figure 3.1 (b) & (c). It can also be seen that some peaks which are present for one composition, are not found to be present in another composition. This is due to the fact that the relative intensities of the components are different in different composition. In figure 4.5, even the most intense peak of NaCl line is negligibly smaller than that of the KCl lines in the mixed halide matrix pattern. This can be attributed to the proportionate amount of NaCl which is less in the mixed matrix. The presence of ZrO_2 with adequate intensities is seen in the composite electrolyte pattern. The system in figure 5.4 has also shown no new compound formation either in the matrix or in composite electrolyte preparations.

6.1.2 SEM micrographs

The microstructural studies of the systems were carried out primarily:

(i) to confirm the grain structure that develops due to sintering,

(ii) to observe the oxide dispersion characteristics in the resultant microstructure of composite electrolytes and thereby

(iii) the development of interface between oxide and matrix phases as the interconnecting interfaces is the main cause of space charge layer for high conductivity.

The microstructural analyses of matrices and composites were carried out in almost all the systems. The sintered samples in $(KCl)_{1-x} + (ZrO_2)_x$ system are found to consist of grains whose size and shape changes with increase in oxide content. On careful observations on the micrographs, it can be seen that the oxides are not present in the form of agglomerate. The oxide dispersion characteristic in the system $[(KCl)_{1-x} + (NaCl)_x]_{1-y} + (ZrO_2)_y$ is clearly revealed from the micrographs. The presence of oxide as a separate phase in the microstructure is clearly revealed. However, the oxide dispersion is not free from agglomeration. However, the continuity of the inter dispersoid particles contact are more and as a result larger oxide–matrix interface area developed in $[(KCl)_{0.9}+(NaCl)_{0.1}]_{0.5}+(ZrO_2)_{0.5}$ composite. The micrographs in figure 4.9 refer to the dispersion with very fine (20-50 nm) ZrO_2 particles in $[(KCl)_{0.9}+(NaCl)_{0.1}]_{1-y}+(ZrO_2)_y$

system. The grain structure of the matrix and the presence of oxides as dispersoid can be seen in the micrographs (figure 4.9). However, relatively high distinct grain boundaries and the presence of dispersoid as a separate phase are found for the sample with composition y = 0.2. The dispersoid contents are found to be excessive for the samples with y = 0.4, 0.5 and this microstructural feature supports the lower conductivities of these compositions. The conductivity maximum at y = 0.2 within the composition range studied is thus explained. The microstructure of the sample in the composition $[(BaCl_2)_{0.9}+(KCl)_{0.1}]_{0.5}+(ZrO_2)_{0.5}$, consists of grains and oxide dispersion. The grains in this system are more uniform in size than in the other systems studied in this thesis. Well-defined interconnecting interphase region due to the oxide dispersion is evident from the micrograph. The formation of interfacial layer between interconnecting oxide particles and the matrix phase is also evident from the micrograph.

6.1.3 Transport characteristics

6.1.3.1 Electrical conductivity (σ) of mixed halide matrices

The electrical conductivities at room temperature of the single halide matrix (KCl) and mixed halide matrices ($(KCl)_{1-x}+(NaCl)_x$, $(KCl)_{1-x}+(CuCl)_x$, $(BaCl_2)_{1-x}+(KCl)_x$ and $(KCl)_{1-x}+(KI)_x$) were studied. The room temperature conductivity of the KCl was estimated to be 0.24 x 10^{-8} $\Omega^{-1}cm^{-1}$ and this was enhanced to about 50 times for the mixed matrix $(KCl)_{0.9}+(NaCl)_{0.1}$, which was found to be highest conducting composition over the composition range studied. The possible explanation for the conductivity enhancement is lattice distortion as explained in section 4.2.1. The defect reactions that occur due to the partial substitution of host cations by guest ions are also described in that section. The conductivity enhancement at room temperature in $(KCl)_{0.5}+(CuCl)_{0.5}$ composition was about 500 times the conductivity of KCl. This situation demonstrates that the substitution of alkali halide by metallic halide for mixed matrix preparation has superior effect, although the conductivity maximum obtained for the two systems $(KCl)_{1-x}+(NaCl)_x$, $(KCl)_{1-x}+(CuCl)_x$ investigated were at different compositions i.e. at different x values. The conductivity begins to rise at around x = 0.3 for the KCl+CuCl system, whereas, the enhancement begins right from x = 0.0 for KCl+NaCl system.

The electrical conductivity in $(BaCl_2)_{1-x}+(KCl)_x$ system was studied between x = 0.0 to x = 0.5 and the conductivity maximum was found to occur at x = 0.1. However, this enhancement is nominal with respect to the conductivity of $BaCl_2$. The reason for small conductivity rise is due to very small value of the factor "f" as explained in section 5.2.1. The conductivity maximum in the system $(KCl)_{1-x}+(KI)_x$ arises at x = 0.4 and the value is about 2 orders of magnitude higher than the conductivity of KCl. The study was conducted in the composition range x = 0.0 to x = 0.5. The higher conductivity rise in $(KCl)_{0.6}+(KI)_{0.4}$ is attributed to the higher lattice distortion caused in the matrix as characterized by the factor "f" in sections 5.2.8.

6.1.3.2 Electrical Conductivity (σ) of Composite electrolytes

The conductivity maximum in the system $(KCl)_{1-x}+(ZrO_2)_x$ was occurred at x = 0.7, and the value becomes 3 orders of magnitude of that of KCl. The conductivity increases with increase in temperature and the value at about 500°C becomes 4670 times when compared to the conductivity of KCl at room temperature. The ionic mobility was estimated as a function of temperature in the temperature range of 300°C to 460°C. The mobility was found to increase gradually with increase in temperature and the value at 460°C becomes 1.4 times the mobility value at 300°C.The conductivity enhancement at room temperature in the system $[(KCl)_{0.9}+(NaCl)_{0.1}]_{0.5}+(ZrO_2)_{0.5}$ was found to be maximum for y = 0.5 and the magnitude is estimated to be 500 times the room temperature conductivity of KCl. On increasing the temperature to about 450°C, the conductivity of the maximum conducting composite has increased to about 3000 times the room temperature conductivity of KCl. The room temperature conductivity of the SnO_2 dispersed $[(KCl)_{0.5}+(CuCl)_{0.5}]_{0.7}+(SnO_2)_{0.3}$ samples was found to be about 3000 times the conductivity of KCl. The conductivity maximum at room temperature in $[(BaCl_2)_{1-x}+(KCl)_x]_{1-y}+(ZrO_2)_y$ system was found to occur at y = 0.5 and the value becomes 2 orders of magnitude higher than the conductivity of KCl. On increasing temperature, the conductivity value at 270°C becomes 4000 times the room temperature conductivity of KCl. The ionic mobility as a function of temperature shows 2 times the

room temperature mobility at 300°C. Therefore, the large conductivity variation with increase in temperature largely depends on the variation of carrier concentration.

In order to determine the ionic contribution to the electrical conductivity in the material, the ionic transference number in the composition $[(BaCl_2)_{0.9}+(KCl)_{0.1}]_{0.5}+(ZrO_2)_{0.5}$ was estimated and this was found to be 0.964 indicating that the conductivity is predominantly due to ions.

6.2 Conclusion

The work presented in the thesis describes the preparation of composite solid electrolytes for potential applications in solid state batteries and other electrochemical devices. As the performance of the electrochemical devices depends primarily on the ionic conductivity, there has been a continuous upsurge to develop electrolytes with higher and higher ionic conductivity. Though insulating phase dispersed ionic crystals paved a long way towards developing highly conducting electrolytes, efforts are on to find better electrolytes. In this line, the dissertation work was undertaken to develop composite electrolytes primarily on mixed halide matrix as electrolyte base and then dispersing the base with oxide particles. In order to address the present issue, the electrolytes chosen to study were divided into two categories i.e. type I in which the conductivity is by the cations and type II for which anions are the main conducting species. The fact that the conductivity enhancement can be achieved by mixed halides compared to single halide used as base for preparations of composite electrolytes was exploited in this study. The superiority of mixed halides in relation to ionic conductivity was established in all the systems studied. A many fold increase in conductivity could be achieved with oxide dispersion. The conductivities at room temperature of all the systems and as a function of temperature for some of these systems were reported. The conductivity data were explained, in majority of the cases, by the measurements of other transport properties and microstructural features. The mobility data at room temperature and as function of temperature for a few systems gives further insight about the predominant factor on which the conductivity depends. In the systems $(KCl)_{1-x}+(ZrO_2)_x$ and $[(BaCl_2)_{1-x}+(KCl)_x]_{1-y}+(ZrO_2)_y$, the mobility studied over a temperature range show a nominal rise. The charge carrier concentration as a function of

temperature was calculated from the measured mobility and conductivity data. It can be inferred from the calculated data that the carrier concentration plays a substantial role in giving rise to the conductivity. The electrical characterizations of the materials were made to correlate with the physical characterizations results. The possibility of formation of new compound (during the synthesis of the materials), which may offer high ionic conductivity, was ruled out by the X-ray diffraction analyses. This fact leads one to resort on the phenomenological models as proposed by many researches for the conductivity enhancement due to oxide dispersion. Interconnecting interface between the matrix and the dispersoid that develops during sintering is the prevailing mechanism in the literature. In order to make an attempt to reveal such interface formation in the present study, microstructural investigations were carried out. The microstructural features as discussed earlier indicated the formation of pathway which is optimum with a particular composition depending on the system.

6.3 Scope of the further work

In the light of the present work, it is suggested that the following investigations can be carried out for further study:

(i) The effect of matrix grain size on its conductivity as well as composite's conductivity can be studied. The grain size, in turn, depends on the sample preparative parameters. Therefore preparative parameters are required to be controlled for the conductivity enhancement.

(ii) The relationship between the second-phase particle size and the matrix grain size must be clearly understood if maximum enhancements in conductivity are to be engineered.

(iii) The relationship between structural (crystal structure) behaviour and the ionic conductivity of mixed matrices needs to be developed.

(iv) In order to understand the structural effect on high temperature transport characteristics, the samples can be characterized by high temperature X-ray diffraction analysis.

(v) A method suitable for the determination of carrier concentration (n) both at room temperature and as a function of temperature, should be devised for knowing the relative

contributions of the mobility and carrier concentration to the ionic conductivity at different temperature of different materials.

(vi) The effect of dispersoid particle size can be considered in the electrolytes development.

(vii) The performance of the electrolytes developed should be tested in an actual configuration for electrochemical devices applications.

(viii) It is required to establish a relationship between the ionic conductivity of the electrolytes and its defect chemistry.

(ix) A relationship can be developed between lattice strain and the increased vacancy concentration in mixed matrices.

(x) Impedance plots in the form of depressed semi circles for composite electrolytes can be resolved very accurately for separating the contributions due to the different interfaces formed, in the material.

BIBLIOGRAPHY

[1] W. Nernst, Z. Elektrochem., 6 (1899) 41-43.

[2] S. Chandra and R. C. Agrawal, in "The National Academy of Sciences, India, Golden Jubilee Commemoration Volume" edited by U. S. Srivastava (Naya Prokash, Calcutta, 1980) p. 429.

[3] C. A. C. Sequeira and A. Hooper (eds) "Solid State Batteries" (Martinus Nijhoff, Dordrecht, 1985).

[4] M. Z. A. Munshi and B. B. Owens, in "Superionic Solids and Solid Electrolytes – Recent Trends" edited by A. L. Laskar and S. Chandra (Academic Press, New York, 1989) p. 631.

[5] S. Megahed and B. Scrosati, J. Electrochem. Soc. "Interface" Winter (1995) 34.

[6] J. N. Bradley and P. D. Greene, Trans. Faraday Soc., 62 (1966) 2069.

[7] J. N. Bradley and P. D. Greene, Trans. Faraday Soc., 63 (1967) 424.

[8] B. B. Owens and G. R. Argue, Science, 157 (1967) 308.

[9] Y. F. Y. Yao and J. T. Kummer, J. Inorg. Nucl. Chem., 29 (1967) 2453.

[10] J. H. Edwards, S. P. S Badwal, G. J. Duffy, J. Lasich and G. Ganakas, Solid State Ionics, 152-153 (2002) 843.

[11] J. Coetzer, J. Power Sources, 18 (1986) 377.

[12] S. P. S. Badwal, M. J. Bannister and W. G. Garrett, J. Phys. E: Sci. Instrum., 20 (1987) 531.

[13] P. R. Somani and S. Radhakrishnan, Mat. Chem. Phy., 77 (2003) 117.

[14] A. Donnadieu, Mater. Sci. and Engg. B, 3 (1989) 185.

[15] H. Iwahara, in : Solid State Ionic Devices, July 18-23, Singapore : B. V. R. Chowdari and S. Radhakrishna, (Eds.) Singapore : World Scientific, (1988) 289-323.

[16] D. M. Rowe, Renewable Energy, 5 (1994) 1470.

[17] D. M. Rowe, Renewable Energy, 16 (1999) 1251.

[18] J. M. Tarascon, A. S. Gozdz, C. Schmutz, F. Shokoohi and P. C. Warren, Solid State Ionics, 86-88 (1996) 49.

[19] E. J. Cairns and P. Shimotake, Science, 164 (1969) 1347.

[20] A. Vanzyl, Solid State Ionics, 86-88 (1996) 883.

[21] V. Venugopal, Progress in Crystal Growth and Characterization of Materials, 45 (2002) 139.

[22] R. A. Pett, A. N. Theodore, G. J. Tennenhouse and F. D. Runkle, Am. Ceram. Soc. Bull., 164 (1969) 1347.

[23] B. C. H. Steele and A. Heinzel, Nature, 414 (2001) 345.

[24] H. Iwahara, T. Esaka, H. Uchida and T. Yamauch, Solid State Ionics, 18-19 (1986) 1003.

[25] A. M. Azad, S. A. Akbar, S. G. Mhaisalkar and L. D. Birkefeld and K. S. Goto, J. Electrochem. Soc., 139 (1992) 3690.

[26] N. Yamazoe and N. Miura, Sensors and Actuators B, 20 (1994) 95.

[27] N. Fukatsu, N. Kurita, K. Kiode and T. Ohashi, Solid State Ionics, 113-115 (1998) 219.

[28] O. Takikawa, A. Imai and M. Horata, Solid State Ionics, 7 (1982) 101.

[29] T. Takahashi, K. Kuwabara and O. Yamamoto, J. Electrochem. Soc., 116 (1959) 357.

[30] M. Wittingham and R. Huggins, J. Chem. Phys., 54 (1971) 414.

[31] J. Wang, M. Gaffari and S. Choi, J. Chem. Phys., 63 (1975) 772.

[32] M. A. Ratner and A. Nitzan, Solid State Ionics, 28-30 (1988) 3.

[33] F. T. Ciacchi, K. M. Crane and S. P. S. Badwal, Solid State Ionics, 73 (1994) 49.

[34] S. Chandra, " Superionic Solids-Principles and Applications" (North Holland, Amsterdam, 1981).

[35] A. B. Lidiard, Handb. Phys., 20 (1951) 246.

[36] Y. V. G. S. Murti and R. D. Banhatti, Ind. J. Pure and App. Phys., 37 (1999) 285.

[37] J. Maier, Solid State Ionics, 131 (2000) 13.

[38] F. W. Poulsen, N. H. Andersen, B. Kindl and J. Schoonman, Solid State Ionics, 9/10 (1983) 119.

[39] R. C. T. Slade and I. M. Thompson, Solid State Ionics, 26 (1988) 287.

[40] Y. Saito, J. Mayne, K. Ado, Y. Yamamoto and O. Nakamura, Solid State Ionics, 40/41 (1990) 72.

[41] M. Vidyullatha and C. S. Sunandana, Solid State Commun., 88 (1993) 553.

[42] L. M. Navarro, P. Recio and J. R. Jurado, J. Mater. Sci., 30 (1995) 1949.

[43] D. Kunze, in "Fast Ion Transport in Solids," Ed., W. vanGool (North Holland, Amsterdam) (1973) 405.

[44] C. A. Angell, Solid State Ionics, 9/10 (1983) 3.

[45] M. D. Ingram, Phys. Chem. Glasses, 28 (1987) 215.

[46] S. S. Sekhon, Phys. News, Bull. Indian Phys. Assoc., 26 (1995) 80.

[47] M. Tatsumisago, Y. Shinkuma and T. Minami, Nature, 354 (1991) 217.

[48] P. G. Bruce and C. A. Vincent, J. Chem. Soc. Faraday Trans., 89 (1993) 3187.

[49] M. Watanbe and N. Ogata, " Polymer Electrolyte Reviews-1" Ed., J. R. MacCallum and C. A. Vincent (Elsevier, London) (1987) 39.

[50] P. Mustarelli, E. Quartarone, C. Tomasi and A. Magistris, Solid State Ionics, 86/88 (1996) 347.

[51] B. Kumar, J. D. Schaffer, M. Nookala and L. G. Scanlon Jr., J. Power Sources, 47 (1994) 63.

[52] S. Skaarup, K. West, P. M. Julian and D. M. Thomas, Solid State Ionics, 40/41 (1990) 1021.

[53] W. Wieczorek, Solid State Ionics, 53-56 (1992) 1064.

[54] J. A. Subramony and A. R. Kulkarni, Mater. Sci. Eng., B22 (1994) 206.

[55] S. L. Agrawal, P. K. Shukla and P. K. Srivastava, Bull. Electrochem. Soc., 12 (1996) 683.

[56] A. M. Sukeshini, A. Nishimoto and M. Watanbe, Solid State Ionics, 86/88 (1996) 385.

[57] S. Pack, Abstract No. 133, Electrochemical Society Meeting, Los Angeles (1979).

[58] K. Shahi and J. B. Wagner Jr., J. Electrochem. Soc., 128 (1981) 6.

[59] K. Shahi and J. B. Wagner Jr., J. Solid State Chem., 42 (1982) 107.

[60] J. Mejerovich, J. Power Sources, 38 (1992) 345.

[61] L. Chen, " Materials for Solid State Batteries" Ed., B. V. R. Chowdari and S. RadhaKrishna (World Scientific, Singapore), (1986) 69.

[62] M. C. R. Shastry and K. J. Rao, Solid State Ionics, 51 (1992) 311.

[63] S. Furusawa, S. Miyaoka and Y. Ishibashi, J. Phys. Soc. Jpn, 60 (1991) 1666.

[64] T. Takekuchi, K. Ado, Y. Saito, M. Tabuchi, H. Okuyama and O. Nakamura, Solid State Ionics, 86/88 (1996) 565.

[65] Y. Saito and J. Maier, Solid State Ionics, 86/88 (1996) 581.

[66] F. W. Poulsen, J. Power Sources, 20 (1987) 317.

[67] Y. Saito, K. Ado, T. Asai, H. Kageyama and O. Nakamura, Solid State Ionics, 53/56 (1992) 723.

[68] T. Jow and J. Bruce Wagner Jr., J. Electrochem. Soc., 126 (1979) 1963.

[69] N. J. Dudney, Ann. Rev. Mater. Sci., 19 (1989) 103.

[70] N. F. Uvarov, M. C. R. Shastry and K. J. Rao, Rev. Solid State Sci., 4 (1990) 61.

[71] A. kumar and K. Shahi, J. Solid State Chem., 109 (1994) 15.

[72] C. C. Liang and P. Bro, J. Electrochem. Soc., 116 (1969) 1322.

[73] C. C. Liang, J. Epstein and G. H. Boyle, J. Electrochem. Soc., 116 (1969) 1452.

[74] C. R. Schlaikjer and C. C. Liang, J. Electrochem. Soc., 118 (1971) 1447.

[75] C. R. Schlaikjer and C. C. Liang, in " Fast Ion Transport in Solids," Ed. W. vanGool (North Holland Publishing Co., Amsterdam) (1973) 685-694.

[76] C. C. Liang, J. Electrochem. Soc., 120 (1973) 1289.

[77] J. Maier, Ber. Bunsenges. Phys. Chem., 88 (1984) 1057.

[78] J. Maier, J. Phys. Chem. Solids, 46 (1985) 309.

[79] S. Fujitsu, K. Koumoto and H. Yanagida, Solid State Ionics, 18 & 19 (1986) 1146.

[80] O. Nakamura and J. B. Goodenough, Solid State Ionics, 7 (1982) 119.

[81] O. Nakamura and J. B. Goodenough, Solid State Ionics, 7 (1982) 125.

[82] N. F. Uvarov, V. P. Isupov, V. Sharma and A. K. Shukla, Solid State Ionics, 51 (1992) 41.

[83] M. Nagai and T. Nishino, Solid State Ionics, 53-56 (1992) 63.

[84] M. Nagai and T. Nishino, J. Am. Ceram. Soc., 76 (1993) 1057.

[85] Ashok Kumar and K. Shahi, Bull. Mater. Sci., 17 (1994) 209.

[86] Ashok Kumar and K. Shahi, J. Phys. Chem. Solids, 56 (1995) 215.

[87] Ashok Kumar and k. Shahi, Solid State Communications, 94 (1995) 813.

[88] A. Brune and J. B. Wagner Jr., Solid State Ionics, 25 (1987) 165.

[89] A. Kumar and K. Shahi, J. Mater. Sci., 28 (1993) 1257.

[90] A. Kumar and K. Shahi, J. Mater. Sci., 30 (1995) 4407.

[91] R. W. Ure, J. Chem. Phys., 26 (1957) 1363.

[92] T. L. Wen, R. A. Huggins, A. Rabenau and W. Weppner, Rev. Chim. Miner., 20 (1983) 643.

[93] S. Fujitsu, K. Koumoto, H. Yanagida and T. Kanazawa, J. Mater. Sci., 20 (1985) 2103.

[94] A. Khandkar, V. B. Tare and J. B. Wagner, Rev. Chim. Miner., 23 (1986) 274.

[95] G. Rog, A. Kielski, A. Kozlowska-Rog and M. Bucko, Ceram. Int., 24 (1998) 91.

[96] G. Rog, M. M. Bucko, A. Kielski and A. Kozlowska-Rog, Ceram. Int., 25 (1999) 623.

[97] H. H. Hoffer, W. Eysel and U. V. Alpen, J. Solid State Chem, 36 (1981) 365.

[98] S. Hull, D. A. Keen and P. Berastegui, Solid State Ionics, 147 (2002) 97.

[99] P. Manoravi and K. Shahi, Solid State Ionics, 58 (1992) 243.

[100] K. Singh, S. D. Wachasunder and S. S. Bhoga, Bull. Mater. Sci., 18 (1995) 147.

[101] K. Singh and V. K. Deshpande, Solid State Ionics, 7 (1982) 295.

[102] U. Lauer and J. Maier, Ber. Bunsenges. Phys. Chem., 96 (1992) 111.

[103] L. S. Cain and L. M. Slifkin, J. Phys. Chem. Solids, 41 (1980) 173.

[104] K. Shahi and J. B. Wagner Jr., Phys. Rev. B, 23 (1981) 6417.

[105] H. H. Hoffer, W. Eysel and U. V. Alpen, J. Solid State Chem., 36 (1981) 365.

[106] K. Shahi and J. B. Wagner Jr., J. Phys. Chem. Solids, 43 (1982) 713.

[107] K. Shahi and J. B. Wagner Jr., J. Phys. Chem. Solids, 44 (1983) 89.

[108] K. Shahi and J. B. Wagner Jr., Solid State Ionics, 12 (1984) 511.

[109] K. Singh, Solid State Ionics, 28/30 (1988) 1371.

[110] R. B. Beeken and K. L. Menningen, J. Appl. Phys., 66 (1989) 5340.

[111] R. Mercier, M. Tachez, J. P. Malugani and G. Robert, Solid State Ionics, 15 (1985) 109.

[112] M. Lumbreras, J. Protas, S. Jebbari, G. J. Dirksen and J. Schoonman, Solid State Ionics, 20 (1986) 295.

[113] S Gupta, S. Patmaik, S. Chaklanobis and K. Shahi, Solid State Ionics, 31 (1988) 5.

[114] P. Manoravi and K. Shahi, Solid State Ionics, 45 (1991) 83.

[115] P. Manoravi and K. Shahi, Solid State Ionics, 52 (1991) 527.

[116] U. Lauer and J. Maier, Solid State Ionics, 51 (1992) 209.

[117] R. C. Agrawal, R. K. Gupta, R. Kumar and Ajay Kumar, J. Mat. Sci., 29 (1994) 3673.

[118] N. Rao, J. Schoonman and O. T. Sorensen, Solid State Ionics, 57 (1992) 159.

[119] K. Singh, S. M. Pande and S. S. Bhoga, Bull. Mater. Sci., 18 (1995) 237.

[120] K. Singh and S. S. Bhoga, Apply. Phys. A, 67 (1998) 475.

[121] B. K. Choi, H. K. Lee and Y. W. Kim, Solid State Ionics, 113/115 (1998) 493.

[122] B. M. Suleiman, A. Lunden and E. Karawacki, Solid State Ionics, 136/137 (2000) 325.

[123] S. Gomathy, M. Shukla, P. Gopalan and A. R. Kulkarni, Mat. Res. Bull., 36 (2001) 397.

[124] S. Hull, P. Berastegui, S. G. Eriksson and N. J. G. Gardner, J. Phys.: Condens. Matter, 10 (1998) 8429.

[125] S. Hull and P. Berastegui, J. Phys.: Condens. Matter, 11 (1999) 5257.

[126] S. Hull, D. A. Keen and P. Berastegui, Solid State Ionics, 147 (2002) 97.

[127] J. S. Bae and S. I. Pyun, J. Mater. Sci. Lett., 13 (1994) 573.

[128] P. Chowdary, V. B. Tare and J. B. Wagner Jr., J. Electrochem. Soc., 132 (1985) 123.

[129] J. C. Maxwell, " A Treatise on Electricity and Magnetism," Vol. 1, 2^{nd} ed. (Clarendon Press, Oxford, 1881) p. 435.

[130] J. C. Raleigh, Phil. Mag., 34 (1892) 481.

[131] K. Lichtenecker, Phys. Z., 25 (1924) 225.

[132] R. Landauer, J. Appl. Phys., 23 (1952) 779.

[133] C. Wagner, J. Phys. Chem. Solids, 33 (1972) 1051.

[134] G. Crosbie, J. Solid State Chem., 25 (1978) 367.

[135] K. L. Kliewer, J. Phys. Chem. Solids, 27 (1966) 705.

[136] J. Maier, Solid State Ionics, 70/71 (1994) 43.

[137] J. Maier, Phys. Status Solidi (b), 123 (1984) K89.

[138] J. Maier, Solid State Ionics, 18/19 (1986) 1141.

[139] J. Maier, Ber. Bunsenges. Phys. Chem., 89 (1985) 355.

[140] A. Bunde, W. Dieterich and E. Roman, Phys. Rev. Lett., 55 (1985) 5.

[141] R. Blender and W. Dieterich, J. Phys. C, 20 (1987) 6113.

[142] E. Roman, A. Bunde and W. Dieterich, Phys. Rev. B, 34 (1986) 3439.

[143] S. Chandra, Superionic solids – principles and applications, (North Holland, Amsterdam), 1981.

[144] J. R. Macdonald, (ed), Impedance Spectroscopy (John Wiley and Sons, NY), 1987.

[145] M. Watanabe, K. Sanui, N. Ogata, T. Kobayashi and Z. Ontaki, J. Appl. Phys., 57 (1985) 123.

[146] S. Chandra, S. K. Tolpadi and S. A. Hashmi, Solid State Ionics, 28-30 (1988) 651.

[147] J. B. Wagner Jr. and C. Wagner, J. Chem. Phys., 26 (1957) 1597.

[148] CRC Handbook of Solid State Chemistry, Eds. P. J. Gellings and H. J. M. Boumeester (CRC Press. Inc., USA, 1997).

[149] G. J. Dudley and B. C. H. Seele, J. Solid State Chem., 21 (1977) 1.

[150] D. W. Marquardt, J. Soc. Indust. Appl. Math., 11 (1963) 431.

[151] B. A. Boukamp, Solid State Ionics, 20 (1986) 31.

[152] T. H. Etsell and S. N. Flengas, Chem. Rev., 70 (1970) 339-376.

[153] L. Heyne (1977), S. Geller (Ed.), Solid Electrolytes, New York : Springer Verlag, pp. 169-221.

[154] P. H. Bottelberghs (1978), Solid Electrolytes, General Principles, Characterization, Materials, Applications : P. Hagenmuller and W. Vangool (Eds.), New York : Academic Press, pp. 145-172.

[155] H. Schmalzried, Z. Phys. Chem., 38 (1963) 87-102.

[156] T. H. Etsell and S. N. Flengas, Chem. Rev., 70 (1970) 339-376.

[157] C. Wagner, Proc. Int. Committee Electrochem. Thermodyn. Kinetics (CITEC), 7 (1957) 361-377.

[158] W. Weppner, J. Solid State Chem., 20 (1977) 305.

[159] W. Weppner and R. A. Huggins, J. Electrochem. Soc., 124 (1977) 35.

[160] G. J. Dudley, K. Y. Cheung and B. C. H. Steele, J. Solid State Chem., 32 (1980) 259-267.

[161] A. Mangla and A. Sil, Ind. J. Pure and Appl. Phys., 39 (2001) 267.

[162] R. C. Agrawal and R. K. Gupta, Bull. Mater. Sci., 19 (1996) 573.

List of Publications in reviewed Journals

1. "Transport characteristics of 0.3 KCl : 0.7 ZrO_2 solid electrolyte", Archana Mangla and Anjan Sil, Ind. J. of Pure & Appl. Physics, 39 (2001) 267–270.

2. "Preparation, characterization and ionic conductivity measurements of (1–x) KCl : x ZrO_2 solid electrolyte system", Archana Gupta and Anjan Sil, Indian Journal of Engg. and Materials Science, 9 (2002) 65–68.

3. "Preparation and characterization of mixed halide systems as solid electrolyte base", Archana Gupta, Anjan Sil and N K Verma, Indian Journal of Engg. & Materials Science, 11 (2004) 212–216.

4. "Transport characteristics of ZrO_2 dispersed mixed KCl – $BaCl_2$ solid electrolytes", Archana Gupta and Anjan Sil, Materials Research Bulletin, 40 (2005) 67–77.

5. "Preparation, characterization and ionic conducitvity studies of ZrO_2 dispersed mixed halide matrix $(KCl)_{1-x}$: $(NaCl)_x$", Archana Gupta, Anjan Sil and N K Verma, Current Applied Physics (under review).

List of Papers presented in Conferences

1. Archana Mangla and Anjan Sil, "Preparation, characterization and ionic conductivity measurements of (1 – x) KCl : x ZrO_2 solid electrolyte system", National Seminar on "Materials Science : Trends and Future", at SLIET, Longowal, Sangrur, Punjab Feb. 24 – 25, 2000.

2. Archana Gupta, Anjan Sil and N K Verma, "Role of mixed halides as solid electrolyte base matrix ", 5th Punjab Science Congress, "Science and Technology in New Millennium", at TIET, Patiala, Feb. 7 – 9, 2002.

3. Archana Gupta, Anjan Sil and N K Verma, "Electrical conductivity measurements of ZrO_2 dispersed mixed $(KCl)_{1-x} - (KI)_x$ solid electrolytes", National Conference on "Materials and Related Technologies", at TIET, Patiala, Sept. 19 – 20, 2003.